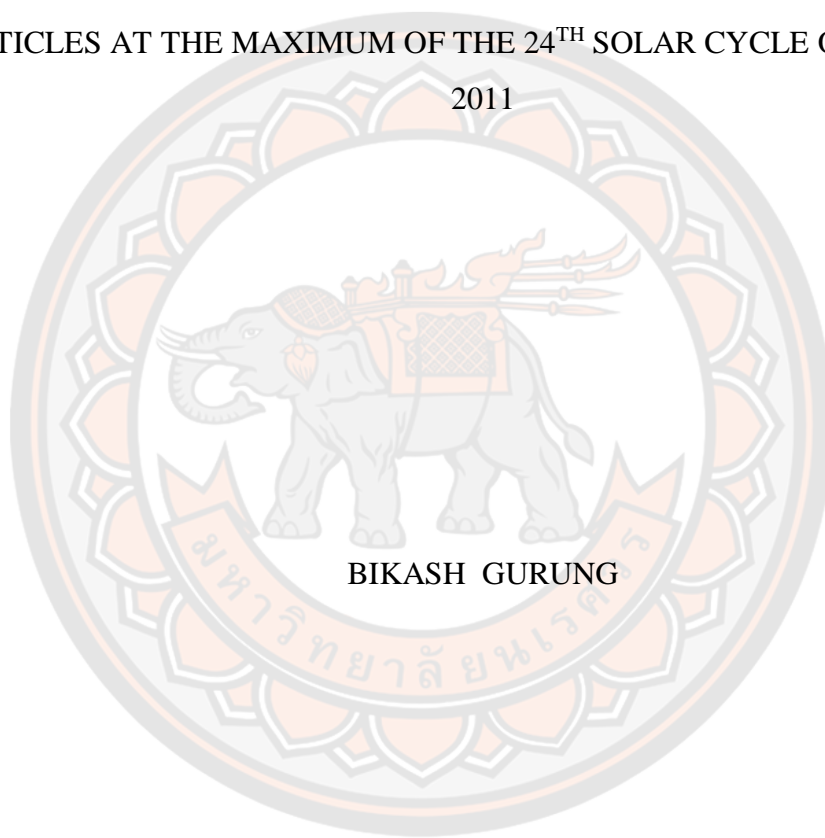




AN ANALYSIS OF INTENSITY PROFILE OF THE SOLAR ENERGETIC
PARTICLES AT THE MAXIMUM OF THE 24TH SOLAR CYCLE ON AUGUST 9,
2011



BIKASH GURUNG

A Thesis Submitted to the Graduate School of Naresuan University
in Partial Fulfillment of the Requirements
for the Master of Science in (Physics)

2020

Copyright by Naresuan University

AN ANALYSIS OF INTENSITY PROFILE OF THE SOLAR ENERGETIC
PARTICLES AT THE MAXIMUM OF THE 24TH SOLAR CYCLE ON AUGUST 9,
2011



A Thesis Submitted to the Graduate School of Naresuan University
in Partial Fulfillment of the Requirements
for the Master of Science in (Physics)
2020
Copyright by Naresuan University

Thesis entitled "An analysis of intensity profile of the solar energetic particles at the maximum of the 24th solar cycle on August 9, 2011"

By BIKASH GURUNG

has been approved by the Graduate School as partial fulfillment of the requirements
for the Master of Science in Physics of Naresuan University

Oral Defense Committee

..... Chair
(Assistant Professor Charuangrit Channok, Ph.D.)

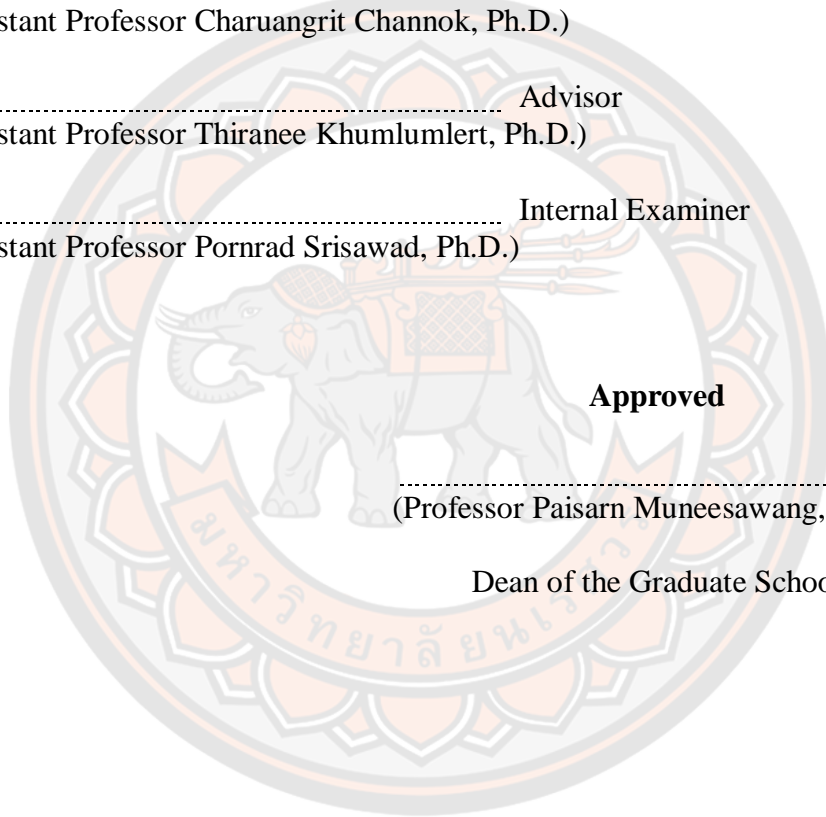
..... Advisor
(Assistant Professor Thiranee Khumlumlert, Ph.D.)

..... Internal Examiner
(Assistant Professor Pornrad Srisawad, Ph.D.)

Approved

.....
(Professor Paisarn Muneesawang, Ph.D.)

Dean of the Graduate School



Title AN ANALYSIS OF INTENSITY PROFILE OF THE SOLAR ENERGETIC PARTICLES AT THE MAXIMUM OF THE 24TH SOLAR CYCLE ON AUGUST 9, 2011

Author BIKASH GURUNG

Advisor Assistant Professor Thiranee Khumlumlert, Ph.D.

Academic Paper Thesis M.S. in Physics, Naresuan University, 2020

Keywords Sun, solar flare, solar cycle, solar energetic particles, coronal mass ejections

ABSTRACT

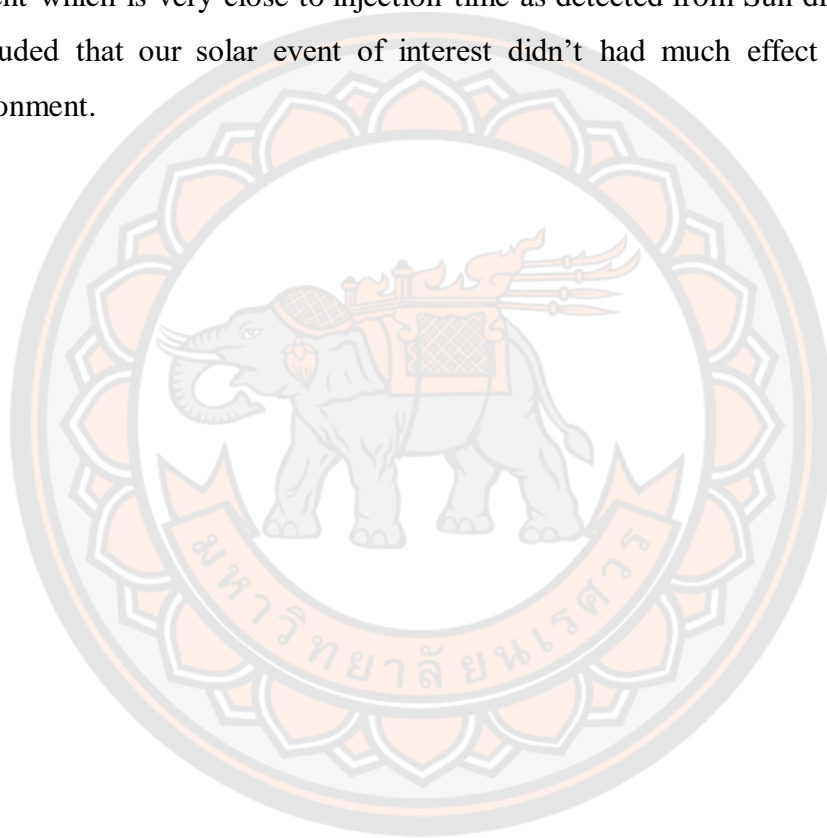
Our Sun releases large amount of coronal matter into outer space due to violent eruption known as solar flare. This phenomenon has large impact on Earth by disrupting radio communication on satellites. It happens every solar cycle corresponding to change in Sun's activity every periodic 11 year with varying number of sunspots on its surface.

In this research we study the behavior of solar energetic particle at the maximum of 24th solar cycle on August 9, 2011. The X-ray class of the selected solar event is X6.9 with solar flare position on the Sun as N18W68 and solar wind speed of 551.5 kms⁻¹. The chosen element were He, C, N, O and Fe which are the elements having lower mass, medium mass and higher mass. The kp index for our event of interest was equal to 3 which indicated that it did not have much effect to earths magnetic field due to solar flare.

We collect data of an event from the SIS (Solar Isotope Spectrometer) instrument on ACE spacecraft (Advanced Composition Explorer). The data are then simulated for the motion of particles from the solar flare using transport equation of Ruffolo (1995, 1998) solved by numerical technique of finite different method in C++ program. Mean free path and injection time are obtained for particles that propagate from Sun to Earth by using compared fitting method of piecewise linear function between the data collected from spacecraft and simulation results. We determine the best piecewise linear injection function and chi square value for each

mean free path. Chi square is defined as the difference between data from simulation result and data from spacecraft. We then, work out the injection time duration by the means of method called full width at half maximum of the injection function.

We found out that most particles with higher energy level propagated from Sun to Earth faster than particles with lower energy levels due to their higher speed. The trend of mean free path is found to be roughly constant for each event. The calculated approximate injection time for our event was between 30 – 60 min for each element which is very close to injection time as detected from Sun directly. Thus, we concluded that our solar event of interest didn't had much effect from the space environment.



ACKNOWLEDGEMENTS

It is my great privilege to acknowledge my sincere thanks of gratitude to my advisor Assistant Professor Thiranee Khumlumlert, Ph.D., for her tremendous guidance, support, motivation, and immense knowledge without which completion of this research would have been impossible. Her dynamism, vision, and sincerity have deeply inspired me and would like to thank for her friendship, empathy, and great sense of humor.

The scale of appreciation can't be completed without acknowledging to the Thailand International Cooperation Agency (TICA) and Royal Government of Bhutan (RGoB) for proposition of the scholarship and generous financial support they have rendered during this entire course.

Transport equation for explaining the behavior of solar energetic particles and C++ program for the simulation have been one the major means of source for this research. Let me not forget to thank Professor Dr. David Ruffolo, Department of Physics, Mahidol University for approving the usage of such fundamental tools.

My deepest indebtedness to all the dynamic staffs of the Department of Physics, Naresuan university who have helped me to this delightful voyage. I am also pleased in all humbleness and gratefulness to acknowledge my deepest to all those friends of the physics department who have helped me to put these ideas, well above the simplicity into something rational.

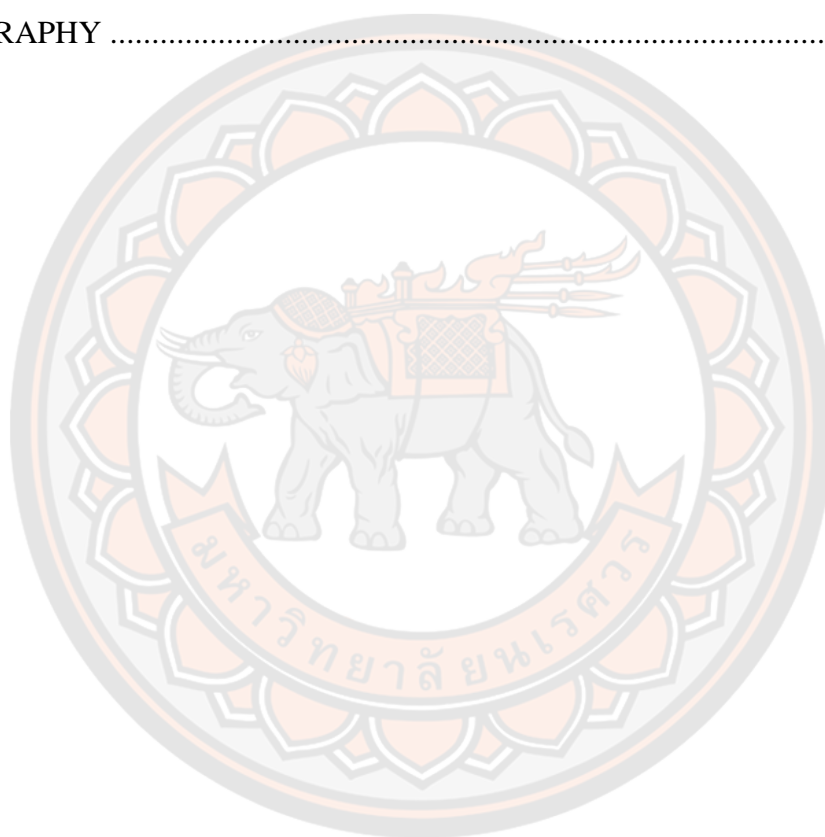
BIKASH GURUNG

TABLE OF CONTENTS

	Page
ABSTRACT	C
ACKNOWLEDGEMENTS	E
TABLE OF CONTENTS.....	F
List of tables	I
List of figures	J
CHAPTER I INTRODUCTION	1
1.1 Importance and background of the research	1
1.2 Research objectives	2
1.3 Hypothesis of research.....	2
1.4 Scope of research.....	3
1.5 Expected benefits	3
1.6 Purposes of the Study	3
1.7 Research Plan	4
CHAPTER II LITERATURE REVIEW	5
2.1 The Structure of Sun.....	5
2.1.1 Internal structure of the Sun	5
2.1.2 The atmosphere of Sun	6
2.2 Solar Cycle	7
2.3 Solar flare.....	8
2.3.1 Impulsive solar flares.....	10
2.3.2 Gradual solar flares.....	10
2.4 Classification of X-rays	10
2.5 Solar Energetic Particles (SEPs)	11
2.6 Coronal Mass Ejection (CME).....	12
2.7 Solar wind	13

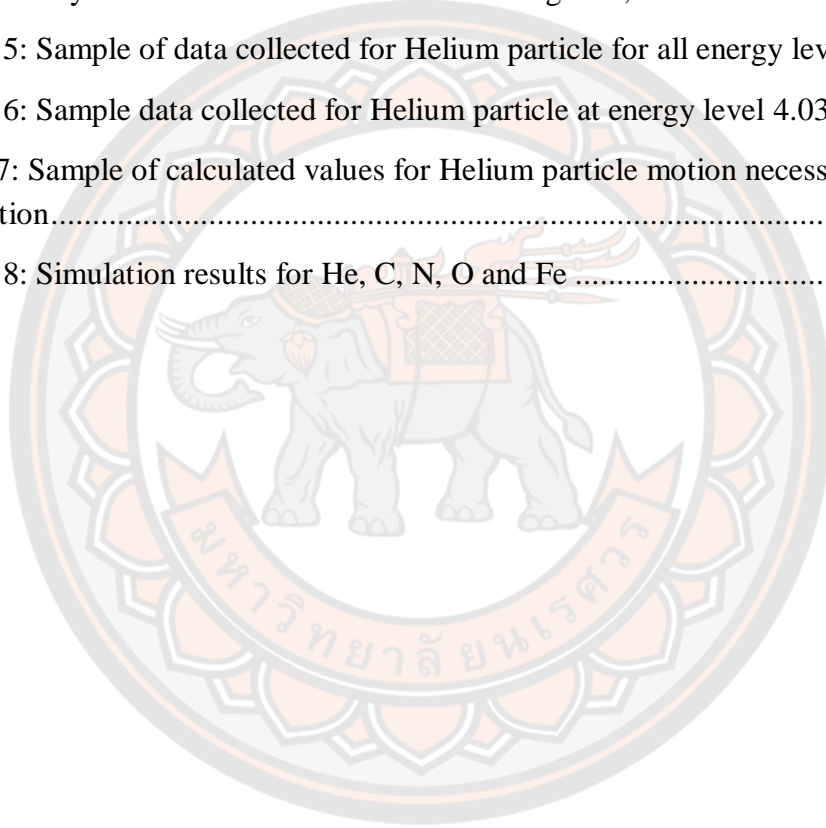
2.8 Archimedean spiral magnetic field.....	14
2.9 Transport Equation	18
2.10 Numerical methods used in research operations	24
2.10.1 Explicit method	25
2.10.2 Implicit method	27
2.10.3 Crank-Nicolson method.....	28
CHAPTER III RESEARCH METHODOLOGY	30
3.1 Research guidelines	30
3.2 Research Procedures of the Study	31
3.2.1 Flow chart of the research procedures in brief	32
3.3 Tools used in research operations	33
3.3.1 Data from the ACE (Advanced Composition Explorer) spacecraft	33
3.3.2 Program written in C++ for the simulation of particle motion	34
3.4 Selecting an event for the release of high-energy particles from the Sun's eruption	35
3.5 Position of solar flare and kp index on an event of interest	36
3.6 Data collection from SIS instrument on ACE spacecraft	37
3.7 Preparation of data for simulation in C++ program	40
3.8 Determination of the necessary values for simulation of particle motion	42
3.9 Simulation of high energy particle motion	45
3.10 Fit to compare data	46
3.11 Sample procedures for FWHM method for Helium element at energy level 4.032 MeV/n.....	47
CHAPTER IV RESULTS AND DISCUSSION	50
4.1 Best mean free path λ	50
4.2 Fitting data (compare.dat).....	55
4.3 Injection Function and FWHM (Full Width Half Maximum)	60
4.4 The simulation result for solar event on August 9, 2011	66
4.5 Relationship between solar cycle and galactic cosmic rays.....	67
CHAPTER V CONCLUSIONS.....	69

5.1 Discussion	69
5.2 Conclusion	70
5.3 Suggestion.....	71
REFERENCES.....	72
APPENDIX A:	74
APPENDIX B:	76
APPENDIX C:	78
BIOGRAPHY	80



List of tables

	Page
Table 1: Displays a research plan.....	4
Table 2: Classification of intensity of X-ray emission.....	11
Table 3: Description of each term of transport equation.....	23
Table 4: Physical characteristics of events on August 9, 2011.....	35
Table 5: Sample of data collected for Helium particle for all energy level.....	40
Table 6: Sample data collected for Helium particle at energy level 4.032 MeV/n....	41
Table 7: Sample of calculated values for Helium particle motion necessary for simulation.....	44
Table 8: Simulation results for He, C, N, O and Fe.....	66



List of figures

	Page
Figure 1: The structure of the Sun.....	5
Figure 2: Eruption of the Sun.....	9
Figure 3: Series of solar flares as detected by NOAA satellites in July 2000	11
Figure 4: Spherical Co-ordinates.....	15
Figure 5: Characteristics of the magnetic field that emits from the Sun in a spherical coordinate.....	16
Figure 6: Systematic flux conduction (left) and Random flux conduction (right)	19
Figure 7: Diagram displaying the pitch angle θ between the velocity of the particle and magnetic field line direction.....	20
Figure 8: Flow of particles through cells	24
Figure 9: Flow chart of research procedures.....	32
Figure 10: ACE (Advanced Composition Explorer) spacecraft	33
Figure 11: The flare as seen by the Solar Dynamic Observatory (SDO) at 8:05 UT in 304 angstrom light on august 9, 2011.....	36
Figure 12: Kp index on august 9, 2011 as detected by NOAA GOES satellite	37
Figure 13: The overview of the webpage to download data.....	37
Figure 14: Selecting data from the spacecraft.....	38
Figure 15: Data type selection.....	38
Figure 16: Choosing data on an event of interest.....	39
Figure 17 : Downloading data of high energy particles [He, C, N, O, and Fe]	39
Figure 18: Element selection for analysis.....	40
Figure 19: A sample of the particle distribution chart Helium at the energy level 4.032 MeV/n.	42
Figure 20: A sample of graph for Helium showing the relationship between momentum log values and spectrum spectra of events on August 9, 2011.	45
Figure 21: A sample graph of Helium particle at energy level 5.390 MeV/n showing relationship between Chi square and λ mean free path.	46

Figure 22: Sample graph of injection profile for Helium element at energy level 4.032 MeV/n.	47
Figure 23: Displaying best mean free path for corresponding minimum Chi square value for Helium particle at energy level (a) 4.032 MeV/n, (b) 5.390 MeV/n, (c) 6.685 MeV/n, and (d) 8.418 MeV/n.....	51
Figure 24: Displaying best mean free path for corresponding minimum Chi square value for Carbon particle at energy level (a) 7.443 MeV/n, (b) 9.839 MeV/n, (c) 12.267 MeV/n, and (d) 15.505 MeV/n.	52
Figure 25: Displaying best mean free path for corresponding minimum Chi square value for Nitrogen particle at energy level (a) 8.009 MeV/n, (b) 10.660 MeV/n, (c) 13.317 MeV/n, and (d) 16.854 MeV/n.	53
Figure 26: Displaying best mean free path for corresponding minimum Chi square value for Oxygen particle at energy level (a) 8.538 MeV/n, (b) 11.427 MeV/n, (c) 14.293 MeV/n, and (d) 18.104 MeV/n.	54
Figure 27: Displaying best mean free path for corresponding minimum Chi square value for Iron particle at energy level (a) 18.461 MeV/n, and (b) 30.902 MeV/n.....	55
Figure 28: Comparison of simulated data and spacecraft data for Helium particle at energy level (a) 4.032 MeV/n, (b) 5.390, (c) 6.685 MeV/n, and (d) 8.418 MeV/n. ...	56
Figure 29: Comparison of simulated data and spacecraft data for Carbon particle at energy level (a) 7.443 MeV/n, (b) 9.839 MeV/n, (c) 12.267 MeV/n, and (d) 15.505 MeV/n.	57
Figure 30: Comparison of simulated data and spacecraft data for Nitrogen particle at energy level (a) 8.009 MeV/n, (b) 10.660 MeV/n, (c) 13.317 MeV/n, and (d) 16.854 MeV/n.	58
Figure 31: Comparison of simulated data and spacecraft data for Oxygen particle at energy level (a) 8.538 MeV/n, (b) 11.427 MeV/n, (c) 14.293 MeV/n, and (d) 18.104 MeV/n.	59
Figure 32: Comparison of simulated data and spacecraft data for Iron particle at energy level (a) 18.461 MeV/n, and (b) 30.902 MeV/n.	60
Figure 33: Injection profile for Helium particle at energy level (a) 4.032 MeV/n, (b) 5.390, (c) 6.685 MeV/n, and (d) 8.418 MeV/n.	61
Figure 34: Injection profile for Carbon particle at energy level (a) 7.443 MeV/n, (b) 9.839 MeV/n, (c) 12.267 MeV/n, and (d) 15.505 MeV/n.....	62
Figure 35: Injection profile for Nitrogen particle at energy level (a) 8.009 MeV/n, (b) 10.660 MeV/n, (c) 13.317 MeV/n, and (d) 16.854 MeV/n.....	63

Figure 36: Injection profile for Oxygen particle at energy level (a) 8.538 MeV/n, (b) 11.427 MeV/n, (c) 14.293 MeV/n, and (d) 18.104 MeV/n.....	64
Figure 37: Injection profile for Iron particle at energy level (a) 18.461 MeV/n, and (b) 30.902 MeV/n.	65
Figure 38: Data collected by Inuvik Neutron monitor illustrating the relationship between sunspot number and neutron rate.....	67
Figure 39: Data collected (Corr Vs Time) for the duration of 216/2011 to 229/2011 from Princess Sirindhorn Neutron monitor, Thailand.	68
Figure 42: Displaying best mean free path for corresponding minimum Chi square value for Helium particle at energy level (e) 11.493 MeV/n, and (f) 15.623 MeV/n.	74
Figure 43: Displaying best mean free path for corresponding minimum Chi square value for Oxygen particle at energy level (e) 24.838 MeV/n, (f) 33.847 MeV/n, and (g) 49.832 MeV/n.	75
Figure 44: Comparison of simulated data and spacecraft data for Helium particle at energy level (e) 11.483 MeV/n, and (f) 15.623 MeV/n.....	76
Figure 45: Comparison of simulated data and spacecraft data for Oxygen particle at energy level (e) 24.838 MeV/n, (f) 33.847 MeV/n, and (g) 49.832 MeV/n.	77
Figure 46: Injection profile for Helium particle at energy level (e) 11.493 MeV/n, and 15.623 MeV/n.....	78
Figure 47: Injection profile for Oxygen particle at energy level (e) 24.838 MeV/n, (f) 33.847 MeV/n, and (g) 49.832 MeV/n.	79

CHAPTER I

INTRODUCTION

1.1 Importance and background of the research

The energy from our Sun plays an essential role in ensuring balanced survival of all living organism on Earth. However, every 11 year the Sun's activity will change with varying number of sunspots on its surface which is known as solar cycle. Solar flare is one such solar event and is defined as a sudden, rapid and intense variation in brightness and occurs when magnetic energy built up in the solar atmosphere is suddenly released (Paluk, Khumlumlert, Kanlayaprasit, & Aiemsa-ad, 2017).

Generally, they are classified into two types, impulsive flare and gradual flare. Impulsive flare causes rapid increasing of solar particle density in time whereas gradual flare causes the coronal mass ejection and shock wave in the interplanetary medium.

Solar flare occurs when the particles on the Sun outrun the tension of the magnetic field lines, which forces large amounts of high energy particles to the interplanetary medium in outward direction. The explosion would be more intense if at that time the release of material from the outermost atmosphere of the Sun, called the Coronal Mass Ejection (CMEs), causes the particles that leave the Sun to have more serious and able to move to Earth for a long time and multiply in the case of mass release of the Sun.

In this research, close investigative study is done in order to analyze solar flare at maximum of 24th solar cycle on August 9, 2011. We make use of data for solar flare from the SIS (Solar Isotope Spectrometer) instrument on the ACE (Advanced Composition Explorer) spacecraft. We then, simulate the motion of particles from the solar flare on precise date with the help of transport equation of Ruffolo (1995, 1998) solved by numerical technique of finite differential method. By using, compared fitting method of piecewise linear function between the data collected from spacecraft and simulation results, injection duration of particles from Sun to Earth is determined (Paluk et al., 2017).

The X-ray class of the selected solar event is X6.9, the solar flare position on the Sun is N18W68 and the solar wind speed is 551.5 kms^{-1} . This flare had the long

injection time from the Sun to the Earth corresponding to the shock wave detected after explosion in the interplanetary space 13 minutes.

The main objective of this thesis is to predict and prevent incidents due to a solar eruption that may affect the world in a timely manner by studying the time when high energy particles reach Earth after the Sun's eruption, and the intensity profile of solar energetic particle for each element at the maximum of this solar cycle.

1.2 Research objectives

- 1.1.1 To analyze the data collected by SIS instrument on ACE spacecraft which consist of particles flux and counts of different energy level.
- 1.1.2 To calculate the injection time for particles to travel from Sun to Earth due to eruption on Sun's surface using transport equation solved by numerical technique of finite different method.
- 1.1.3 To study the behavior of the movement of particles caused by the eruption of the Sun's surface.
- 1.1.4 To compare the injection time for particles to travel from the Sun to earth between simulated result and the actual values from the spacecraft.

1.3 Hypothesis of research

The hypothesis of our work are as follows:

- 1.3.1 If the magnetic field affects the movement of high energy particles then, the high energy particles from the Sun's eruption will move in a spiral direction along the magnetic field lines to Earth.
- 1.3.2 If the particle's energy affects the speed of the particles movement then, the particle with higher energy will reach Earth faster than particles with lower energy.
- 1.3.3 If the particles energy effects the particle count then, the particles with higher energy are less common than particles with lower energy.
- 1.3.4 If the highest solar flare occurs in maximum of every solar cycle, then prediction of next solar flare would be easier to compute.

1.4 Scope of research

- 1.4.1 Select an event of interest based on solar eruption and study its characteristics from the data as measured by SIS instrument on ACE spacecraft.
- 1.4.2 Simulate motion of particle with the transport equation of Ruffolo (1995, 1998) which is solved using numerical technique of finite difference method in C++ program.
- 1.4.3 Compare the injection time for particles to travel from the Sun to earth between simulated data and the spacecraft data.

1.5 Expected benefits

The results as obtained from these research plays an important role which are as discussed below:

- 1.5.1 To learn about physical characteristics of solar eruption resulting in the movement of high energy particle towards the Earth.
- 1.5.2 To understand and explain the movement of high energy particle by using transport equation solved by numerical technique of finite differential method.
- 1.5.3 To know the impact of SEP (Solar energetic particles) towards Earth due to eruption on the Sun.
- 1.5.4 To possess skill in computing physics problems related to particles motion due to solar activity on the Sun.

1.6 Purposes of the Study

The purpose of our work is to examine and analyze the intensity profile of solar energetic particle at the maximum of 24th solar cycle on August 09, 2011. The data of high energy particles and space environment is measured and collected by SIS instrument on the ACE spacecraft. We use C++ programming language to simulate the motion of particles from the solar flare with the help of transport equation and compute the injection time as well as mean free path of particles as release from the Sun to Earth (Ruffolo, 1994).

Thus, the above trial helps us in directing our main objective, which is to analyze the behavior of the movement of particles as caused by the solar flare during its event. These studies will help us to predict and prevent future incidents due to a

solar eruption that may affect our world in a timely manner by reviewing the time when high energy particles reach Earth after the Sun's eruption.

1.7 Research Plan

The table below gives the brief description of our research plan which we intend to finish within the time frame as stated by university.

Table 1: Displays a research plan

Activities	Time (months)																	
	1	2	3	4	5	6	7	8	9	10	11	12	13	14	15	16	17	18
1. Study background of the thesis and selection of topic.	█	█	█	█	█	█	█											
2. Study of research related to the movement of high energy particles from the Sun and changes that occur in the solar cycle.					█	█	█	█	█									
3. Simulate the transport of particles and fitting the data in C language on the Ubuntu operating system.						█	█	█	█	█	█							
4. Analyze the data obtained from simulations and actual data from spacecraft.										█	█	█	█					
5. Summary, analyze the findings and write a book.													█	█	█	█	█	█

CHAPTER II

LITERATURE REVIEW

2.1 The Structure of Sun

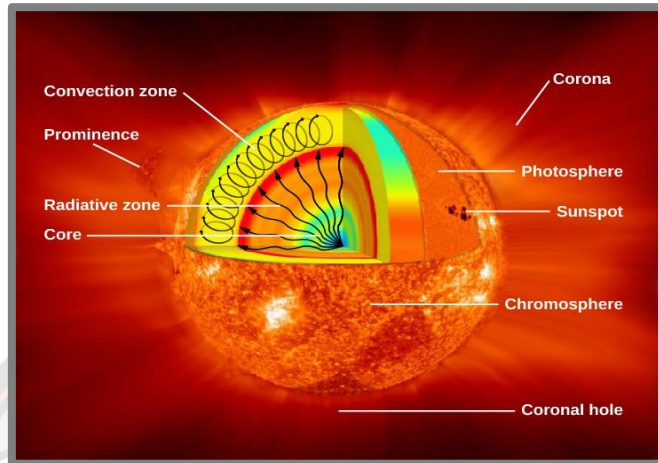


Figure 1: The structure of the Sun

Source: https://www.nasa.gov/mission_pages/sunearth/science/solar-anatomy.html

The Sun, located at the heart of our solar system is about 1.39×10^6 km in its diameter has a mass of 1.9884×10^{30} kg. It is composed mostly of hydrogen (~73%), helium (~25%) and some other elements in small quantities such as oxygen, carbon, iron, etc. It is theorized that our Sun was formed 4.6×10^9 years ago with the collapse of matter of large molecular cloud due to gravity. Most of the matter were accumulated at the center and the rest of which was flattened into orbiting disk which we now call “Solar System”. The accumulated matter became hot and dense resulting into nuclear fusion within its core. Thus, our Sun was born (Wikipedia contributors, 2021, February 27). The structure of the Sun consists of two parts which are as discussed below:

2.1.1 Internal structure of the Sun

Internal structure of the Sun consists of following layers:

- Core

The core is the only region in the Sun that produces a massive amount of thermal energy via fusion of four free protons of hydrogen nuclei to produce a single alpha particle known as p-p chain nuclear reaction. It is about 20-25% of the solar radius and has a temperature approximately about 1.57×10^7 K. The energy produced in the core

transfers outward to other parts of Sun through successive layers and escapes into space through radiation (photons) or advection (massive particles) (Wikipedia contributors, 2021, February 27).

- **Radiative zone**

The Radiative zone starts at about 25% of the distance to the solar surface and extends up to about 70% of the way to the surface. In this layer the energy in the form of photon (electromagnetic radiation), is mainly transported toward the exterior by radiative diffusion, rather than by convection. Due to dense matter in this region, photon travels a short distance before they are absorbed or scattered by another particle and shifts to longer wavelength as they do so. Thus, it takes an average of 1.71×10^5 years for gamma rays from the core of the Sun to leave the radiation zone. The temperature of the plasma drops from 1.5×10^7 K near the core down to 1.5×10^6 K at the base of the convection zone (Wikipedia contributors, 2021, January 4).

- **Convective zone**

Extending from 0.7 solar radii (5×10^5 km) to near its surface is Sun's convection zone where plasma is not so dense and hot enough to transfer the heat energy of the interior outward via radiation. Thus, convective currents develop and plays a role in moving the Sun's energy outward to its surface.

When the matter cools just beneath the surface of Photosphere, the density increases and moves to base of convection zone which again gets heated up due to radiative zone and the convection cycle continues (Wikipedia contributors, 2021, February 27).

2.1.2 The atmosphere of Sun

The atmosphere of the Sun is composed of several layers, mainly the photosphere, the chromosphere and the corona.

- **Photosphere**

The layer of the Photosphere is about 500km thick and it is the lowest layer of Sun's atmosphere. The photosphere is marked by bright, bubbling granules of plasma and darker, cooler sunspots, which emerge when the Sun's magnetic field breaks

through the surface. Sunspots appear to move across the Sun's disk. Observing this motion led astronomers to realize that the Sun rotates on its axis. Since, the Sun is a ball of gas with no solid form, different regions rotate at different rates. The Sun's equatorial regions rotate in about 24 days, while the polar regions take more than 30 days to make a complete rotation. The photosphere is also the source of solar flares that extend hundreds of thousands of miles above the Sun's surface. Solar flares produce bursts of X-rays, ultraviolet radiation, electromagnetic radiation and radio waves (Sharp, 2017, November 2).

- **Chromosphere**

The chromosphere emits a reddish glow as super-heated hydrogen burns off. but the red rim can only be seen during a total solar eclipse. At other times, light from the chromosphere is usually too weak to be seen against the brighter photosphere. The chromosphere plays a role in conducting heat from the interior of the Sun to its outermost layer, the corona (Sharp, 2017, November 2).

- **Corona**

The third layer of the Sun's atmosphere is the corona. It can only be seen during a total solar eclipse as well. It appears as white streamers or plumes of ionized gas that flow outward into space. Temperature in the Sun's corona can get as high as 3.5×10^6 °F. As the gases cool, they become the solar wind (Sharp, 2017, November 2).

2.2 Solar Cycle

The solar cycle is a nearly periodic 11-year change in the Sun's activity measured in terms of variations in the number of observed sunspots on the solar surface. Levels of solar radiation and ejection of solar material, the number and size of sunspots, solar flares, and coronal loops all exhibit a synchronized fluctuation, from active to quiet and quite to active again, within a period of 11 years.

The sunspots were shown to increase and decrease over time in a regular, approximately 11-year cycle. Although, the exact length of the Solar cycle may vary but sunspots always increase over time and then returns to low again. More the number

of sunspots, more the increased in solar activity where great blooms of radiation known as solar flares or bursts of solar material known as coronal mass ejections (CMEs) shoot off the Sun's surface.

The highest number of sunspots in any given cycle is known as “solar maximum”, while the lowest number is known as “solar minimum”. Each cycle varies dramatically in its intensity with some solar maxima being so low as to be almost indistinguishable from the preceding minimum.

Scientists suggest that the magnetic material inside the Sun is constantly stretching, twisting, and crossing as it rises up to the surface which causes solar cycle. The precise pattern of movements is not mapped out but over time they ultimately lead to the poles reversing completely where north becomes south and south becomes north approximately every 11 years. Some 11 years later, the poles reverse again back to where they started, making the full solar cycle actually a 22-year phenomenon. The Sun then again behaves similarly over the course of each 11-year cycle no matter which pole is on top.

Understanding and predicting the Sunspot cycle remains one of the grand challenges in astrophysics with major consequences for space science and the understanding of certain phenomena elsewhere in the Universe (Fox, 2011; Wikipedia contributors, 2021, January 11).

2.3 Solar flare

A flare is defined as a sudden, rapid and intense variation in brightness of the Sun. The first ever solar flare was recorded on September 1, 1859 by two scientists, Richard C. Carrington and Richard Hodgson, who were observing sunspots at the same time but, independently. The example of solar flare is as displayed in the Figure 2.

The amount of energy released is very large which is comparable to millions of 100-megaton hydrogen bombs exploding at the same time. It is released in the form of almost all electromagnetic waves, such as gamma rays, x-rays, radio waves, etc. Flare occurs when magnetic energy that has built up in the solar atmosphere is suddenly released and the particles including electrons, protons, and heavy nuclei are heated and accelerated in the solar atmosphere. The measured energy released during a flare is typically on the order of 10^{27} ergs per second.

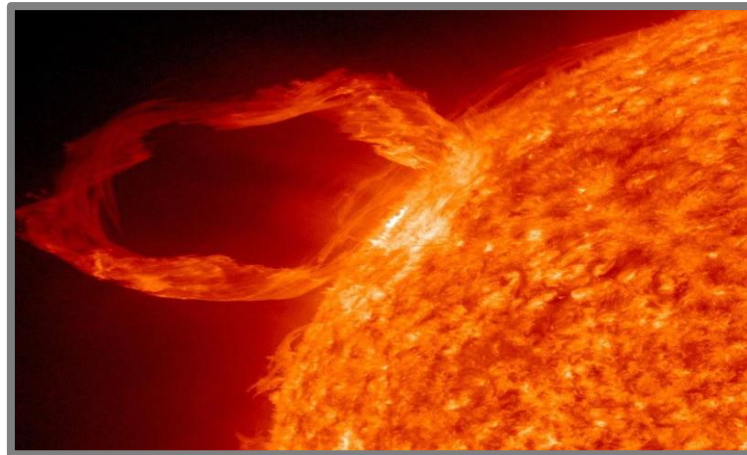


Figure 2: Eruption of the Sun

Source: <https://pixabay.com/photos/solar-flare-sunlight-eruption-978/>

There are typically three stages to a solar flare.

- Precursor stage is the first stage of solar flare where the release of magnetic energy is triggered. Usually Soft x-ray emission is detected in this stage.
- In the second stage known as impulsive stage, protons and electrons are accelerated to energies exceeding 1 MeV. During the impulsive stage, radio waves, hard x-rays, and gamma rays are emitted.
- Decay stage is where the gradual builds up and decay of soft x-rays can be detected. The duration of these stages can be as short as a few seconds or as long as an hour.

Solar flares extend out to the layer of the Sun called the corona which is the outermost atmosphere of the Sun. Inside a flare, the temperature typically reaches $\sim 2 \times 10^7$ K and can be as high as $\sim 1 \times 10^8$ K. It usually happens in the active regions where sunspots are located and the frequency of flares coincides with the Sun's eleven-year cycle. When the solar cycle is at a minimum, active regions are small and rare and few solar flares are detected.

Specialized scientific instruments are used to detect the radiation signatures emitted during a flare. The radio and optical emissions from flares can be observed with telescopes on the Earth. Energetic emissions such as x-rays and gamma rays require telescopes located in space, since these emissions do not penetrate the Earth's atmosphere ("What is a Solar flare?," n.d.).

The eruptions on the Sun are divided into two types, impulsive solar flare and gradual solar flares. Both types of eruptions are violent but the number of particles is released differently. The classification of eruptions can be analyzed based on physical characteristics.

2.3.1 Impulsive solar flares

It is the sudden outburst is an eruption that releases a high number of electron particles and energy within short period of time (less than 1 hour). The density of the particles over time increases rapidly. When these particles move through the space, the increase in the Fe/O and $3\text{He}/4\text{He}$ ratios are 4 times, to the value found in the corona. It is found that there is no release of coronal mass (Coronal Mass Ejection) after the eruption. The solar wind has a normal speed and no shock wave phenomenon are detected.

2.3.2 Gradual solar flares

It is an eruption that releases a high number of energy particles which include many protons. This kind of eruption causes accelerating particles in the interplanetary medium, known as CMEs (coronal Mass Ejection). The solar wind is faster and more normal than the solar storm. The gradation will take more than 1 hour to release the particles.

2.4 Classification of X-rays

We can find out whether there is explosion on Sun by observing the amount of X – ray intensity generated, as shown in Figure 3.

Classification of solar flares are done based on their X-ray brightness in the wavelength ranging from 1 to 8 Angstroms. The X-rays are bright at wavelengths in the range 1 to 8 Angstroms and are divided into 5 levels, A, B, C, M, and X which can be measured near the Earth by the GOES (The Geostationary Operational Environmental Satellite System) spacecraft.

X-class flares are high intensity solar flare which can trigger planet-wide radio blackouts and long-lasting radiation storms. M-class flares are medium-sized, they can cause brief radio blackouts that affect Earth's polar regions.

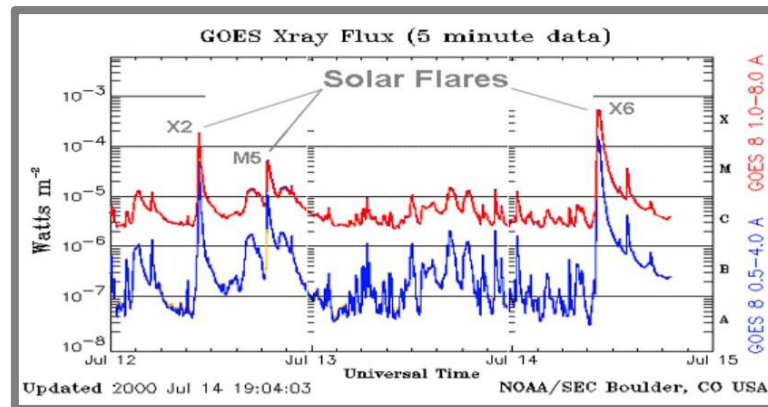


Figure 3: Series of solar flares as detected by NOAA satellites in July 2000

Source: <https://spaceweather.com/glossary/flareclasses.html>

Minor radiation storms sometimes follow an M-class flare. Compared to X-class and M-class events, C-class flares are small with few noticeable consequences here on Earth. A-class and B-class, solar flare also have low level of intensity which has very little effect on Earth. Each category for X-ray flares has further nine subdivisions ranging from, A1 to A9, B1 to B9, C1 to C9, M1 to M9 and X1 to X9 ("The Classification of X-ray Solar Flares," n.d.; "The glare of the Sun (Solar Flares)," n.d.).

Table 2: Classification of intensity of X-ray emission

X-ray class of solar flare	Intensity (Wm^{-2}) of X-rays
A	$10^{-8} - 10^{-7}$
B	$10^{-7} - 10^{-6}$
C	$10^{-6} - 10^{-5}$
M	$10^{-5} - 10^{-4}$
X	$> 10^{-4}$

2.5 Solar Energetic Particles (SEPs)

Solar energetic particles (SEPs) is defined as the high-energy particles from the Sun, such as ion, proton or electron which emits out by various mechanisms such as plasma heating, acceleration etc. They are one of the important phenomena associated with the solar eruptions, e.g., solar flares, filament eruptions, coronal mass ejections

(CMEs), etc. Its intensity depends upon CME speed and magnetic connectivity to Earth ("Solar energetic particles : SEPs," n.d.).

SEP was first detected in 1942 by Geiger counters and other detectors created to measure cosmic rays which frequently observed rapid increase in the radiation associated with solar flares. It was concluded that the cosmic ray intensity returned to normal within minutes or hours, as the acceleration process of ion ends.

The solar-produced ions have relatively low energies, generally below 1 GeV and rarely above 10 GeV which is why such events are often missed by cosmic ray detectors near the equator. The lowest energetic particles are excluded by the Earth's magnetic field and thus, the best detectors for observing solar particles are therefore those sensitive to the lowest energies of the cosmic radiation. In many events the Sun emits enormous numbers of lower-energy ions, with no more than tens of MeV. The Earth's magnetic field diverts them to the vicinity of the magnetic poles, where they may temporarily smother the ionosphere and interfere with radio communications (Space weather prediction center, n.d.).

The particles of each energy level that are emitted by Sun will be detected and measured by ground-based measuring devices such as neutron monitors, muon monitors or by space satellites such as ACE and GOES Ulysses spacecraft. These satellites will measure the varying physical quantities change over time, such as the number of particles, intensity and the direction of the magnetic field within space between planets and can compute density, temperature, speed, etc.

The study will help us to simulate using basic data and will guide to predict and prevent the possible phenomena that are harmful to us. It will also help us to protect our scientific equipment and especially, the readiness of astronauts working in space ("Solar energetic particles : SEPs," n.d.)

2.6 Coronal Mass Ejection (CME)

Coronal Mass Ejection (CME) are large ejections of plasma and magnetic field from the Sun's corona that expels out billions of tons of coronal material as shown in Figure 2. It usually occurs after the solar flare. They can carry an embedded magnetic field (frozen in flux) that is stronger than the background solar wind interplanetary magnetic field (IMF) strength. The speeds of CMEs ranges from 250 kms^{-1} to

3000 kms^{-1} and expands in size as they propagate away from Sun. It only takes about 15 – 18 hours for the fastest CMEs to reach our planet whereas several days for slower CMEs.

Basically, the explosive CMEs begins when highly twisted magnetic field structures contained in the Sun's lower corona become too stressed and realign themselves into a less tense configuration, known as, "magnetic reconnection". This type of CMEs generally take place from areas of the Sun with localized fields of strong and stressed magnetic flux, such as active regions of sunspot groups. CMEs can also occur from locations where relatively cool and denser plasma is trapped and is suspended by magnetic flux extending up to the inner corona, filaments and prominences. When these flux ropes resets, the denser filament or prominence can collapse back to the solar surface and be quietly reabsorbed, or else CME may result. When CMEs travel faster than the background solar wind speed, it can generate a shock wave. These shock waves can accelerate charged particles ahead of them which causes increased radiation storm potential or intensity.

Important CME parameters used in analysis are size, speed, and direction. These properties are inferred from orbital satellite's coronagraph imagery by SWPC forecasters to determine any Earth-impact likelihood (Space weather prediction center, n.d.).

2.7 Solar wind

Solar wind is a high-speed particle that is emitted from the Sun in all directions at all times or may be seen as a particle coming out of the Sun's corona, which has high temperatures. The solar wind is caused by the expansion of the Sun's corona with very high heat energy. The expanding takes places until the particles such as electrons and protons escape the gravitational pull of the Sun and drives away in all direction covering the entire solar system.

This phenomenon occurs at the north and south poles of the Sun which has a large corona cavity. Corona cavity is the certain portion of the Sun where high-speed and intense solar wind blows out of the Sun. Usually, the solar wind that occurs the Sun's equator will have a lower velocity. The calculated, average velocity is about 450 kms^{-1} and accelerates to about 800 kms^{-1} . When the particles are several times

more powerful than normal, they will become solar storm (Gordan D, 2006; "The Solar Wind," n.d.).

The solar wind has a great influence on the planet especially during periods of active Sun or Sunspot maximum. When the solar wind is very strong, it can erupt into flares and coronal mass ejections. The solar wind also affects the Earth's ionosphere by disturbing Earth's magnetic field, aurora and communication systems. For example, a particle eruption from the CME at SOHO (Solar and Heliospheric Observatory) detected 5 days before the danger to the communications satellite Telstar 401 on January 11, 1997.

The solar wind changes the shape of the Earth's magnetic field and the warping (Fluctuation) of the speed, density, direction, etc., of the solar wind also affects the space environment. For example, the shape and position of the Magnetopause and the bow shock will be changed at different world radius levels. These phenomena are collectively referred to as space weather.

The Sun normally releases supersonic particles, which are called solar wind, and because the interior of the Sun's atmosphere consists of high-energy charged particles they are in the fourth state of the substance named, Plasma. The movement of charged particles within the Sun's atmosphere creates a magnetic field which would produce a turbulent magnetic field. Therefore, the solar magnetic field line sometimes has a chance to collide until the phenomena related to magnetic fields such as flare, coronal mass ejections, etc. (Earl, Ruffolo, Pauls, & Bieber, 1995; Wikipedia contributors, 2020, March 11).

2.8 Archimedean spiral magnetic field

The Sun revolves around on its own axis and the charge particles moves along the magnetic field drawn from the Sun by solar wind. The magnetic field worn outward from the Sun in all direction and twisted into a spiral shape is known as "Archimedean spiral". Let us consider magnetic field line in the spherical coordinates along the radius of magnetic field as shown in the Figure 4.

The equation (2.1) and equation (2.2) given below describes the particles moving in the direction parallel to the direction of the magnetic field.

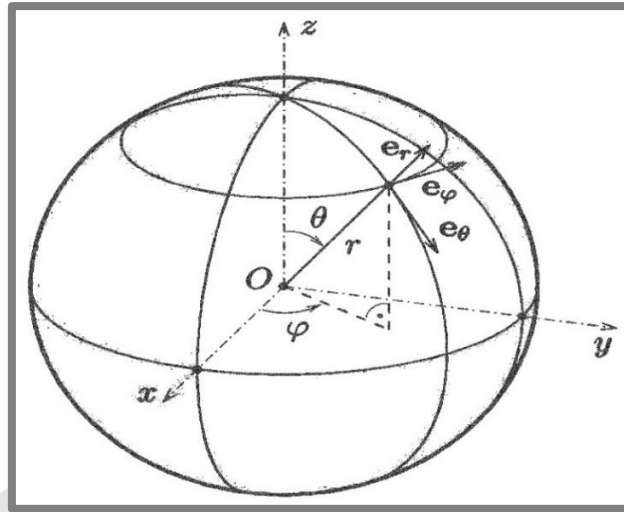


Figure 4: Spherical Co-ordinates

$$\vec{dl} \times \vec{B} = 0 \quad (2.1)$$

$$\vec{\nabla} \times \vec{B} = 0 \quad (2.2)$$

where, \vec{dl} is a spherical coordinate and \vec{B} is a magnetic field with zero electric force.

From the equation (2.1) when considering the magnetic field of the Sun in the spherical coordinates as shown in Figure 5, we obtain:

$$d\vec{l} = dr\hat{e}_r + r d\theta\hat{e}_\theta + r \sin\theta d\phi\hat{e}_\phi$$

$$\vec{B}(r, \theta, \phi) = B_r\hat{e}_r + B_\theta\hat{e}_\theta + B_\phi\hat{e}_\phi$$

$$d\vec{l} \times \vec{B} = 0 = (rd\theta B_\phi - B_\theta r \sin\theta d\phi)\hat{e}_r + (B_r r \sin\theta d\phi - B_\phi dr)\hat{e}_\theta + (B_\theta dr - B_r r d\theta)\hat{e}_\phi$$

Let us consider the magnetic field element radius:

$$rd\theta B_\phi = B_\theta r \sin\theta d\phi$$

$$\frac{rd\theta}{B_\theta} = \frac{r \sin\theta d\phi}{B_\phi} \quad (2.3)$$

Considering the magnetic field element:

$$B_r r \sin\theta d\phi = B_\phi dr$$

$$\frac{r \sin\theta d\phi}{B_\phi} = \frac{dr}{B_r} \quad (2.4)$$

Equating equation (2.3) and equation (2.4) we get:

$$\frac{dr}{B_r} = \frac{rd\theta}{B_\theta} = \frac{r \sin \theta d\phi}{B_\phi} \quad (2.5)$$

Now, we will determine the rate of change of the angle ' φ ' and the radius ' r ' of the magnetic field that is emitted from the Sun.

As shown in Figure 5, let us consider Sun revolving around its own axis having angular velocity (Ω) which is associated to the angle (φ) and let the magnetic field act at radius (r) from the Sun. Thus, the angular displacement per unit time is given by:

$$\Omega = \frac{\phi_0 - \phi}{t - t_0} = -\frac{|\Delta\phi|}{\Delta t} \quad (2.6)$$

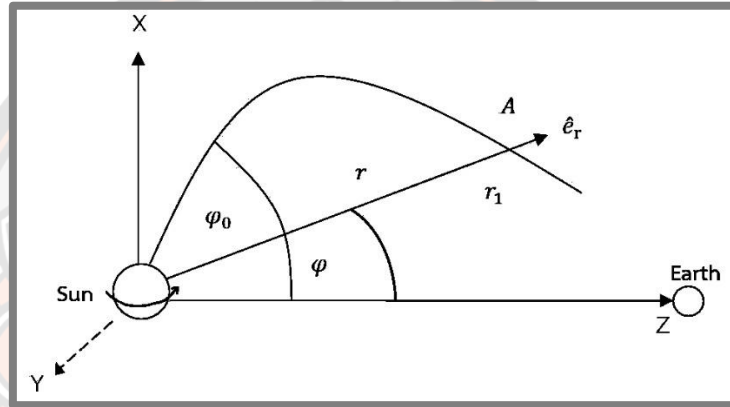


Figure 5: Characteristics of the magnetic field that emits from the Sun in a spherical coordinate

The quantity $-|\Delta\phi|$ indicates that if the value of φ is large it will take less time and if the value of φ is small it will take more time.

Where;

$$\begin{aligned} \Delta\phi &= \phi - \phi_0 \\ \Delta t &= t - t_0 \end{aligned} \quad (2.7)$$

Now, considering the radius of the particles moving in accordance to the solar wind speed we have:

$$\begin{aligned} r &= v_{sw} t \\ \frac{dr}{dt} &= v_{sw} \\ r - r_0 &= v_{sw}(t - t_0) \\ \Delta r &= v_{sw} \Delta t \end{aligned} \quad (2.8)$$

Substituting, Δt from equation (2.7) into equation (2.8) we obtain:

$$\begin{aligned}\Delta r &= v_{sw} \frac{\varphi_0 - \varphi}{\Omega} \\ \frac{\Delta r}{\Delta \varphi} &= -\frac{v_{sw}}{\Omega} \\ \frac{dr}{d\varphi} &= -\frac{v_{sw}}{\Omega}\end{aligned}\quad (2.9)$$

where;

φ is the angle that the magnetic field interacts with the radius when time t at position r_1 (rad).

φ_0 is the angle that the magnetic field acts on the radius of the initial time t_0 (rad).

r is the distance from the Sun to point A (m).

v_{sw} is the speed of the solar wind (m/s).

Ω is the angular velocity of the Sun's rotation ($= 2.7 \times 10^{-6} \text{ rads}^{-1}$)

The relation of $\vec{B}(r, \theta, \varphi)$ for various elements is given by the following equation:

$$\begin{aligned}B_r(r, \theta, \varphi) &= B_r(r, \theta, \varphi) \\ B_\theta(r, \theta, \varphi) &= 0\end{aligned}\quad (2.10)$$

$$B_\varphi(r, \theta, \varphi) = r \sin \theta \frac{d\varphi}{dr} B_r(r, \theta, \varphi)$$

The divergence of the vector field in the spherical coordinate system is given by:

$$\frac{1}{r^2} \frac{\partial r^2}{\partial r} B_r - \frac{1}{r \sin \theta} \frac{\partial}{\partial \theta} \sin \theta B_\theta + \frac{1}{r \sin \theta} \frac{\partial B_\varphi}{\partial \varphi} = 0 \quad (2.11)$$

From the above condition, $B_\theta = 0$ and substituting B_φ from equation (2.10) into (2.11) we get;

$$\begin{aligned}\frac{1}{r^2} \frac{\partial r^2}{\partial r} B_r - \frac{1}{r \sin \theta} \frac{\partial}{\partial \varphi} \left(\frac{\Omega}{v_{sw}} r \sin \theta B_r \right) &= 0 \\ \frac{1}{r^2} \frac{\partial r^2}{\partial r} B_r - \left(\frac{\Omega}{v_{sw}} \right) \frac{\partial B_r}{\partial \varphi} &= 0\end{aligned}\quad (2.12)$$

From the equation (2.12) we get B_r independent of φ and value of $r^2 B_r$ is constant and do not depend on r but depend on θ therefore,

$$B_r = \frac{A(\theta)}{r^2} \quad (2.13)$$

Let us consider r_1 is a magnetic reference point $B_r = B_1$, so

$$A(\theta) = B_1 r_1^2$$

Substituting $A(\theta)$ into the equation (2.8.13), we get;

$$B_r = \frac{B_1 r_1^2}{r^2} \quad (2.14)$$

By substituting:

$$\vec{B}(r, \theta, \varphi) = \frac{B_1 r_1^2}{r^2} \left(\hat{e}_r - \frac{\Omega}{v_{sw}} r \sin \theta \hat{e}_\varphi \right) \quad (2.15)$$

The above equation plays an important role in describing the characteristics of the magnetic field that exists in spherical coordinate.

2.9 Transport Equation

The high energy particles propagating from Sun to Earth are charged and neutral particles. In describing the motion of particles in space that are moving along a magnetic field line that is not smooth or has variability can be explained from the diffusion-conduction equation. Let us consider the distribution of particles in one dimension.

Mathematically;

$$f(x, t) = \frac{dN}{dx}$$

$$dN = f(x, t) dx \quad (2.16)$$

Where, N is the number of particles in the cell. Let, S be flux and is defined as, number of particles (N) moving through a point at unit time t . Mathematically;

$$S = \frac{N}{\Delta t} \quad (2.17)$$

Substituting, equation (2.16) in equation (2.17), we obtain:

$$S = v f(x, t) \quad (2.18)$$

We have;

$$N = f(x, t) \Delta x \quad (2.19)$$

As the particles moves through the cell in the x-direction, the relationships between equation (2.18) and equation (2.19) can be written as:

$$\frac{\partial}{\partial t}(f \cdot \Delta x) = S\left(x - \frac{\Delta x}{2}\right) - S\left(x + \frac{\Delta x}{2}\right)$$

As, $\Delta x \rightarrow 0$

$$\frac{\partial f(x, t)}{\partial t} = -\frac{\partial S(x, t)}{\partial x} \quad (2.20)$$

The distribution of particles over time consists of systematic processes and random processes. The systematic process is when the particles moves in the cell, in the same direction and at the same speed as shown in the Figure 6 (left).

Mathematically, the systematic or convective change is:

$$S(x, t)_{\text{convective}} = \left(\frac{\Delta x}{\Delta t}\right) f(x, t) \quad (2.21)$$

Random changes are the particles moving randomly or disordered manner as shown in the Figure 6 (right).

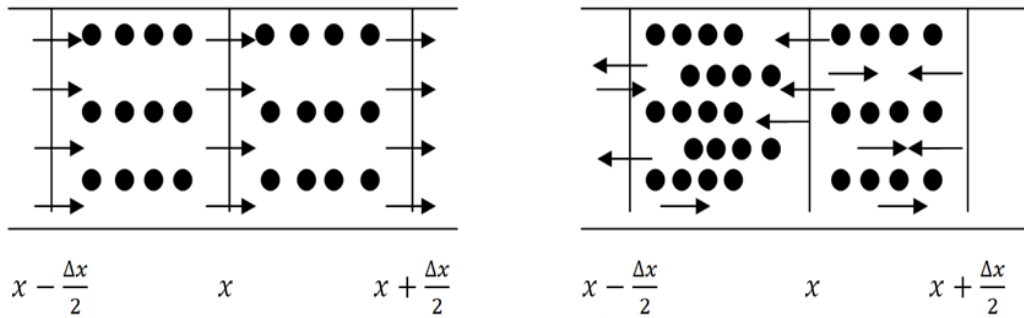


Figure 6: Systematic flux conduction (left) and Random flux conduction (right)

$$S(x, t)_{\text{diffusive}} \propto -\left(\frac{\partial f(x, t)}{\partial x}\right) \quad (2.22)$$

$$\therefore S(x, t)_{\text{diffusive}} = -D \left(\frac{\partial f(x, t)}{\partial x}\right) \quad (2.23)$$

Substituting equations (2.21) and equation (2.23) in equation (2.20), we obtain:

$$\frac{\partial f(x, t)}{\partial t} = -\frac{\partial}{\partial x} \left[\frac{\Delta x}{\Delta t} f(x, t) \right] + \frac{\partial}{\partial x} \left[D \frac{\partial f(x, t)}{\partial x} \right] \quad (2.24)$$

Systematic first order Random process of diffusion second order term

The motion of particles that decay over time can be explained by the diffusion equation, which has the form of partial differential equation as follows:

$$D \frac{\partial^2 F}{\partial x^2} - \frac{\partial F}{\partial t} = 0 \quad (2.25)$$

where; D is the diffusion coefficient, ∂t is the time period in which the particles move through the distance ∂x , $\frac{\partial^2 F}{\partial x^2}$ is the flux of particles per unit volume that flows through the phase ∂x and $\frac{\partial F}{\partial t}$ is the distribution of particles over time consisting of systemic change and random change. The motion of particles is simulated using Fokker-planck equation, based on the time particle distribution equation. It was developed by Ruffolo (1998), an equation describing the transport of high energy particles from the Sun.

$$\frac{\partial F}{\partial t} + \frac{\partial(\dot{a}_i F)}{\partial a_i} = Q \quad (2.26)$$

where, Q is the particle release function (source term), F is the particle diffusion function (distribution function), $\frac{\partial F}{\partial t}$ is the distribution of the flux of particles over time, a_i are parameters of various independent variables related to movement or independent variables in terms $t, \mu, z, \text{ and } p$. Here, t is the time the particle to travel from the Sun to the earth (seconds), μ is the direction of the movement of the particles moving in or out of the Sun, z is the distance along the magnetic field from the Sun to the earth (AU) and p is the momentum of the particle (MeV/c).

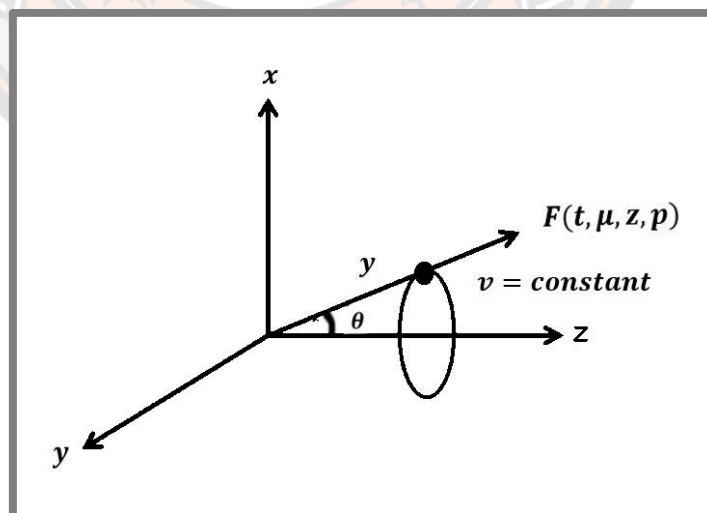


Figure 7: Diagram displaying the pitch angle θ between the velocity of the particle and magnetic field line direction

From Figure 7, when considering independent variables that affect the motion of high energy particles from the Sun, it can be seen that high energetic particles are charged particles. Therefore, the motion of particles moves along the magnetic field lines at the speed \vec{v} .

Considering the independent variables in terms of systemic change, the changed variables can be as follows:

- i. Change of distance along the magnetic field lines in the z-axis
- ii. Change of momentum
- iii. The change of μ , where μ is a variable that shows the direction of particle motion.

We know; $\mu = \cos \theta$; θ is the angle between the velocity v of the particle and the direction of the magnetic field which is also known as spiral phase.

When;

$\theta > 90^\circ, \mu < 0$ the particles move towards the Sun.

$\theta < 90^\circ, \mu > 0$ the particles will move out of the Sun.

Since, the magnetic field lines on the Sun fluctuates due to solar wind, we consider the independent variables of particle motion in terms of random changes. Independent variables in terms of random changes are changes in μ along the line of the magnetic field that has fluctuations and the density of the particles in the distance along the magnetic field lines in the z – axis with the speed v . When considering various independent variables, it follows that the equation is:

$$\frac{\partial F(t, \mu, z, p)}{\partial t} = -\frac{\partial}{\partial z} \left(\frac{\Delta z}{\Delta t} F \right) - \frac{\partial}{\partial \mu} \left(\frac{\Delta \mu}{\Delta t} F \right) - \frac{\partial}{\partial p} \left(\frac{\Delta p}{\Delta t} F \right) + \frac{\partial}{\partial \mu} \left[\frac{\varphi \mu}{2} \frac{\partial}{\partial \mu} \left(\frac{E'}{E} F \right) \right] \quad (2.27)$$

We will have to consider fixed frame, solar wind frame and mixed frame in above equation. The ratio of particles from the solar wind frame to the stationary frame is given by:

$$\frac{E'}{E} = \frac{1 - (\mu v v_{sw} \sec \Psi)}{c^2} \quad (2.28)$$

We know, flux of particles is given by:

$$F(t, \mu, z, p) = \frac{d^3 N}{dz d\mu dp}$$

Where, $F(t, \mu, z, p)$ is the dispersing function of high-energy particles that are released from the sun's eruption, z is the distance that particles travel along the magnetic field line to Earth (AU), p is the momentum of a particle (MeV/c), μ is the direction of movement of the particles, t is the time when particles move from the Sun to the Earth (min) and N is the number of particles.

Simulating the movement of high energy particles using plankton plank and various factors of solar activity such as change in magnetic fluxes and solar wind will give us transport equation. (Ruffolo, 1994; Ruffolo, Khumlumlert, & Youngdee, 1998).

Thus, the transport equation is:

$$\begin{aligned}
 \frac{\partial \vec{F}(t, \mu, z, p)}{\partial t} = & -\frac{\partial}{\partial z} \mu v \vec{F}(t, \mu, z, p) && \text{(streaming)} \\
 & -\frac{\partial}{\partial z} (1 - \mu^2 \frac{v^2}{c^2}) v_{sw} \sec \Psi \vec{F}(t, \mu, z, p) && \text{(convection)} \\
 & -\frac{\partial}{\partial \mu} \frac{v}{2L(z)} \left[1 + \mu \frac{v_{sw}}{v} \sec \Psi - \mu \frac{v_{sw} v}{c^2} \sec \Psi \right] (1 - \mu^2) \vec{F}(t, \mu, z, p) && \text{(focusing)} \\
 & + \frac{\partial}{\partial \mu} v_{sw} (\cos \Psi \frac{d}{dr} \sec \Psi) \mu (1 - \mu^2) \vec{F}(t, \mu, z, p) && \text{(differential convection)} \\
 & + \frac{\partial}{\partial \mu} \frac{\phi(\mu)}{2} \frac{\partial}{\partial \mu} (1 - \mu \frac{v_{sw} v}{c^2} \sec \Psi) \vec{F}(t, \mu, z, p) && \text{(scattering)} \\
 & + \frac{\partial}{\partial p} p v_{sw} \left[\frac{\sec \Psi}{2L(z)} (1 - \mu^2) + \cos \Psi \frac{d}{dr} (\sec \Psi) \mu^2 \right] \vec{F}(t, \mu, z, p) && \text{(deceleration)}
 \end{aligned}$$

where; F is the distribution function; $\vec{F}(t, \mu, z, p) = \frac{d^3 N}{dz d\mu dp}$, θ is the pitch angle, μ is the cosine of pitch angle, v_{sw} is the solar wind speed, Ψ is the angle between \hat{r} and \hat{z} , c is the light speed, v is the particle speed (km/s), $\phi(\mu)$ is the scattering coefficient and p is the momentum of particle.

The table below explains the meaning of each term in brief:

Table 3: Description of each term of transport equation

Terms	Descriptions
1. Streaming	It describes the motion of particles along the magnetic field lines in the z-axis.
2. Convection	It describes the movement of particles along the magnetic field lines caused by solar convection.
3. Focusing	It describes the movement of particles resulting from the adiabatic focusing considered in the stationary reference frame and the frame of the solar wind.
4. Differential convection	It shows the change in solar velocity by position. By considering the rate of change μ with respect to time t in the frame of the solar wind which has no effect on focussing.
5. Scattering	It is a term that shows the scattering of particles in the framework of the solar wind in random changes.
6. Deceleration	It is a term for the rate of change of momentum that depends on the rate of change of velocity along the line of the magnetic field in the frame of the solar wind.

2.10 Numerical methods used in research operations

The transport equation is in the form of a partial differential equation (PDE) consisting many independent variables (Ruffolo, 1994; Ruffolo et al., 1998). Thus, this makes us hard to determine its solution directly. However, as the equation is in the form of PDE we will have the boundary condition where we can apply the finite difference method and determine its solution. There are three methods of finding such solutions as follows:

2.10.1 Explicit method

2.10.2 Implicit method and

2.10.3 Crank-Nicholson method.

From the particle diffusion equation when $f(x_i, t_n)$.

$$\frac{\partial f}{\partial t} = -\frac{\partial S}{\partial x} \quad (2.29)$$

where;

$$S = -D \frac{\partial f}{\partial x} \quad (2.30)$$

Substituting equation (2.30) into the equation (2.29) we obtain:

$$\frac{\partial f}{\partial t} = -\frac{\partial}{\partial x} \left(-D \frac{\partial f}{\partial x} \right) = D \frac{\partial^2 f}{\partial^2 x}$$

where;

S is a flux or number of particles moving through a point in time t

f is the particle flux

D is the coefficient of diffusion

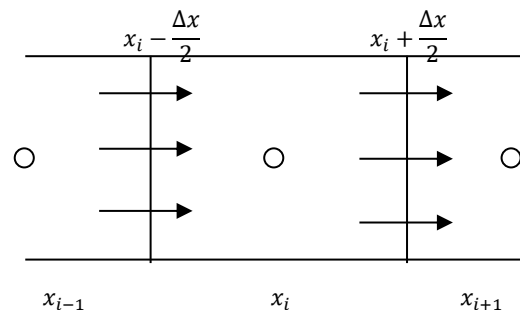


Figure 8: Flow of particles through cells

we know:

Net number of particles = inflow particles – outflow particles

$$\frac{\partial}{\partial t}(f \cdot \Delta x) = s\left(x_i - \frac{\Delta x}{2}\right) - s\left(x_i + \frac{\Delta x}{2}\right) \quad (2.31)$$

Particle flow rate is given by:

$$\frac{\partial f}{\partial t} = \frac{f^{n+1}(x_i) - f^n(x_i)}{\Delta t} = \frac{s\left(x_i - \frac{\Delta x}{2}\right) - s\left(x_i + \frac{\Delta x}{2}\right)}{\Delta x} \quad (2.32)$$

$n = 0, 1, 2, \dots$

$$\frac{f^{n+1}(x_i) - f^n(x_i)}{\Delta t} = \frac{-D\left(x_i - \frac{\Delta x}{2}\right)[f(x_i) - f(x_{i-1})] + D\left(x_i + \frac{\Delta x}{2}\right)[f(x_{i+1}) - f(x_i)]}{(\Delta x)^2}$$

We know;

$$r = \frac{D\Delta t}{(\Delta x)^2}$$

Where; x (distance) = 1

$$\begin{aligned} f^{n+1}(x_i) - f^n(x_i) &= -r[f(x_i) - f(x_{i-1})] + r[f(x_{i+1}) - f(x_i)] \\ &= -rf(x_i) + rf(x_{i-1}) + rf(x_{i+1}) - rf(x_i) \\ f^{n+1}(x_i) &= f^n(x_i) + r[f(x_{i-1}) - 2f(x_i) + f(x_{i+1})] \end{aligned} \quad (2.33)$$

Equation (2.33) describes the main equation for solving transport equation of Ruffolo, using explicit method, implicit method and Crank-Nicolson method.

2.10.1 Explicit method

The technique is to substitute all values on the right-hand side of equation (2.33) by assigning $n + 1$ to as time t increases. Thus, the equation will be:

$$\begin{aligned} f^{n+1}(x_i) - f^n(x_i) &= r[f(x_{i-1}) - 2f(x_i) + f(x_{i+1})] \\ f^{n+1}(x_i) &= f^n(x_i) + r[f(x_{i-1}) - 2f(x_i) + f(x_{i+1})] \end{aligned}$$

Thus,

$$f^{n+1}(x_i) = rf^n(x_{i-1}) + (1 - 2r)f^n(x_i) + rf^n(x_{i+1}) \quad (2.34)$$

Where, $i = 1, 2, 3, \dots, N - 1$

The equation (2.34) can be solved by using the matrix method and substituting the value of i , thus;

$$\begin{aligned} f^{n+1}(x_1) &= rf^n(x_0) + (1 - 2r)f^n(x_1) + rf^n(x_2), i = 1 \\ f^{n+1}(x_2) &= rf^n(x_1) + (1 - 2r)f^n(x_2) + rf^n(x_3), i = 2 \end{aligned}$$

$$\begin{aligned}
f^{n+1}(x_3) &= rf^n(x_2) + (1 - 2r)f^n(x_3) + rf^n(x_4), i = 3 \\
&\vdots \\
f^{n+1}(x_{N-1}) &= rf^n(x_{N-2}) + (1 - 2r)f^n(x_{N-1}) + rf^n(x_N), i = N - 1
\end{aligned}$$

Error analysis:

From the initial equation

$$f^{n+1}(x_i) - f^n(x_i) = r[f(x_{i-1}) - 2f(x_i) + f(x_{i+1})]$$

We know;

$$f(x_{i-1}) - 2f(x_i) + f(x_{i+1})$$

Using the Taylor series distribution method:

$$f(x_{i-1}) = f(x_{i-1}) \tag{2.35}$$

$$f(x_i) = f(x_{i-1}) + \Delta x f'(x_{i-1}) + \frac{(\Delta x)^2 f''(x_{i-1})}{2} + \frac{(\Delta x)^3 f'''(x_{i-1})}{6} + \dots \tag{2.36}$$

$$f(x_{i+1}) = f(x_{i-1}) + 2\Delta x f'(x_{i-1}) + \frac{(2\Delta x)^2 f''(x_{i-1})}{2} + \frac{(2\Delta x)^3 f'''(x_{i-1})}{6} + \dots \tag{2.37}$$

Substitute the equation (2.35), equation (2.36) and the equation (2.37) into $f(x_{i-1}) - 2f(x_i) + f(x_{i+1})$, we get;

$$\begin{aligned}
&f(x_{i-1}) - 2f(x_i) + f(x_{i+1}) \\
&= f(x_{i-1}) - 2f(x_{i-1}) - 2\Delta x f'(x_{i-1}) - (\Delta x)^2 f''(x_{i-1}) \\
&\quad - \frac{1}{3}(\Delta x)^3 f'''(x_{i-1}) + \dots + f(x_{i-1}) + 2\Delta x f'(x_{i-1}) \\
&\quad + 2(\Delta x)^2 f''(x_{i-1}) + \frac{2}{3}(\Delta x)^3 f'''(x_{i-1}) + \dots
\end{aligned} \tag{2.38}$$

Thus;

$$\begin{aligned}
&f(x_{i-1}) - 2f(x_i) + f(x_{i+1}) \\
&\approx -(\Delta x)^2 f''(x_{i-1}) - \frac{1}{3}(\Delta x)^3 f'''(x_{i-1}) + \dots + 2(\Delta x)^2 f''(x_{i-1}) \\
&\quad + \frac{2}{3}(\Delta x)^3 f'''(x_{i-1}) + \dots
\end{aligned}$$

Finally;

$$f(x_{i-1}) - 2f(x_i) + f(x_{i+1}) \approx f''(x_{i,t}) + 0(\Delta x)^2$$

Where, $0(\Delta x)^2$ is the error in the order 2 of the initial equations considered in the terms of $f^{n+1}(x_i) - f^n(x_i)$.

$$f^{n+1}(x_i) - f^n(x_i) = \frac{D\Delta t}{(\Delta x)^2} [f(x_{i-1}) - 2f(x_i) + f(x_{i+1})]$$

$$r = \frac{D\Delta t}{(\Delta x)^2}$$

$$\frac{f^{n+1}(x_i) - f^n(x_i)}{\Delta t} = \frac{\partial f(x_i)}{\partial t}$$

Therefore;

$$\frac{f^{n+1}(x_i) - f^n(x_i)}{\Delta t} = \frac{\partial f(x_i)}{\partial t} \approx O(\Delta t)$$

So, $O(\Delta t)$ is the error, thus the equation is:

$$\mathbf{error} \propto \mathbf{O}(\Delta t) + \mathbf{O}(\Delta x)^2 \quad (2.39)$$

2.10.2 Implicit method

The principle of this method is to reset all values to the right of equation (2.33) by assigning $n + 1$ to the new value as time increases and n is the old value at the initial time.

From the initial equation, the equation (2.33) can be written as:

$$\begin{aligned} f^{n+1}(x_i) - f^n(x_i) &= r[f^{n+1}(x_{i-1}) - 2f^{n+1}(x_i) + f^{n+1}(x_{i+1})] \\ f^n(x_i) &= f^{n+1}(x_i) - rf^{n+1}(x_{i-1}) + 2rf^{n+1}(x_i) - rf^{n+1}(x_{i+1}) \\ \therefore f^n(x_i) &= -rf^{n+1}(x_{i-1}) + (1 + 2r)f^{n+1}(x_i) - rf^{n+1}(x_{i+1}) \end{aligned} \quad (2.40)$$

where; $i = 1, 2, 3, \dots$

From the equation (2.40), we use the matrix method to solve the equation by substituting the value of i . We get;

$$\begin{aligned} -rf^{n+1}(x_0) + (1 + 2r)f^{n+1}(x_1) - rf^{n+1}(x_2) &= f^n(x_1), i = 1 \\ -rf^{n+1}(x_1) + (1 + 2r)f^{n+1}(x_2) - rf^{n+1}(x_3) &= f^n(x_2), i = 2 \\ -rf^{n+1}(x_2) + (1 + 2r)f^{n+1}(x_3) - rf^{n+1}(x_4) &= f^n(x_3), i = 3 \\ &\vdots \\ -rf^{n+1}(x_{N-2}) + (1 + 2r)f^{n+1}(x_{N-1}) - rf^{n+1}(x_N) &= f^n(x_{N-1}), i = N - 1 \end{aligned}$$

Writing in matrix form, we obtain:

$$\begin{pmatrix} (1+2r) & -r & 0 & \cdots & 0 \\ -r & (1+2r) & -r & \ddots & \vdots \\ 0 & -r & (1+2r) & -r & 0 \\ \vdots & \ddots & \ddots & \ddots & \ddots \\ 0 & \cdots & 0 & -r & (1+2r) \end{pmatrix} \begin{pmatrix} f^{n+1}(x_1) \\ f^{n+1}(x_2) \\ f^{n+1}(x_3) \\ \vdots \\ f^{n+1}(x_{N+1}) \end{pmatrix} \\ = \begin{pmatrix} rf^{n+1}(x_0) + f^n(x_1) \\ f^n(x_2) \\ f^n(x_3) \\ \vdots \\ f^n(x_{N+1}) \end{pmatrix}$$

In determining the discrepancy, we make use of the Taylor series distribution method as well as the explicit method where all the tolerances are given as the equation (2.41).

$$\text{error} \propto \mathbf{O}(\Delta t) + \mathbf{O}(\Delta x)^2 \quad (2.41)$$

2.10.3 Crank-Nicolson method

It is the method which involves the combination of explicit methods and implicit methods.

We know;

$$r = \frac{D\Delta t}{(\Delta x)^2}$$

Since;

$$r = 2S$$

$$f^{n+1}(x_i) = rf^n(x_{i-1}) + (1-2r)f^n(x_i) + rf^n(x_{i+1}) \quad (2.42)$$

From the method of explicit in the equation (2.34) we have:

$$f^n(x_i) = -rf^{n+1}(x_{i-1}) + (1+2r)rf^{n+1}(x_i) - rf^{n+1}(x_{i+1})$$

Then, equation (2.10.1.1) + equation (2.10.3.1), we obtain:

$$\begin{aligned} -rf^{n+1}(x_{i-1}) + (2+2r)rf^{n+1}(x_i) - rf^{n+1}(x_{i+1}) &= rf^n(x_{i-1}) \\ &+ (2-2r)f^n(x_i) + rf^n(x_{i+1}) \end{aligned}$$

Substituting and dividing by 2 throughout the above equation we get:

$$\begin{aligned} -Sf^{n+1}(x_{i-1}) + (1+2S)rf^{n+1}(x_i) - Sf^{n+1}(x_{i+1}) &= Sf^n(x_{i-1}) \\ &+ (1-2S)rf^n(x_i) + Sf^n(x_{i+1}) \end{aligned} \quad (2.43)$$

$$i = 1, 2, 3, \dots, N - 1$$

The equation (2.43) can be solved using the matrix method and substituting the value of i as follows:

$$\begin{aligned}
 & -Sf^{n+1}(x_0) + (1 + 2S)f^{n+1}(x_1) - Sf^{n+1}(x_2) = Sf^n(x_0) \\
 & \quad + (1 - 2S)f^n(x_1) + Sf^n(x_2), i = 1 \\
 & -Sf^{n+1}(x_1) + (1 + 2S)f^{n+1}(x_2) - Sf^{n+1}(x_3) = Sf^n(x_1) \\
 & \quad + (1 - 2S)f^n(x_2) + Sf^n(x_3), i = 2 \\
 & -Sf^{n+1}(x_2) + (1 + 2S)f^{n+1}(x_3) - Sf^{n+1}(x_4) = Sf^n(x_2) \\
 & \quad + (1 - 2S)f^n(x_3) + Sf^n(x_4), i = 3 \\
 & \quad \vdots \\
 & -Sf^{n+1}(x_{N-2}) + (1 + 2S)f^{n+1}(x_{N-1}) - Sf^{n+1}(x_N) = Sf^n(x_{N-2}) \\
 & \quad + (1 - 2S)f^n(x_{N-1}) + Sf^n(x_N), i = N - 1
 \end{aligned}$$

$$\begin{pmatrix}
 (1 + 2S) & -S & 0 & \dots & 0 \\
 -S & (1 + 2S) & -S & \ddots & \vdots \\
 0 & -S & (1 + 2S) & -S & 0 \\
 \vdots & \ddots & \ddots & \ddots & \ddots \\
 0 & \dots & 0 & -S & (1 + 2S)
 \end{pmatrix}
 \begin{pmatrix}
 f^{n+1}(x_1) \\
 f^{n+1}(x_2) \\
 f^{n+1}(x_3) \\
 \vdots \\
 f^{n+1}(x_{N+1})
 \end{pmatrix} =$$

$$\begin{pmatrix}
 (1 - 2S) & S & 0 & \dots & 0 \\
 S & (1 - 2S) & S & \ddots & \vdots \\
 0 & S & (1 - 2S) & S & 0 \\
 \vdots & \ddots & \ddots & \ddots & \ddots \\
 0 & \dots & 0 & S & (1 - 2S)
 \end{pmatrix}
 \begin{pmatrix}
 f^{n+1}(x_1) \\
 f^{n+1}(x_2) \\
 f^{n+1}(x_3) \\
 \vdots \\
 f^{n+1}(x_{N+1})
 \end{pmatrix} +$$

$$\begin{pmatrix}
 S[f^{n+1}(x_0) + f^n(x_1)] \\
 f^n(x_2) \\
 f^n(x_3) \\
 \vdots \\
 f^n(x_{N+1})
 \end{pmatrix}$$

Since, this method involves the combination of explicit methods and implicit methods the total error is as given in the equation below:

$$\mathbf{error} \propto \mathbf{O}(\Delta t)^2 + \mathbf{O}(\Delta x)^2 \quad (2.44)$$

CHAPTER III

RESEARCH METHODOLOGY

This chapter discourses the research methodology for the simulation of motion of He, C, N, O, and Fe particles due to solar flare and shows the detail procedures followed. The main focus is given as to how the data was collected, prepared for its initial values and how simulation was done to calculate the injection time and mean free path (λ) from transport equation of Ruffolo (1995, 1998) solved using numerical technique of finite difference method. We use C++ program in ubuntu operating system for simulation of particles for it to propagate from Sun to Earth due to solar eruption. Compiling and linking the program required nine files which are wind.c, decel.c, field.c, initial.c, inject.c, nrutil.c, printout.c, stream.c and tridag.c. The particles were selected which are of low range, medium range and high range energy level to give approximation in precision for our analysis.

Researchers suggested that, the probability of solar flare occurrence should be, on the maximum of every solar cycle. Thus, this brings us to select our solar event of interest on August 9, 2011 which is at the maximum of 24th solar cycle and it is only the event having X class solar flare of X6.9 on this period.

3.1 Research guidelines

The subsequent guidelines as shown below were followed to proceed with our research.

- Study the data of the Sun's surface eruption and the movement of high energy particles along the Archimedean magnetic field lines.
- Study the transport equation of Ruffolo (1995, 1998) used to describe the motion of high energy particles from the Sun.
- Select an event of interest for the release of high energy particles due to solar flare.
- Download the information on the distribution of high-energy particles from the Sun to Earth by the SIS instrument on ACE spacecraft and provide the necessary data needed to be used as the default settings in the simulation.

- Simulate particle motion using numerical technique of finite different method in C++ program.
- Analyze the data obtained from the simulation combined with the motion equation and the actual data from the spacecraft.
- Summary, analyze the findings and write a book.

3.2 Research Procedures of the Study

In this research we use quantitative methodology which involves the empirical investigation of observable and measurable variables used for theory testing. Here, we chose the solar flare event on August 9, 2011 to collect data from the spacecraft. The X-ray class of the selected solar event is X6.9, the solar flare position on the Sun is N18W68 and the solar wind speed is 551.5 kms⁻¹. This flare had the long injection time from the Sun to the Earth corresponding to the shock wave detected after explosion in the interplanetary space of 13 minutes. In the path of the solar flare affected on the Earth, the Kp-index (the value of the Earth's magnetic field variable) was also considered (Baisri, Khumlumlert, & Aiemsa-ad, 2017).

The data collected will be on the particles such as helium, carbon, nitrogen, oxygen, and iron which are distributed as a function of time for each energy of the mean free path. We use the technique of the piecewise linear least square method for optimization of the injection duration. The best fitting will showed by the value of χ^2 (chi square). The χ^2 value is the difference between the results from the transport simulation program and the data from spacecraft and is defined as, $\chi^2 = \sum_{i=1}^N \left[\frac{y_i - \sum_{k=1}^M a_k X_k(x_i)}{\sigma_i} \right]^2$, where (x_i, y_i) is the data point from spacecraft, σ_i is the uncertainty of data point, N is the number of data points, $X_k(x_i)$ are the arbitrary fixed function of x , $\{a_k\}$ are the parameters to be fitted and M is the number of fitted functions. We model the injection function versus time near the Sun as a piecewise linear function, in which the best fitting value with the best λ (mean free path). Finally, we get the best piecewise linear injection function and χ^2 value for each mean free path. We find the injection duration of the interested solar event in the terms of full width at half maximum of the injection function (Paluk et al., 2017).

3.2.1 Flow chart of the research procedures in brief

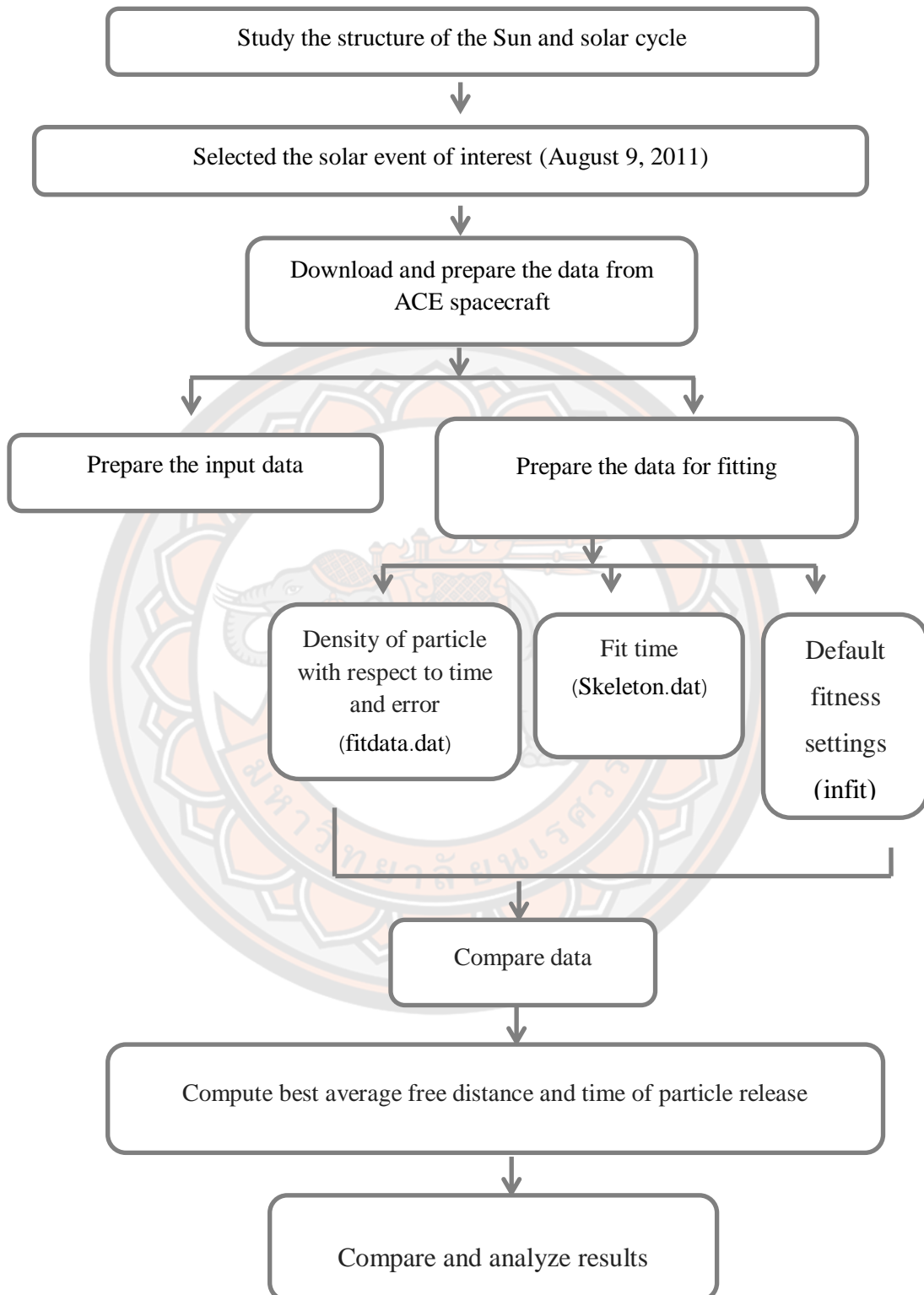


Figure 9: Flow chart of research procedures

3.3 Tools used in research operations

The necessary tools that we have used in the research are, SIS instrument on ACE spacecraft for retrieving data and C++ program in ubuntu operating system for the simulation of particle using the transport equation of Ruffolo (1995, 1998). The explanation of each operation are given in detail as follows:

3.3.1 Data from the ACE (Advanced Composition Explorer) spacecraft

The spacecraft was designed by NASA to study spaceborne energetic particles from the Sun to Earth at L1 Lagrange point, about 1.4×10^6 km from Earth. It was launched on August 25, 1997 and the main function was to investigate the matter ejected from the Sun to establish the commonality and interaction between the Sun, Earth and the Milky Way galaxy.

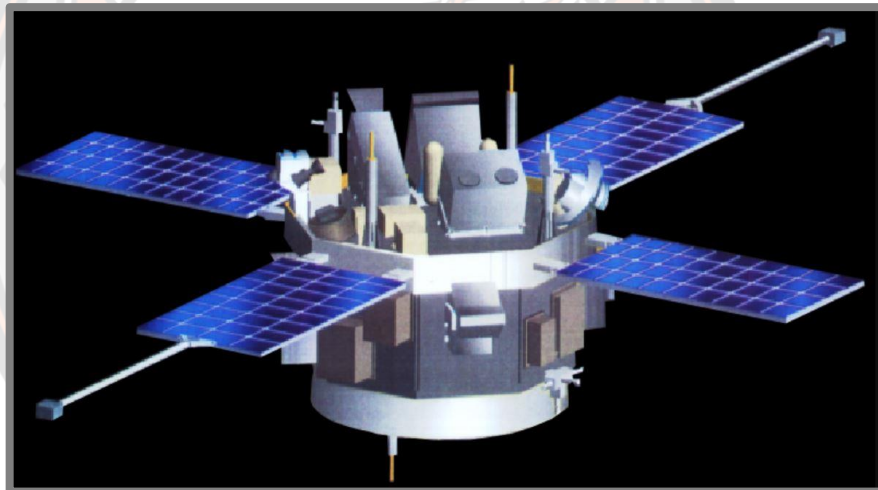


Figure 10: ACE (Advanced Composition Explorer) spacecraft

Source: <https://solarsystem.nasa.gov/missions/ace/in-depth/>

In addition, ACE also provides real-time space weather data and advanced warning of geomagnetic storms (Siddiqi, July 25, 2019). The weight of the spacecraft combined with the fuel tank was approximately 758 kg. There were total of nine instruments installed on the ACE spacecraft but for this research we use only Solar Isotopic Spectrometer (SIS) instrument designed to observed the energetic nuclei from He to Ni over the energy range from ~ 10 to ~ 100 MeV/n. We have mainly focussed on using SIS instrument to collect data on ACE spacecraft which is uploaded in website and freely available for researchers (Siddiqi, July 25, 2019).

3.3.2 Program written in C++ for the simulation of particle motion

We use C++ program to simulate particle motion from Ruffolo's (1995, 1998) transport equation, which is processed on the ubuntu operating system. The program consisted of further nine programs which are discussed as follows:

- wind.c: It is the main program for the simulation of particle motion. The program will receive various variable values from the data and retrieve files from other programs to do processing. The variables that are used to simulate particle motion are:
 - starts: Starting distance (AU) in the simulation.
 - stops: Final distance (AU) of the simulation.
 - s step: The increment of distance (AU).
 - prints: It is the printing for output.
 - nmu: The number of points of μ .
 - length: The length (AU) of the simulation.
 - np: Amount of momentum.
 - p [1 ... np]: Momentum of each energy.
 - m: Mass of the particle.
 - β (Beta) of sw: The ratio of solar wind speed to light speed.
 - λ (Lambda): The average free distance.
 - q: Index of particle scattering.
 - printextra: To print the information on the screen or not.
- decel.c: This program is used in processing of the gradual decomposition of the particle in transport equation of Ruffolo (1995, 1998). It updates $F(t, \mu, z, p)$ for the effects of deceleration.
- field.c: It is a program used for processing the motion of particles along magnetic field lines in an interplanetary medium. The program will calculate the coefficient of scattering in terms of the flaring of the magnetic field, as well as the effect of the solar wind.
- initial.c: The program determines the distribution of particle for processing particle motion simulation, by comparing the maximum distribution of particles

in the least energy to the default values. It is used to determine the initial value of the distribution function $F(\mu, z, p)$.

- inject.c: It is a program to calculate the injection of particles after start of the simulation.
- nrutil.c: The program contains routines to reserve and unreserve the memory for arrays.
- printout.c: It is a program for displaying required information.
- stream.c: It considers the movement of particles along the z-axis by the convection of the solar wind.
- tridag.c: It is a program for solving tridiagonal matrix equations.

3.4 Selecting an event for the release of high-energy particles from the Sun's eruption

The selected incidents of interest are the event on August 9, 2011, which occurred during the maximum of 24th solar cycle of the Sun. The intensity of X-rays is X6.9 located at N18W68 and has solar wind speed of 551.5 kms^{-1} . The event started at 7.48 UT and ended 8.08 UT with 20 min of release time. Hit waves at 8.05 UT are gradual. The physical characteristics of this event are as shown in Table 4 below.

Table 4: Physical characteristics of events on August 9, 2011

Physical characteristics	An event on August 9, 2011
Solar cycle	24
X- ray classification of solar flare	X6.9
Start of eruption	7.48 UT
End of eruption	8.08 UT
Eruption duration	20 mins
Solar wind speed	551.5 kms^{-1}
Shock wave encountered	8.05 UT

The data of an event of interest on August 9, 2011 is obtained from the SIS instrument on ACE spacecraft which is freely available in the website. The number of

particles per unit of time is used as data to simulate the motion of high energy particles from the Sun along the Archimedian magnetic field lines with the Ruffolo's (1995, 1998) transport equation solved in C++ program using ubuntu operating system.

3.5 Position of solar flare and kp index on an event of interest

Figure 11, displays the position of solar flare, N18W68 on august 9, 2011 as seen by the SDO (Solar Dynamic Observatory) at 8:05 UT in 304 angstrom lights. The X-ray class of the flare was X6.9 with solar wind speed of 551.5 kms^{-1} .

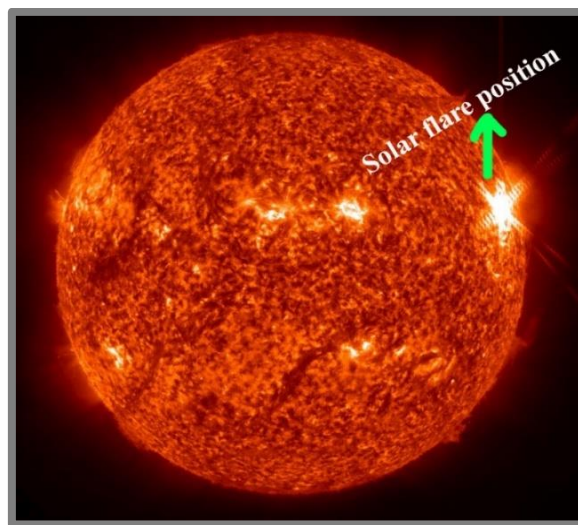


Figure 11: The flare as seen by the Solar Dynamic Observatory (SDO) at 8:05 UT in 304 angstrom light on august 9, 2011.

Source: <https://svs.gsfc.nasa.gov/11500>

Kp index tells the disturbances in the horizontal component of earth's magnetic field by an integer ranging from 0-9 with 1 being calm and ≥ 5 indicates geomagnetic storm. The Figure 12 shows the kp index on an event of interest as detected by NOAA GOES satellite within the time interval of 3 hours. By reading the graph the approximate kp index was found to be >3 and thus didn't had much impact on the livelihood of Earth. However, some sources pointed out that it produced increased solar energetic proton radiation, enough to affect humans in space if they do not protect themselves. They had also disrupted some GPS and communication signal but was not strong enough to cause radio communication blackouts (Fox, 2011, August 9).

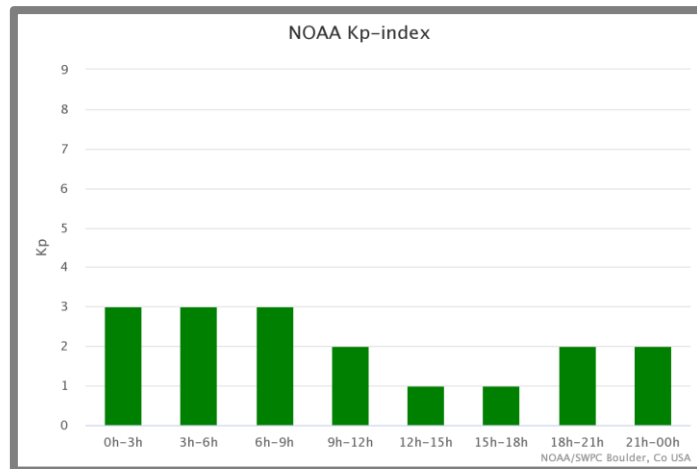


Figure 12: Kp index on august 9, 2011 as detected by NOAA GOES satellite

Source: https://www.nasa.gov/mission_pages/sunearth/news/News080911-xclass.html

3.6 Data collection from SIS instrument on ACE spacecraft

For the preparation of high-energy particle dispersion data from the solar eruption, the data was downloaded from the ACE spacecraft on the day of the solar eruption. After that, we prepare initial data values necessary for the simulation of particle motion. Downloading data from the ACE spacecraft comprises the following steps:

- Enter the website “<http://www.srl.caltech.edu/ACE/>” as shown in the Figure 13 and click on “Online data”.

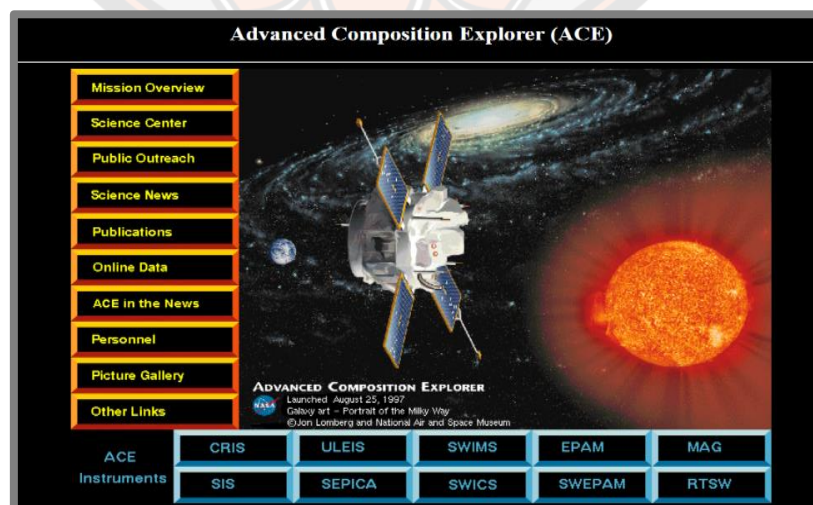
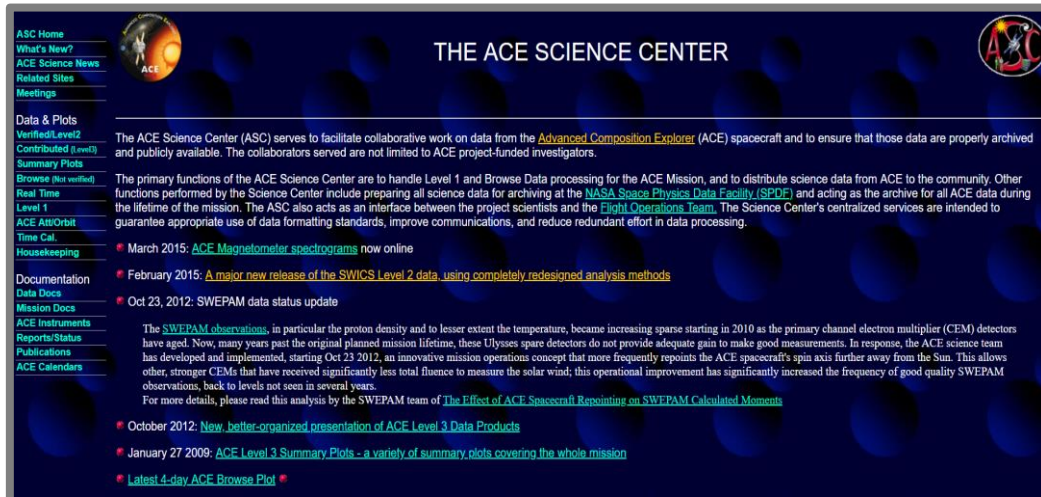


Figure 13: The overview of the webpage to download data

Source: <http://www.srl.caltech.edu/ACE/>

- Click on “Verified / Level2” as shown in Figure 14 to select the measured data from various devices on the spacecraft.



The ACE Science Center (ASC) serves to facilitate collaborative work on data from the [Advanced Composition Explorer \(ACE\)](#) spacecraft and to ensure that those data are properly archived and publicly available. The collaborators served are not limited to ACE project-funded investigators.

The primary functions of the ACE Science Center are to handle Level 1 and Browse Data processing for the ACE Mission, and to distribute science data from ACE to the community. Other functions performed by the Science Center include preparing all science data for archiving at the [NASA Space Physics Data Facility \(SPDF\)](#) and acting as the archive for all ACE data during the lifetime of the mission. The ASC also acts as an interface between the project scientists and the [Flight Operations Team](#). The Science Center's centralized services are intended to guarantee appropriate use of data formatting standards, improve communications, and reduce redundant effort in data processing.

- March 2015: [ACE Magnetometer spectrograms](#) now online
- February 2015: [A major new release of the SWICS Level 2 data, using completely redesigned analysis methods](#)
- Oct 23, 2012: [SWEPAM data status update](#)

The [SWEPAM observations](#), in particular the proton density and to lesser extent the temperature, became increasingly sparse starting in 2010 as the primary channel electron multiplier (CEM) detectors have aged. Now, many years past the original planned mission lifetime, these Ulysses spare detectors do not provide adequate gain to make good measurements. In response, the ACE science team has developed and implemented, starting Oct 23 2012, an innovative mission operations concept that more frequently repoints the ACE spacecraft's spin axis further away from the Sun. This allows other, stonger CEMs that have received significantly less total fluence to measure the solar wind; this operational improvement has significantly increased the frequency of good quality SWEPAM observations, back to levels not seen in several years.

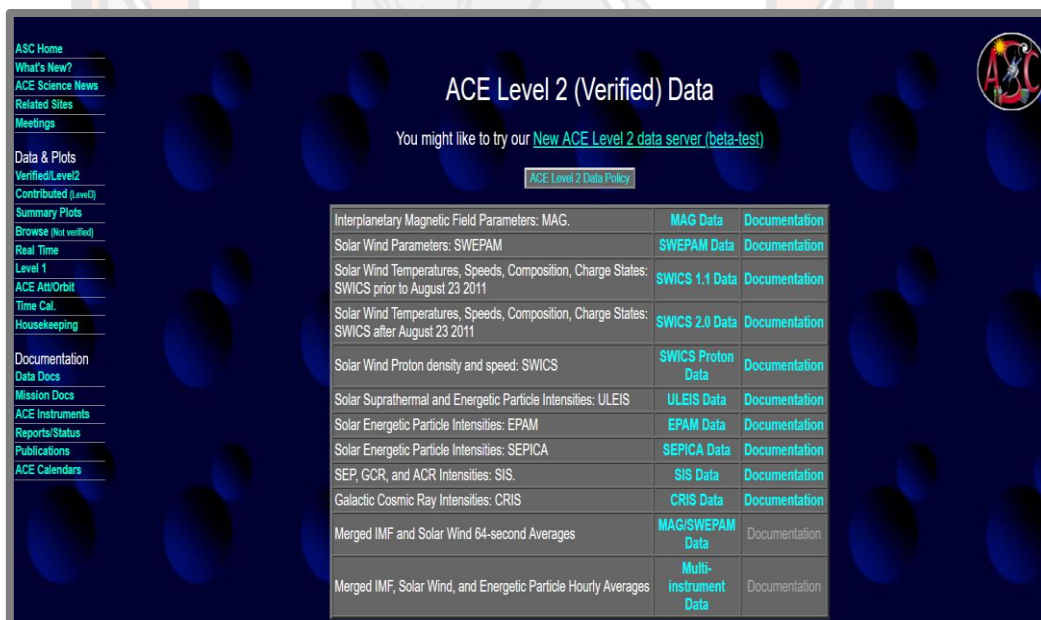
For more details, please read this analysis by the SWEPAM team of [The Effect of ACE Spacecraft Repointing on SWEPAM Calculated Moments](#)

- October 2012: [New, better-organized presentation of ACE Level 3 Data Products](#)
- January 27 2009: [ACE Level 3 Summary Plots - a variety of summary plots covering the whole mission](#)
- [Latest 4-day ACE Browse Plot](#)

Figure 14: Selecting data from the spacecraft

Source: <http://www.srl.caltech.edu/ACE/ASC/>

- As illustrated in Figure 15 select “SEP, GCR, and ACR Intensities: SIS”, by clicking on SIS Data.



ACE Level 2 (Verified) Data

You might like to try our [New ACE Level 2 data server \(beta-test\)](#)

[ACE Level 2 Data Policy](#)

Interplanetary Magnetic Field Parameters: MAG.	MAG Data	Documentation
Solar Wind Parameters: SWEPAM	SWEPAM Data	Documentation
Solar Wind Temperatures, Speeds, Composition, Charge States: SWICS prior to August 23 2011	SWICS 1.1 Data	Documentation
Solar Wind Temperatures, Speeds, Composition, Charge States: SWICS after August 23 2011	SWICS 2.0 Data	Documentation
Solar Wind Proton density and speed: SWICS	SWICS Proton Data	Documentation
Solar Suprathermal and Energetic Particle Intensities: ULEIS	ULEIS Data	Documentation
Solar Energetic Particle Intensities: EPAM	EPAM Data	Documentation
Solar Energetic Particle Intensities: SEPICA	SEPICA Data	Documentation
SEP, GCR, and ACR Intensities: SIS	SIS Data	Documentation
Galactic Cosmic Ray Intensities: CRIS	CRIS Data	Documentation
Merged IMF and Solar Wind 64-second Averages	MAG/SWEPAM Data	Documentation
Merged IMF, Solar Wind, and Energetic Particle Hourly Averages	Multi-instrument Data	Documentation

Figure 15: Data type selection

- We click on “Verified/Level2”, to select the measured data from various devices on the spacecraft and then select the “Day of year (DOY)” and the year at the “Hourly Averages” box and click “Go”. In this research since our DOY/Year is 221/2011, we chose the data within the time interval of “216/2011 - 242/2011”.

Figure 16: Choosing data on an event of interest

- We can now download the data by clicking on “SIS Hourly Averaged Element Fluxes” as shown in the Figure 17, check the element of interest and element counts. Since, for this research “YR / DOY is 11/221” we select starting “YR / DOY” as 11/221 and ending "YR / DOY" as 11/226, to eliminate unnecessary data. Finally, we click the “Text file download box”, click on “Retrieve data” and save the data file for use in the simulation.

Accessing data from: [sis_data_1hr_2459.hdf](#)

Ancillary Data: [SIS Energy Band Information](#)

ACE Data Set:

SIS Hourly Averaged Element Fluxes

The following documentation is contained within the data file:

Data Description	View Documentation
Contact Info	
Energy Bands, Geometry Factors	
Release Notes	

Figure 17 : Downloading data of high energy particles [He, C, N, O, and Fe]

SIS Hourly Averaged Element Fluxes.

Select the data items you want to retrieve.
Click on items in first column for more information.
Note: Data for each element consists of particle fluxes in 8 energy ranges.

Time (UT)	<input type="checkbox"/> year	<input type="checkbox"/> day	<input type="checkbox"/> hour	<input type="checkbox"/> min	<input type="checkbox"/> sec	<input type="checkbox"/> year (float)	<input type="checkbox"/> day (float)	<input type="checkbox"/> ACE epoch
Element Fluxes	<input checked="" type="checkbox"/> He	<input checked="" type="checkbox"/> C	<input checked="" type="checkbox"/> N	<input checked="" type="checkbox"/> O	<input type="checkbox"/> Ne	<input type="checkbox"/> Na	<input type="checkbox"/> Mg	<input type="checkbox"/> Al
Element Counts	<input checked="" type="checkbox"/> He cnt	<input checked="" type="checkbox"/> C cnt	<input checked="" type="checkbox"/> N cnt	<input checked="" type="checkbox"/> O cnt	<input type="checkbox"/> Ne cnt	<input type="checkbox"/> Na cnt	<input type="checkbox"/> Mg cnt	<input type="checkbox"/> Al cnt
Other Info	<input type="checkbox"/> uptime fraction	<input type="checkbox"/> solar activity						

or check here to select all the data (over 100 columns!)

Starting "YR/DOY": Ending "YR/DOY": (Example: 98/37, note: no leading zeros)

Figure 18: Element selection for analysis

3.7 Preparation of data for simulation in C++ program

For the initial preparation of data, we follow the procedures as given below to simulate in C++ program. Intended for the illustration of the procedures used, we have shown only a sample data for Helium particle. However, similar procedures are followed for all the element considered, at every energy level. Table 5 shows a sample data of helium element as obtained from the SIS instrument on the ACE spacecraft. We follow the following procedures for preparation of the data:

Table 5: Sample of data collected for Helium particle for all energy level

Time	He [Flux] at 4.032 MeV/n	He [Flux] at 5.39 MeV/n	He [Flux] at 6.685 MeV/n	He [Flux] at 8.418 MeV/n	He [Flux] at 11.493 MeV/n	He [Flux] at 15.623 MeV/n	He [Flux] at 22.959 MeV/n	He [Flux] at 34.77 MeV/n	Count1 for He at 4.032 MeV/n	Count2 for He at 5.39 MeV/n	Count3 for He at 6.685 MeV/n	Count4 for He at 8.418 MeV/n	Count5 for He at 11.493 MeV/n	Count6 for He at 15.623 MeV/n	Count7 for He at 22.959 MeV/n	Count8 for He at 34.77 MeV/n
30	1.09E-01	5.81E-02	2.87E-02	1.19E-02	3.30E-03	1.07E-03	0.00E+00	1.89E-04	1.09E+02	6.30E+01	2.50E+01	2.10E+01	9.00E+00	3.00E+00	0.00E+00	1.00E+00
90	1.10E-01	5.43E-02	2.48E-02	2.02E-02	3.22E-03	1.11E-03	0.00E+00	0.00E+00	1.11E+02	5.90E+01	2.20E+01	3.40E+01	9.00E+00	3.00E+00	0.00E+00	0.00E+00
150	9.22E-02	4.12E-02	2.36E-02	5.35E-03	4.06E-03	1.32E-03	0.00E+00	0.00E+00	1.15E+02	5.30E+01	2.50E+01	1.30E+01	1.30E+01	5.00E+00	0.00E+00	0.00E+00
210	5.77E-02	3.59E-02	1.61E-02	7.31E-03	2.86E-03	1.49E-03	7.68E-04	0.00E+00	9.10E+01	5.60E+01	2.10E+01	1.90E+01	1.20E+01	7.00E+00	7.00E+00	0.00E+00
270	6.76E-02	2.89E-02	1.78E-02	6.54E-03	2.77E-03	1.69E-03	1.23E-04	9.64E-05	1.15E+02	5.20E+01	2.60E+01	2.00E+01	1.20E+01	9.00E+00	2.00E+00	1.00E+00
330	4.45E-02	3.00E-02	1.17E-02	7.02E-03	2.02E-03	6.47E-04	2.87E-04	0.00E+00	8.10E+01	5.70E+01	1.70E+01	2.10E+01	1.00E+01	4.00E+00	3.00E+00	0.00E+00
390	5.11E-02	2.27E-02	1.14E-02	7.60E-03	3.80E-03	5.86E-04	3.64E-04	0.00E+00	8.80E+01	4.50E+01	1.70E+01	2.40E+01	2.00E+01	3.00E+00	4.00E+00	0.00E+00
450	4.80E-02	2.18E-02	1.24E-02	7.17E-03	2.77E-03	7.77E-04	2.76E-04	0.00E+00	1.01E+02	4.80E+01	2.30E+01	2.60E+01	1.60E+01	4.00E+00	4.00E+00	0.00E+00
510	3.18E-02	1.77E-02	7.43E-03	3.56E-03	1.61E-03	6.50E-04	3.84E-04	6.80E-04	7.90E+01	4.50E+01	1.60E+01	1.60E+01	1.10E+01	5.00E+00	6.00E+00	7.00E+00
570	2.76E-02	2.17E-02	1.28E-02	1.16E-02	9.61E-03	1.31E-02	6.66E-03	3.53E-03	3.30E+01	2.90E+01	1.30E+01	2.00E+01	3.00E+01	4.40E+01	5.60E+01	2.10E+01
630	1.28E-01	8.97E-02	7.76E-02	4.23E-02	2.46E-02	1.69E-02	5.55E-03	1.29E-03	6.40E+01	5.20E+01	3.30E+01	4.00E+01	3.50E+01	2.60E+01	1.90E+01	4.00E+00
690	3.90E-01	2.40E-01	2.08E-01	8.38E-02	3.99E-02	1.73E-02	1.13E-02	3.69E-03	1.08E+02	7.00E+01	4.70E+01	4.10E+01	3.00E+01	1.50E+01	2.10E+01	5.00E+00
750	4.67E-01	2.38E-01	1.33E-01	6.60E-02	2.54E-02	1.46E-02	5.05E-03	0.00E+00	1.47E+02	7.80E+01	3.50E+01	3.60E+01	2.10E+01	1.30E+01	1.20E+01	0.00E+00

- Data are collected from SIS instrument on ACE spacecraft as shown in Table 5. We then create “Start time [min]” at, 0, 60, 120 ... and “End time [min]” at, 60, 120, 180, ... The time, He [Flux] at 4.032 MeV/n, Counts are copied and arranged as given in the Table 6 below.

Table 6: Sample data collected for Helium particle at energy level 4.032 MeV/n

Time	He [Flux] at 4.032 MeV/n	Counts for He at 4.032 MeV/n	Error	Start time [min]	End time [min]
30	1.09E-01	1.09E+02	1.04E-02	0	60
90	1.10E-01	1.11E+02	1.05E-02	60	120
150	9.22E-02	1.15E+02	8.60E-03	120	180
210	5.77E-02	9.10E+01	6.05E-03	180	240
270	6.76E-02	1.15E+02	6.31E-03	240	300
330	4.45E-02	8.10E+01	4.94E-03	300	360
390	5.11E-02	8.80E+01	5.44E-03	360	420
450	4.80E-02	1.01E+02	4.77E-03	420	480
510	3.18E-02	7.90E+01	3.58E-03	480	540
570	2.76E-02	3.30E+01	4.80E-03	540	600
630	1.28E-01	6.40E+01	1.61E-02	600	660
690	3.90E-01	1.08E+02	3.75E-02	660	720

- Separate column of “Error” is made. We then, delete every row which contains the error value of, “# DIV/0!”. This is done in order to eliminate the unnecessary data during the time of simulation.

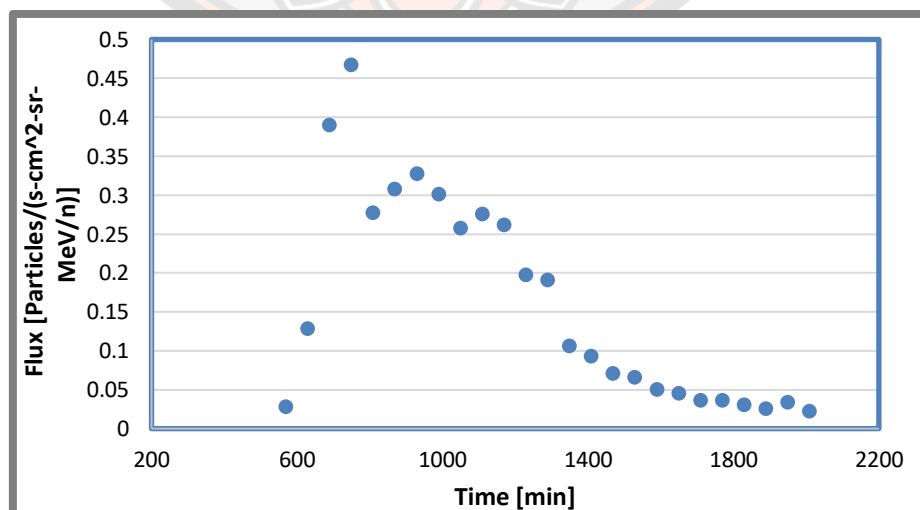


Figure 19: A sample of the particle distribution chart Helium at the energy level 4.032 MeV/n.

- Plot a graph of time distribution and “He [Flux] at 4.032 MeV/n” to record the “start time” of the graph and also to delete unnecessary as shown in Figure.
- Copy the numeric values of “Start time” and “End time” into a new excel file and save it as text (MS-DOS) as “He1timecut.txt”.
- Similarly we, copy the numeric values of “Time”, “He [Flux] at 4.032 MeV/n” and “Error” into new excel file and save it as text (MS-DOS) as “He1datacut.txt”.
- Repeat the above steps for all the elements at all energy levels.

3.8 Determination of the necessary values for simulation of particle motion

For the simulation of data in transport equation we need to prepare some values from the data which will be discussed as follows:

- Obtaining average energy value for each energy (E_k)

From the maximum energy E_{max} and minimum energy E_{min} , each average energy level E_k is obtained by the equation:

$$E_k = \sqrt{E_{min} + E_{max}}$$

The true mass or real mass can be obtained from the formula:

$$Real\ mass = \frac{(931.5\text{MeV}/c^2)(A)}{Z}$$

where;

Z = Mass number

A = Atomic mass

- Determining the momentum of each energy level (P) from the formula:

$$P = \sqrt{(E_k + m_0)^2 - m_0^2}$$

where;

E_k is the average energy value of each energy level

P is the momentum (MeV/c)

m_0 is the true mass of the element (MeV/c²)

- Finding the speed in each energy level from the formula

$$v = \beta(c)$$

where;

$$\beta = \frac{v}{c} = \frac{P}{E_k + m_0}$$

β is the ratio between solar wind speed and light speed

v is the speed of particle at each energy level (AU/min)

c is the speed of light equal to 0.1202 AU/min

- Determining the spectrum

$$\text{Spectrum} = \frac{\text{Maximum flux in energy level } N}{\text{The maximum flux at the power level}}$$

where;

$$N = 1,2,3,4,5,6,7,8$$

- Determining the constant value for the particle decay

Since, the decomposition of high energy particles from the Sun has a tendency of continuous decay which is in accordance with the power law as given in the equation.

$$\frac{dE}{dN} \propto E^{-\gamma}$$

where;

E is the energy of particles.

N is the number of particles in each energy level.

γ is the particle's constant decay.

Constant decay of the particle can be obtained from the slope of the graph between the momentum log value and the spectral log value as show in Figure 20.

- Particle release time can be obtained from the equation:

$$s = v(t)$$

where;

s (AU) is the distance from Sun to Earth.

v (AU/min) is the velocity of each particle of different energy level.

t (min) is the time period for the high energy particle to move from Sun to Earth.

Table 7: Sample of calculated values for Helium particle motion necessary for simulation

E_k (Energy) in MeV/n	m_0 (mass)	p (momentum)	β	v (velocity)
4.032	932.108	86.793	0.093	0.0111
5.390	932.108	100.389	0.107	0.0129
6.685	932.108	111.834	0.119	0.0143
8.418	932.108	125.552	0.133	0.0160
11.493	932.108	146.826	0.156	0.0187
15.623	932.108	171.372	0.181	0.0217
22.959	932.108	208.154	0.218	0.0262
34.770	932.108	256.957	0.266	0.0319

He [Flux]	spectrum	$\log(p)$	$\log(\text{spec})$	The distance (AU)
0.467	1.000	1.938	0.000	64.191
0.240	0.513	2.002	-0.290	74.138
0.208	0.445	2.049	-0.351	82.476
0.084	0.179	2.099	-0.746	92.423
0.040	0.085	2.167	-1.068	107.731
0.017	0.037	2.234	-1.432	125.194
0.011	0.024	2.318	-1.616	150.896
0.004	0.008	2.410	-2.103	183.999

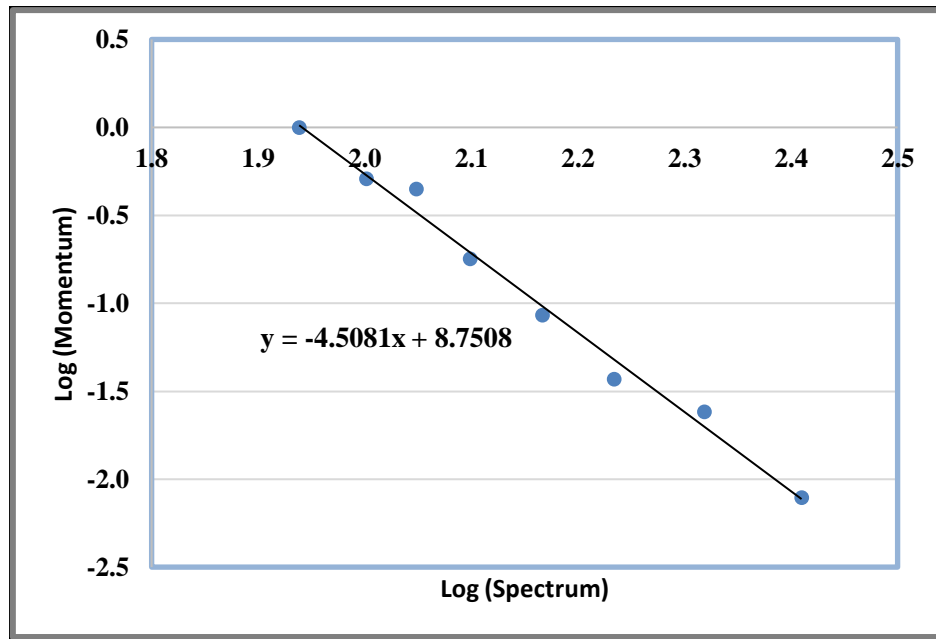


Figure 20: A sample of graph for Helium showing the relationship between momentum log values and spectrum spectra of events on August 9, 2011.

3.9 Simulation of high energy particle motion

The transport equation of Ruffolo (1995, 1998) is given by:

$$\begin{aligned}
 \frac{\partial F}{\partial t} = & -\frac{\partial}{\partial z} \mu v F - \frac{\partial}{\partial z} \left(1 - \mu^2 \frac{v^2}{c^2} \right) v_{sw} \sec \psi F \\
 & - \frac{\partial}{\partial \mu} \frac{v}{2L(z)} \left[1 + \mu \frac{v_{sw}}{v} \sec \psi - \mu \frac{v_{sw} v}{c^2} \sec \psi \right] (1 - \mu^2) F \\
 & + \frac{\partial}{\partial \mu} v_{sw} \left(\cos \psi \frac{d}{dr} \sec \psi \right) \mu (1 - \mu^2) F \\
 & + \frac{\partial}{\partial \mu} \frac{\phi(\mu)}{2} \frac{\partial}{\partial \mu} \left(1 - \mu \frac{v_{sw} v}{c^2} \sec \psi \right) F \\
 & + \frac{\partial}{\partial p} p v_{sw} \left[\frac{\sec \psi}{2L(z)} (1 - \mu^2) + \cos \mu \frac{d}{dr} (\sec \psi) \mu^2 \right] F
 \end{aligned}$$

It can be seen that the equation is a complex linear partial differential equation. Thus, C++ program in ubuntu operating system was used to solve the above equation through numerical technique of finite difference method. The condition applied was the initial data prepared from SIS instrument on ACE spacecraft.

3.10 Fit to compare data

After the results of the particle motion simulation are obtained, we compare the data from the spacecraft with the data from simulated data using the linear least squares fitting technique. The method involves the following equation;

$$\chi^2 = \sum_{i=1}^N \left[\frac{y_n - y(x_n)}{\sigma_n} \right]^2$$

where,

χ^2 is the sum of squared differences of data n .

y_n is the actual data from the spacecraft in the particle flux data (fitdata.dat).

$y(x_n)$ is the data from simulation of particle motion in counts.dat file format.

σ_n is the discrepancy of each data point.

n is the number of data.

We will fit distances to simulate the λ (mean free path) compared with the actual data in order to find trend of the mean free path that gives the minimum χ^2 (chi square) value from all 3 or 5 neighboring points.

When the minimum λ (mean free path) is obtained the result of fitting the data will get the function of particle release according to time which can be used to draw graphs and determine the time of particle release.

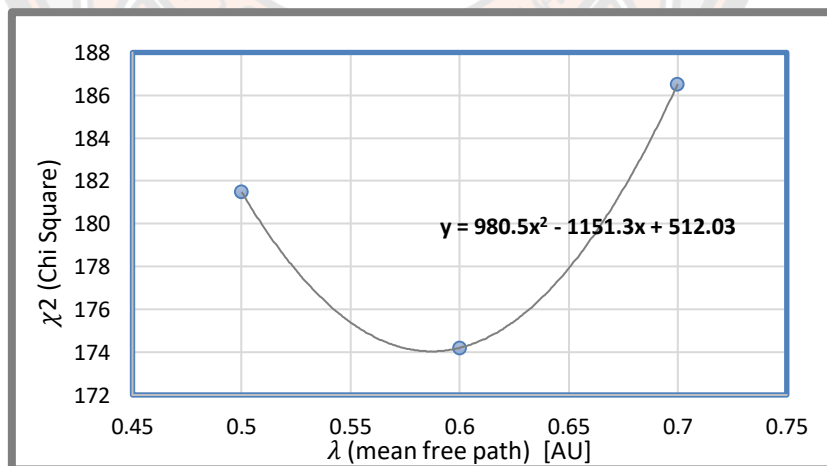


Figure 21: A sample graph of Helium particle at energy level 5.390 MeV/n showing relationship between Chi square and λ mean free path.

In order to find the time of particle release, we used the FWHM (Full Width at Half Maximum) method to determine the period of particle release using injection

profile obtained as output from C++ program in ubuntu operating system. FWHM method involves finding the width from highest point of the graph reduced to half. A sample is as shown in the Figure 22 below:

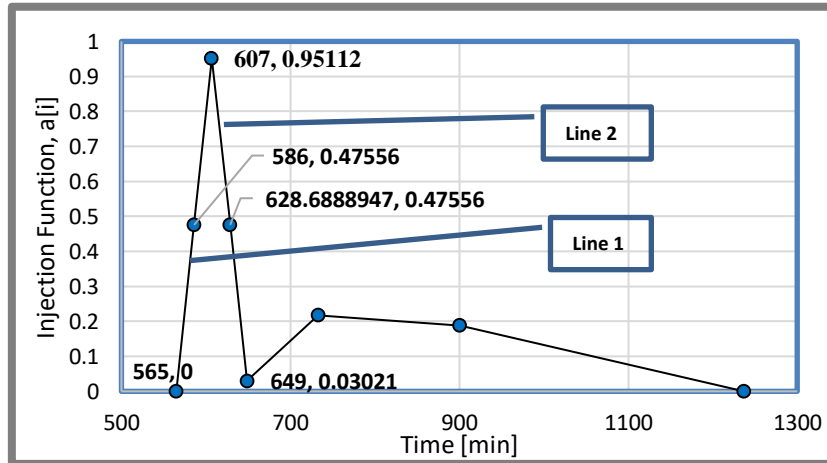


Figure 22: Sample graph of injection profile for Helium element at energy level 4.032 MeV/n.

3.11 Sample procedures for FWHM method for Helium element at energy level 4.032 MeV/n

The following are the procedures followed in FWHM method to determine the time for particle release from Sun to Earth.

- Determining the half maximum by locating the highest flux

$$\text{Half maximum} = \frac{y_2}{2} = \frac{0.95112}{2} = 0.47556$$

- Determining the slope from line 1

$$\text{Slope (m)} = \frac{\Delta y}{\Delta x} = \frac{y_2 - y_1}{x_2 - x_1}$$

From the graph:

$$(y_2, y_1) = (0.95112, 0)$$

$$(x_2, x_1) = (607, 565)$$

$$\text{Slope (m)} = \frac{0.95112 - 0}{607 - 565} = 0.022645714$$

Thus; the equation of line 1 is:

$$y = (0.022645714)x + C \quad (1)$$

- Determining the slope from line 2

$$\text{Slope } (m) = \frac{\Delta y}{\Delta x} = \frac{y_2 - y_1}{x_2 - x_1}$$

From the graph:

$$(y_2, y_1) = (0.95112, 0.03021)$$

$$(x_2, x_1) = (607, 649)$$

$$\text{Slope } (m) = \frac{0.95112 - 0.03021}{607 - 649} = -0.021926429$$

Thus; equation of line 2 is:

$$y = (-0.021926429)x + C \quad (2)$$

- Determine the value of C for equation of line 1

We have;

$$y_1 = (0.022645714)x_1 + C$$

Let us choose the co-ordinate:

$$(x_1, y_1) = (607, 0)$$

Substituting the value in above equation we get:

$$C = 12.79482857$$

- Substitute the value of half maximum and C in the equation of line 1

From equation 1, we have:

$$y_1 = (0.022645714)x_1 + C$$

$$0.47556 = (0.022645714)x_1 + 12.79482857$$

$$x_1 = t_1 = \frac{0.47556 - 12.79482857}{0.022645714} = 545 \text{ min}$$

- Determine the value of C for equation of line 2

From equation (2), we have;

$$y = (-0.021926429)x + C$$

Let us choose the co-ordinate from line 2:

$$(x_1, y_1) = (649, 0.03021)$$

Substituting the value in above equation we get:

$$C = 14.26046214$$

- Substitute the value of half maximum and C in the equation of line 2

From equation (2), we have:

$$0.47556 = (-0.021926429)x_2 + 14.26046214$$

$$x_2 = t_2 = \frac{0.47556 - 14.26046214}{-0.021926429} = 628.68 \text{ min}$$

- Now, subtracting $t_2 - t_1$ we will obtain injection time

$$t_2 - t_1 = 628.68 \text{ min} - 545 \text{ min} = 42.689 \text{ min}$$

- Similarly, we followed all the above steps for determining injection time for every element (C, N, O and Fe) at all energy level.

CHAPTER IV

RESULTS AND DISCUSSION

The spacecraft data are collected from the website and further prepared for its initial values necessary for simulation in C++ program which uses transport equation of Ruffolo (1995, 1998), in ubuntu operating system. The equation is solved using numerical technique of finite different methods in the program itself. The solar event of interest was chosen on August 9, 2011 having X-ray class flare of X6.9 and solar wind speed of 551.5 kms^{-1} at the Sun's position of N18W68.

The fitting results (compare.dat) and injection profile are obtained as auto generated files through simulation using initial data from spacecraft. Fitting results (compare.dat) file explains the accuracy of the results. Closer the values between flux (spacecraft) and flux (simulation), accurate would be the output result. However, we tried to bring the values of flux (spacecraft) and flux (simulation) close to each other as far as possible for precision of the result. This chapter deliberates the results of best mean free path (λ) corresponding to its minimum chi square value, its error and simulated value. It also discusses how we computed the injection time using FWHM in the injection profile for the propagation of SEP from Sun to Earth. We also gave our analysis on the relationship of solar cycle and data collected for cosmic rays from Princess Sirindhorn Neutron Monitor at an event of interest.

4.1 Best mean free path (λ)

We will fit distances to simulate the mean free path (λ) compared with the actual data in order to find trend of the best mean free path corresponding to the minimum chi square (χ^2) value from all 3 to 5 neighboring points. The mean free path of particles for solar event on August 9, 2011 is as shown in the Figure 23 – 27 used for simulating the injection profile. We then, obtained the best mean free path by differentiating the equation with respect to x and determining the value of $x = \lambda$. To work out mean free path from graph we follow the procedures as indicated in chapter III section 3.10. The results along with some corrected error are displayed in Table 8 for all elements at all energy level considered.

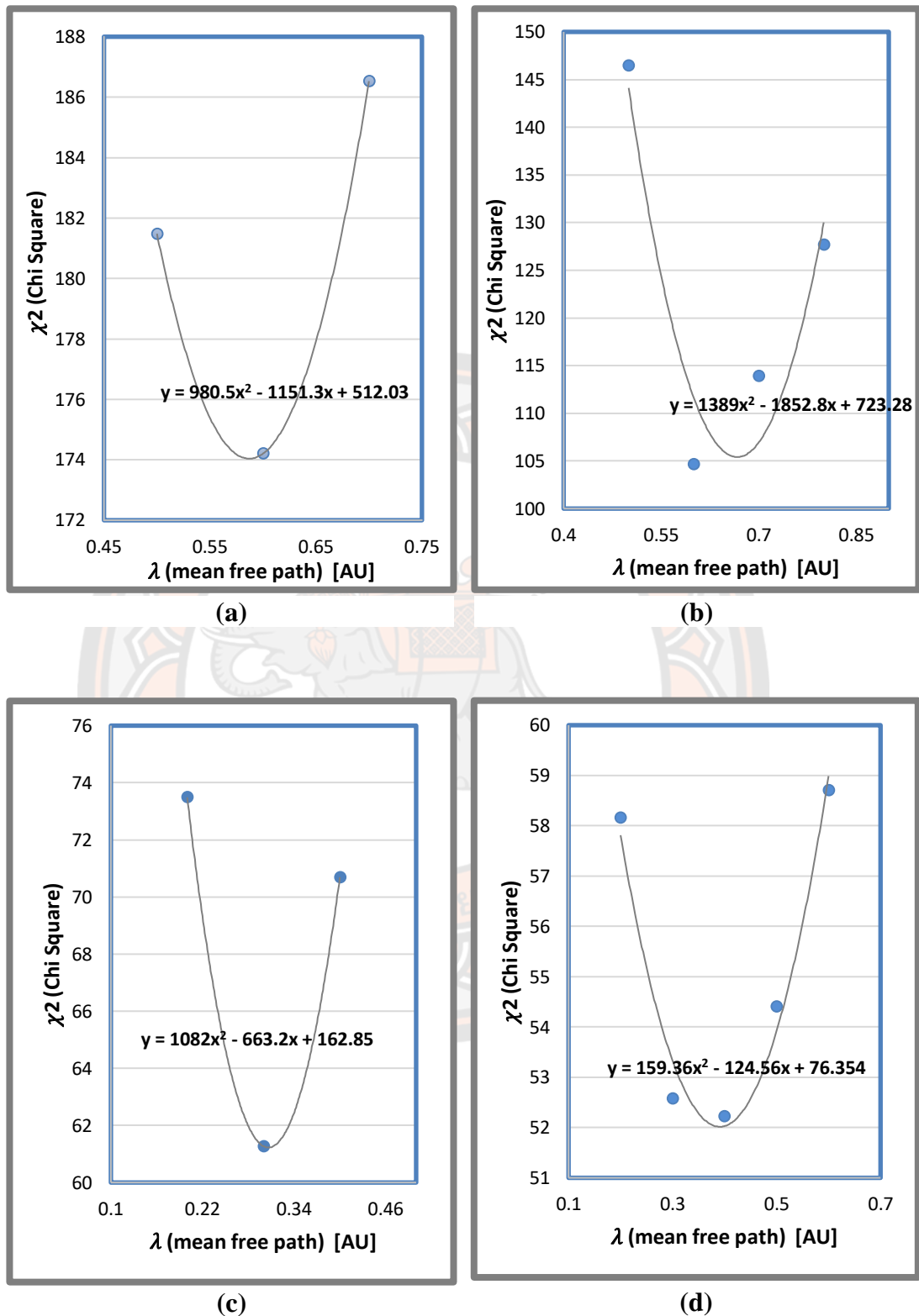


Figure 23: Displaying best mean free path for corresponding minimum Chi square value for Helium particle at energy level (a) 4.032 MeV/n, (b) 5.390 MeV/n, (c) 6.685 MeV/n, and (d) 8.418 MeV/n.

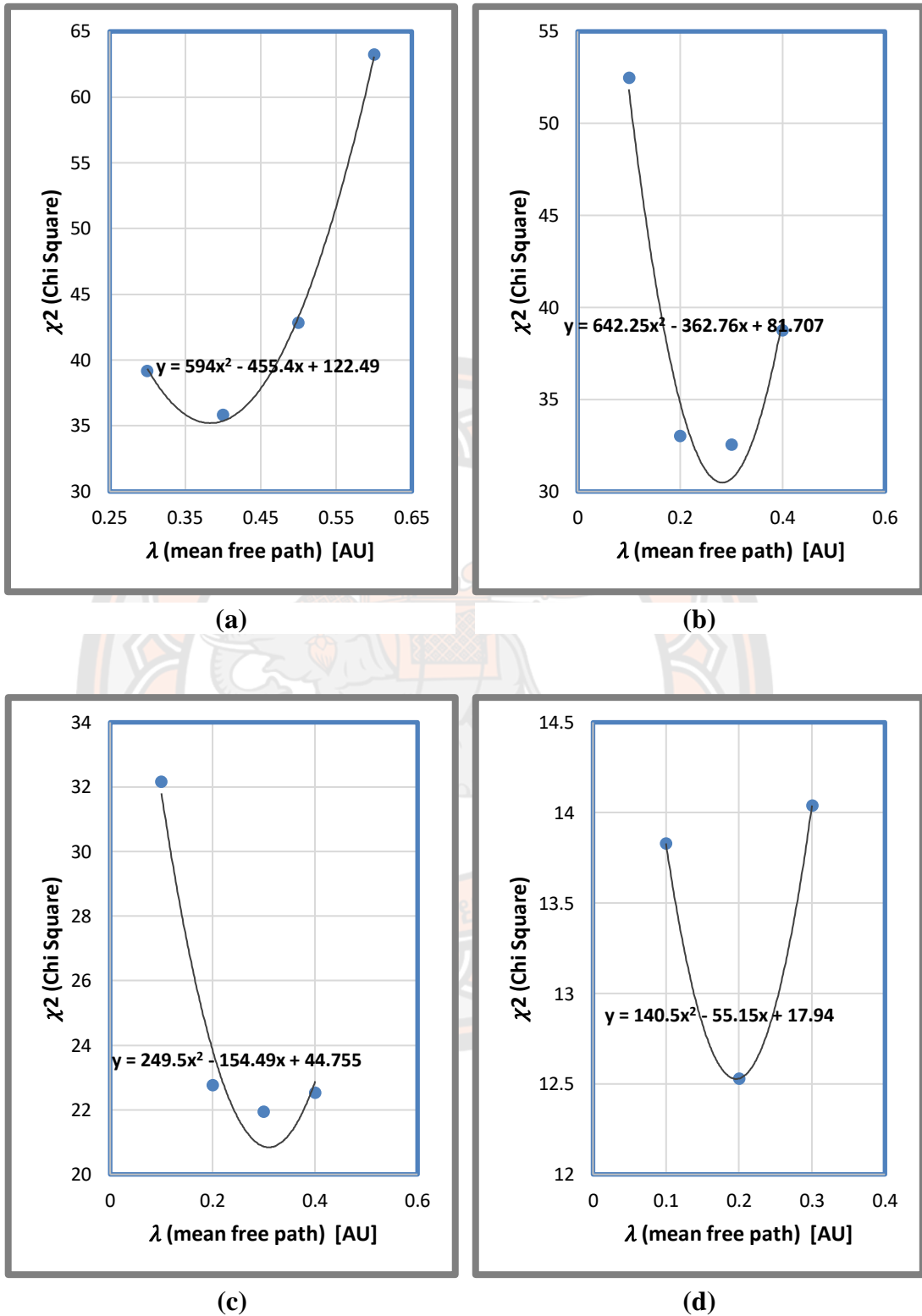


Figure 24: Displaying best mean free path for corresponding minimum Chi square value for Carbon particle at energy level (a) 7.443 MeV/n, (b) 9.839 MeV/n, (c) 12.267 MeV/n, and (d) 15.505 MeV/n.

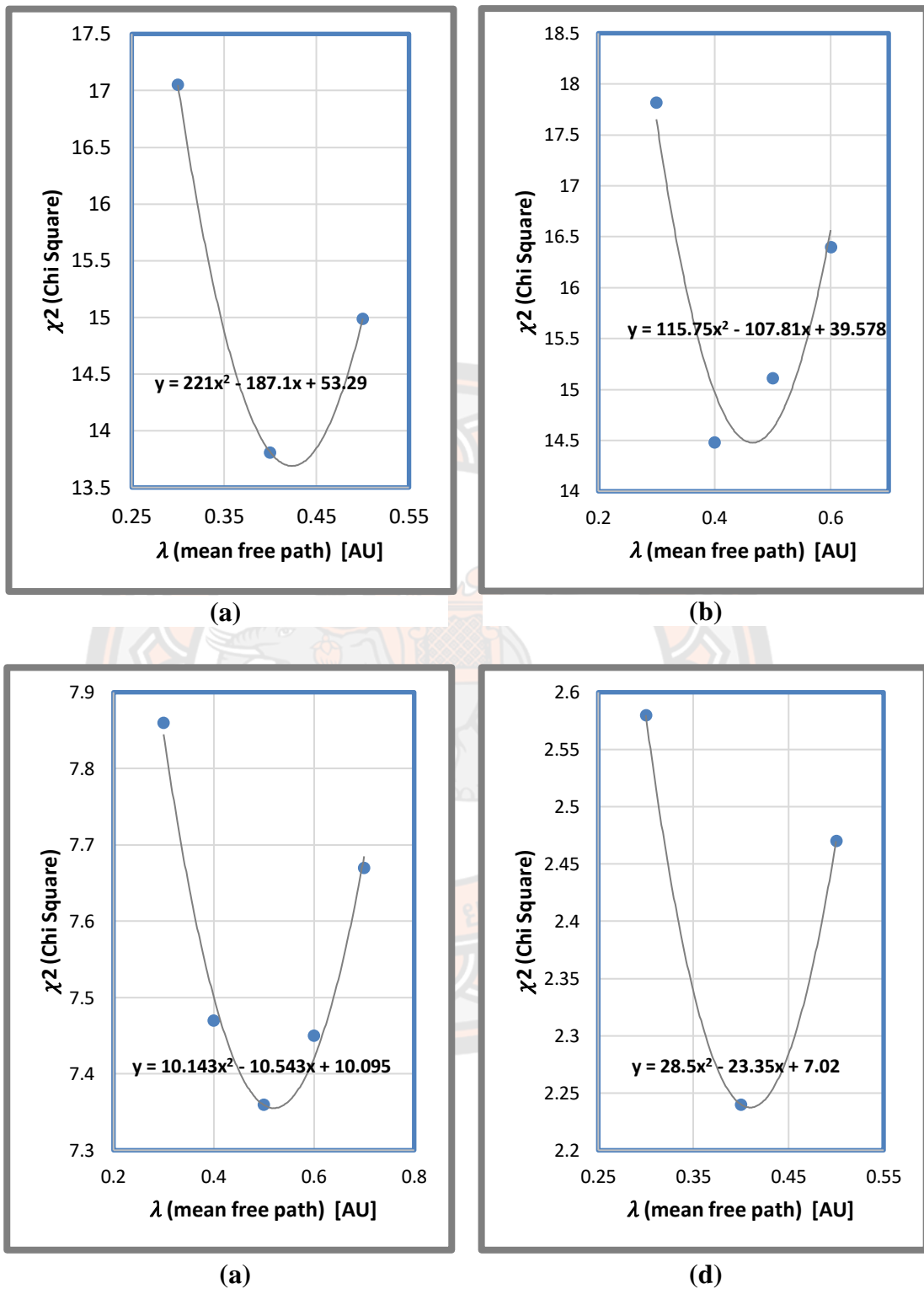


Figure 25: Displaying best mean free path for corresponding minimum Chi square value for Nitrogen particle at energy level (a) 8.009 MeV/n, (b) 10.660 MeV/n, (c) 13.317 MeV/n, and (d) 16.854 MeV/n.

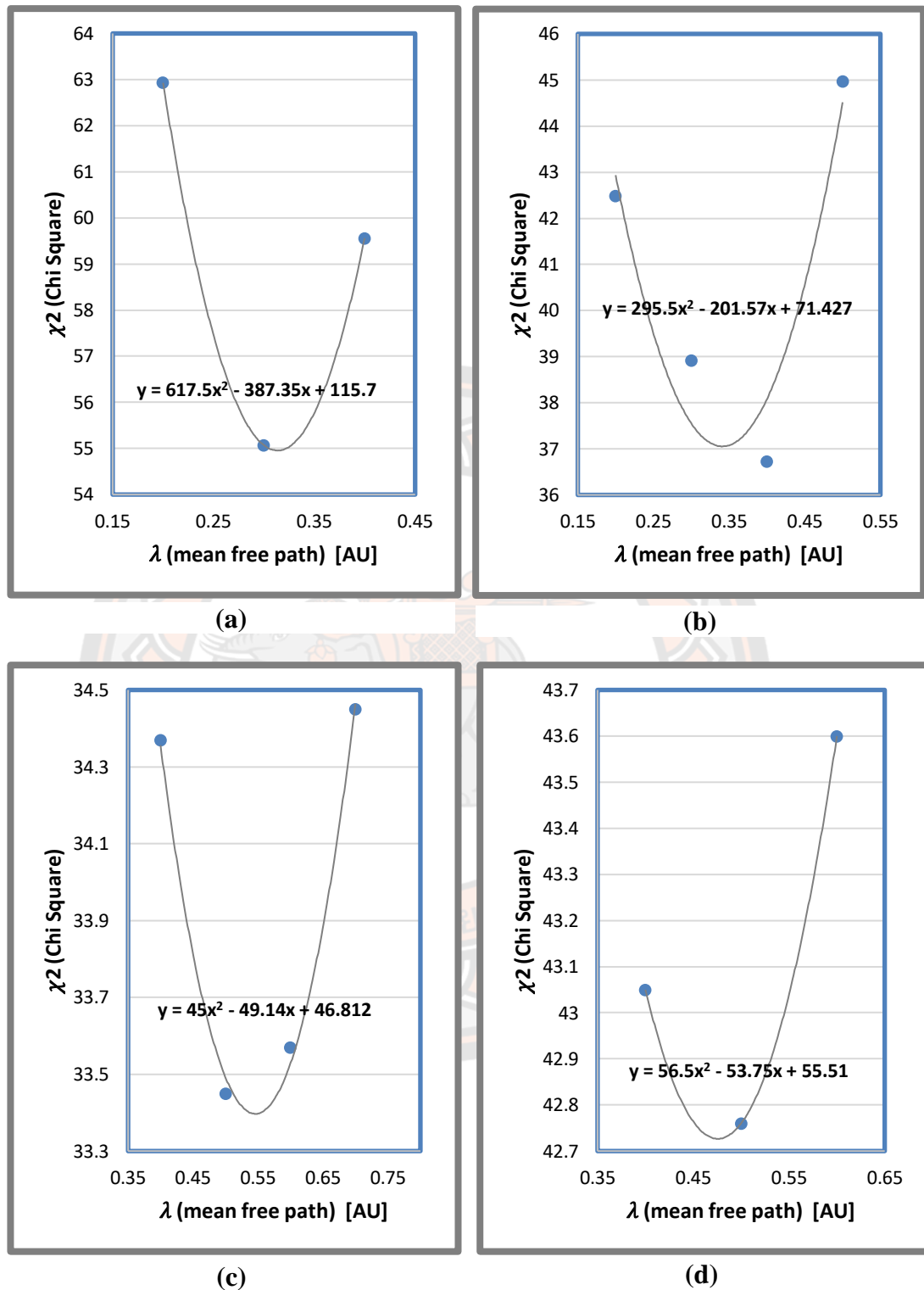


Figure 26: Displaying best mean free path for corresponding minimum Chi square value for Oxygen particle at energy level (a) 8.538 MeV/n, (b) 11.427 MeV/n, (c) 14.293 MeV/n, and (d) 18.104 MeV/n.

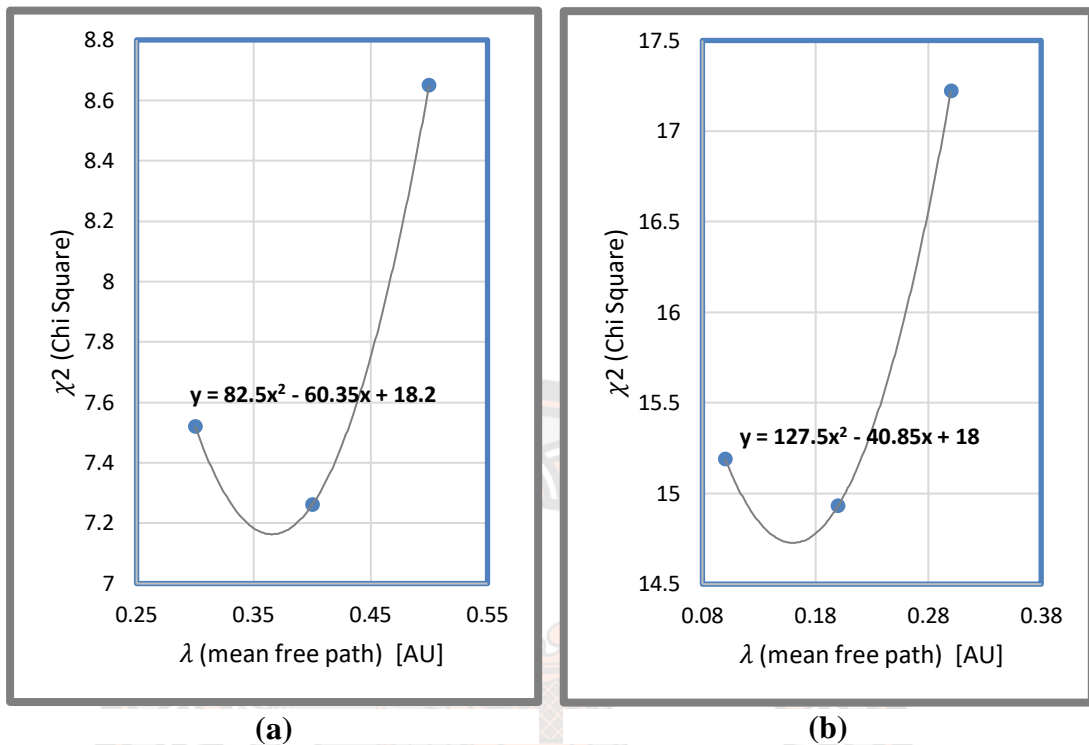


Figure 27: Displaying best mean free path for corresponding minimum Chi square value for Iron particle at energy level (a) 18.461 MeV/n, and (b) 30.902 MeV/n.

4.2 Fitting data (compare.dat)

The fitting results corresponding to the comparison of actual data from the spacecraft and with those obtained from simulation results for each element at all energy level is as displayed in Figure 28 - 32. We find the best fitting between spacecraft data and simulated data for best mean free path. The spacecraft data is in blue dot and simulation results in red dot computed in the best mean free path (λ) from corresponding minimum chi square (χ^2) value. The graph consists of time [min] in x-axis and flux [particles/s-cm²-sr-MeV/n] in y-axis. We use compared fitting method of piecewise linear function between the simulation results and spacecraft data.

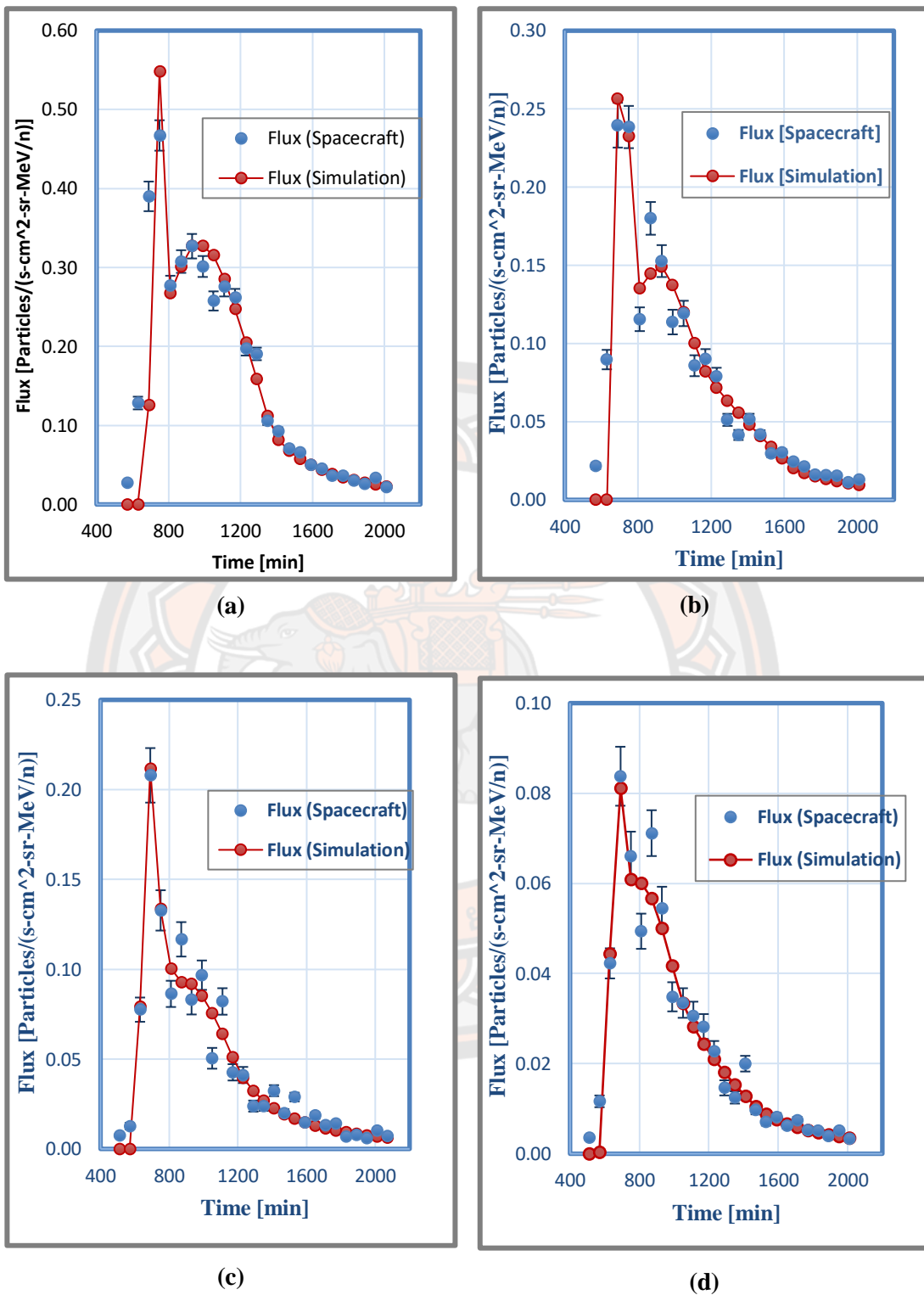


Figure 28: Comparison of simulated data and spacecraft data for Helium particle at energy level (a) 4.032 MeV/n, (b) 5.390, (c) 6.685 MeV/n, and (d) 8.418 MeV/n.

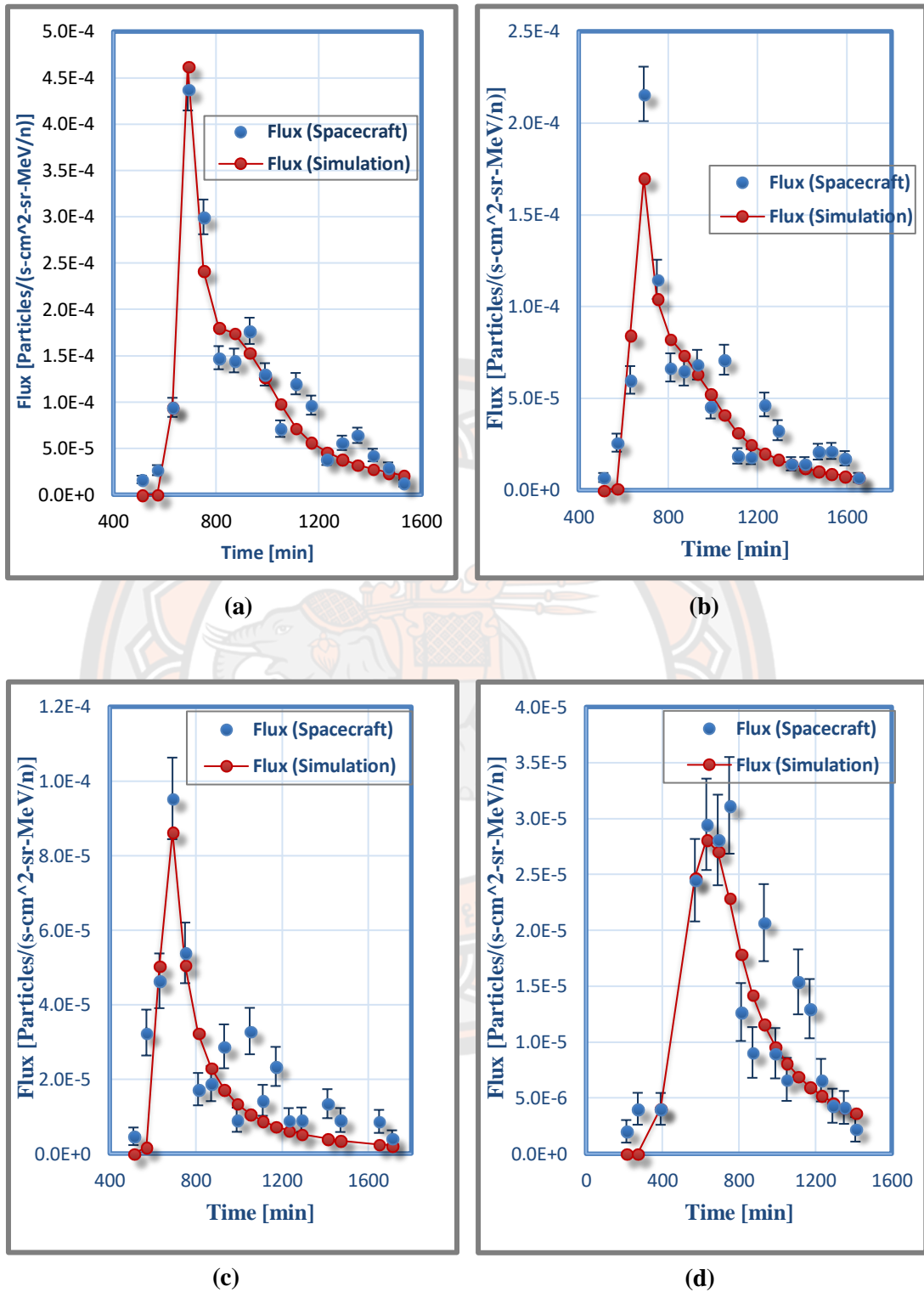


Figure 29: Comparison of simulated data and spacecraft data for Carbon particle at energy level (a) 7.443 MeV/n, (b) 9.839 MeV/n, (c) 12.267 MeV/n, and (d) 15.505 MeV/n.

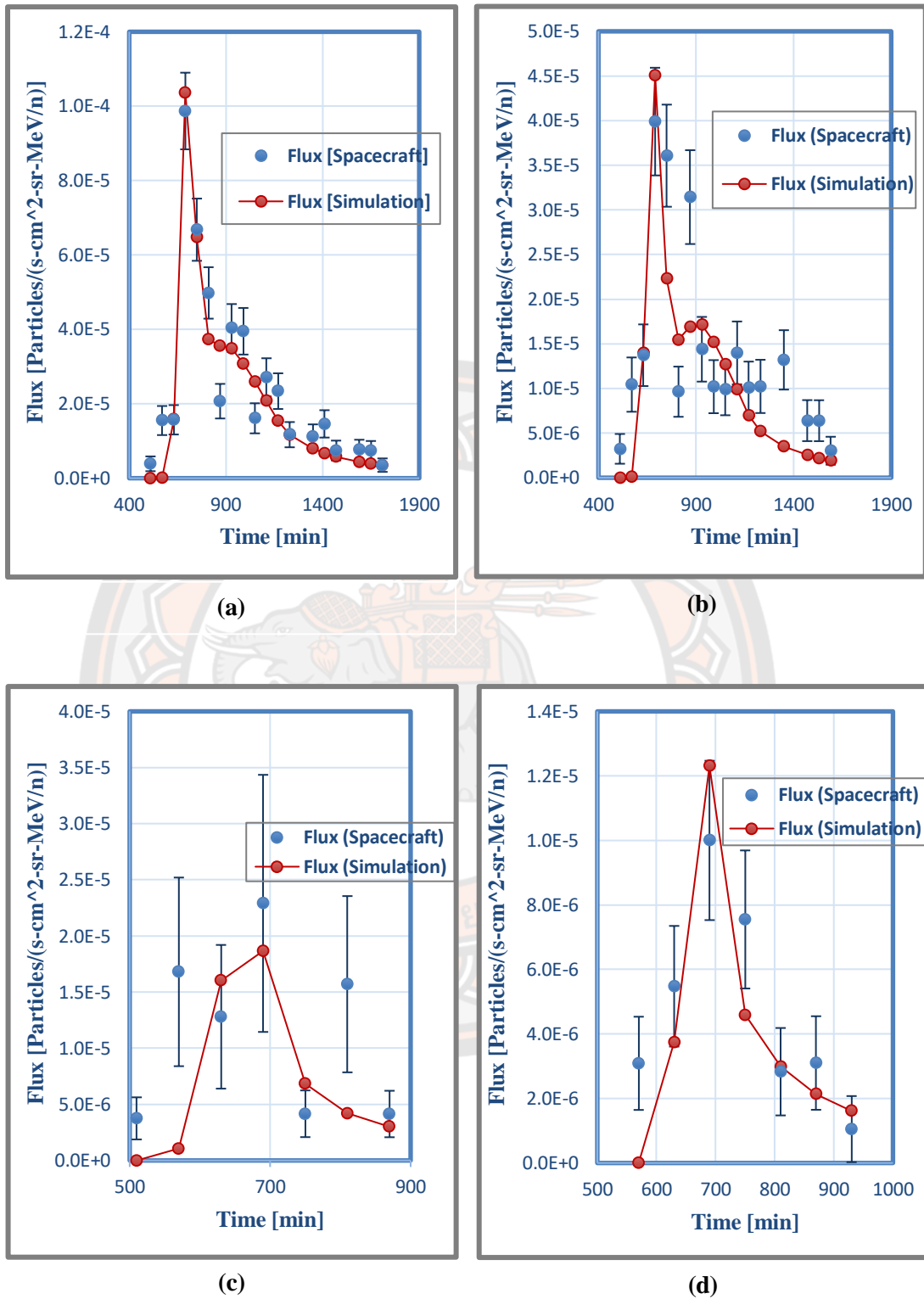


Figure 30: Comparison of simulated data and spacecraft data for Nitrogen particle at energy level (a) 8.009 MeV/n, (b) 10.660 MeV/n, (c) 13.317 MeV/n, and (d) 16.854 MeV/n.

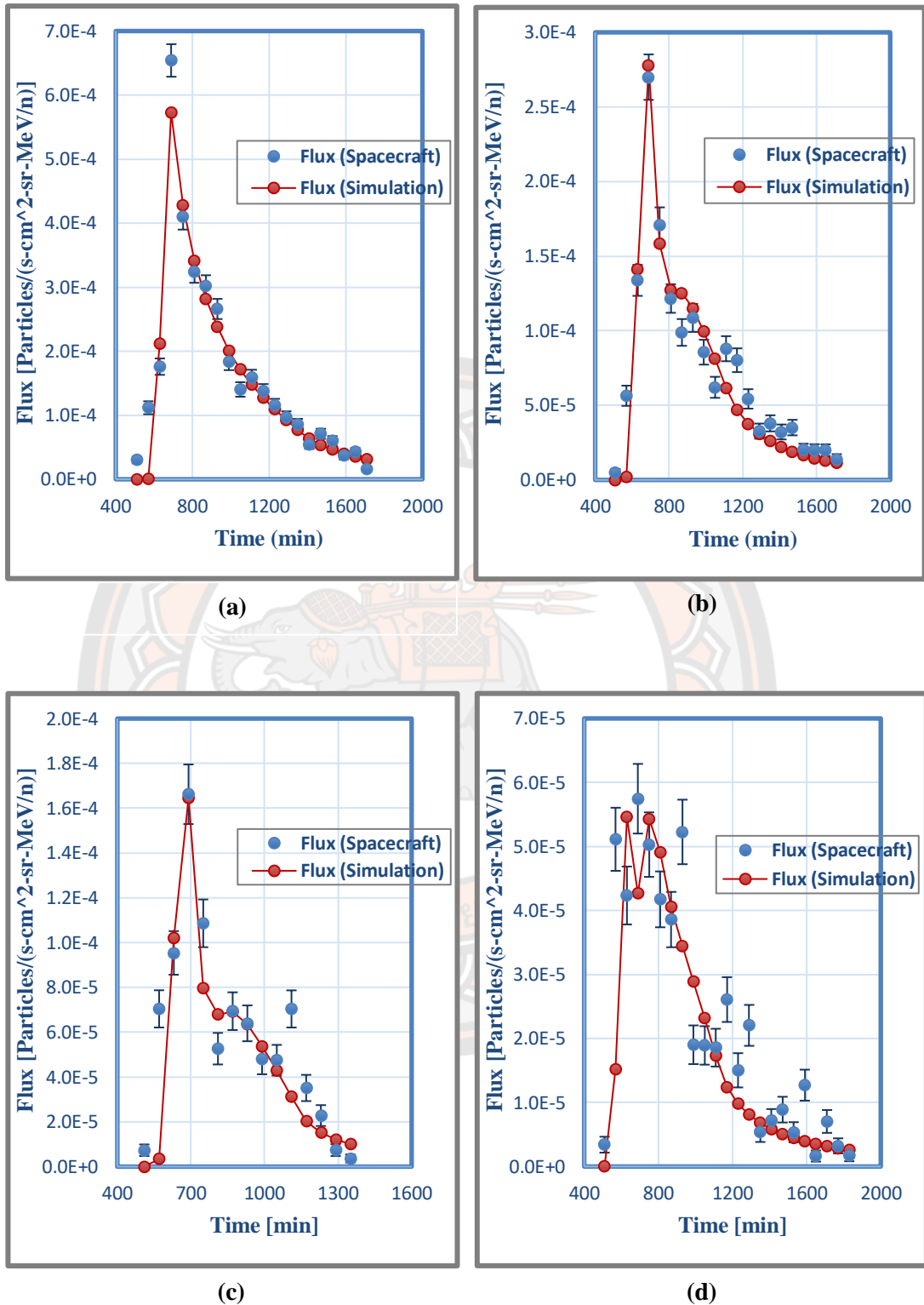


Figure 31: Comparison of simulated data and spacecraft data for Oxygen particle at energy level (a) 8.538 MeV/n, (b) 11.427 MeV/n, (c) 14.293 MeV/n, and (d) 18.104 MeV/n.

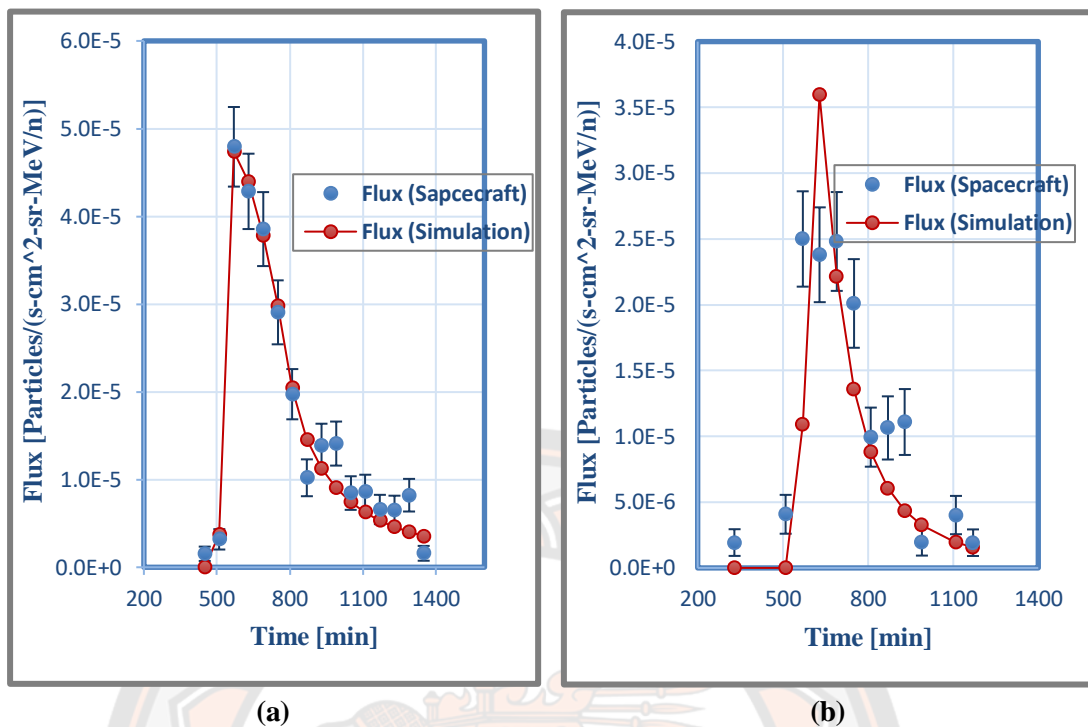


Figure 32: Comparison of simulated data and spacecraft data for Iron particle at energy level (a) 18.461 MeV/n, and (b) 30.902 MeV/n.

4.3 Injection Function and FWHM (Full Width Half Maximum)

After getting best mean free path and fitting data we then, determine the particle release time by from Sun to Earth by using FWHM technique in injection profile. We found injection time for every considered element at all energy level. Injection time is the time taken by the SEP (Solar Energetic Particle) to travel from Sun to Earth. It plays an important role in helping us to understand the way solar flare behaves.

FWHM is the technique which involves, the finding of the width of the highest point in the graph and reduce it to half from the injection profile as shown in the Figure 33 – 37. The detailed procedure of the technique is as discussed in section 3.11 of chapter III. The x-axis of the graph is time [min] and y-axis is the injection function, $a[i]$. The calculated injection time is shown in Table 8.

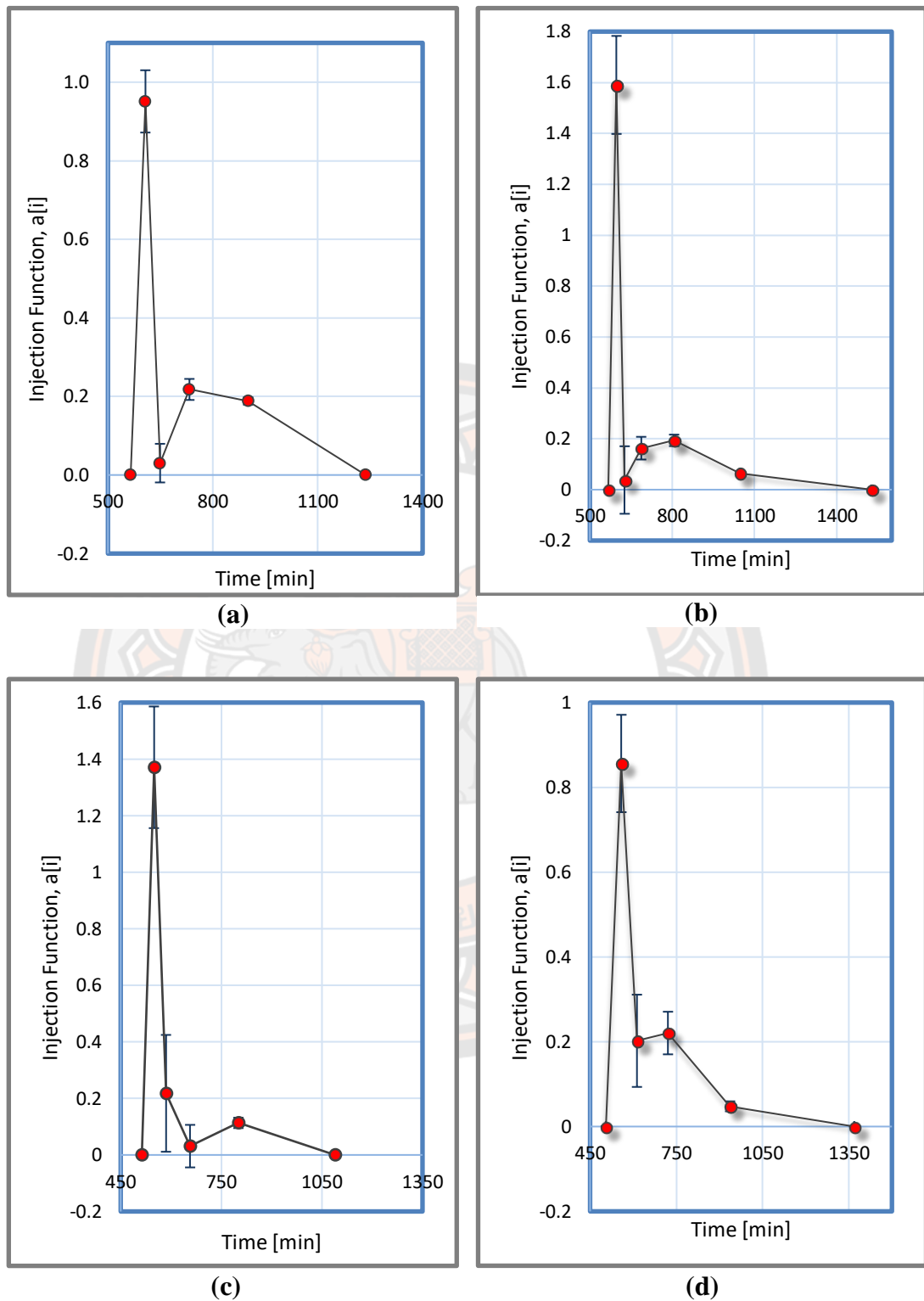


Figure 33: Injection profile for Helium particle at energy level (a) 4.032 MeV/n, (b) 5.390, (c) 6.685 MeV/n, and (d) 8.418 MeV/n.

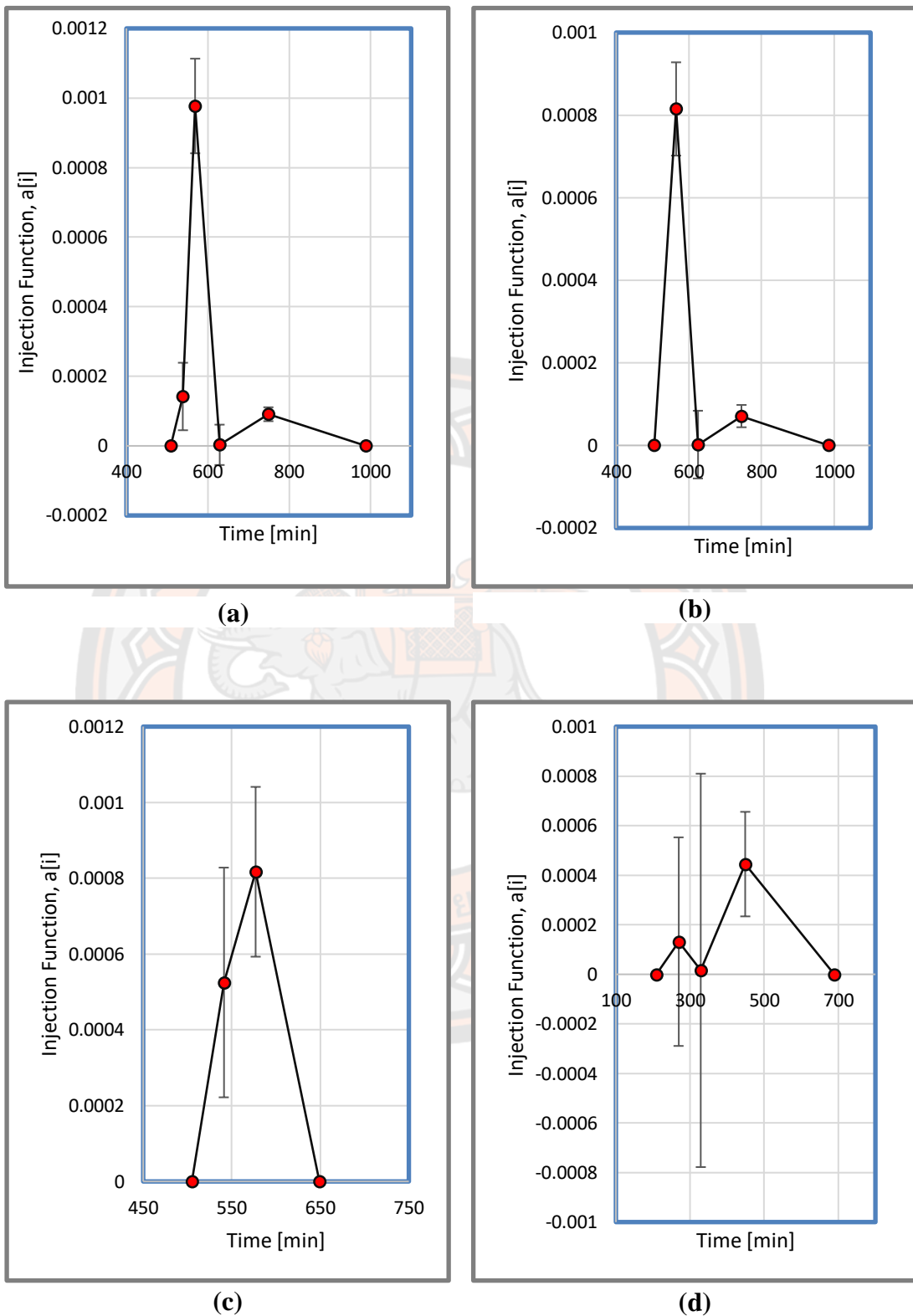


Figure 34: Injection profile for Carbon particle at energy level (a) 7.443 MeV/n, (b) 9.839 MeV/n, (c) 12.267 MeV/n, and (d) 15.505 MeV/n.

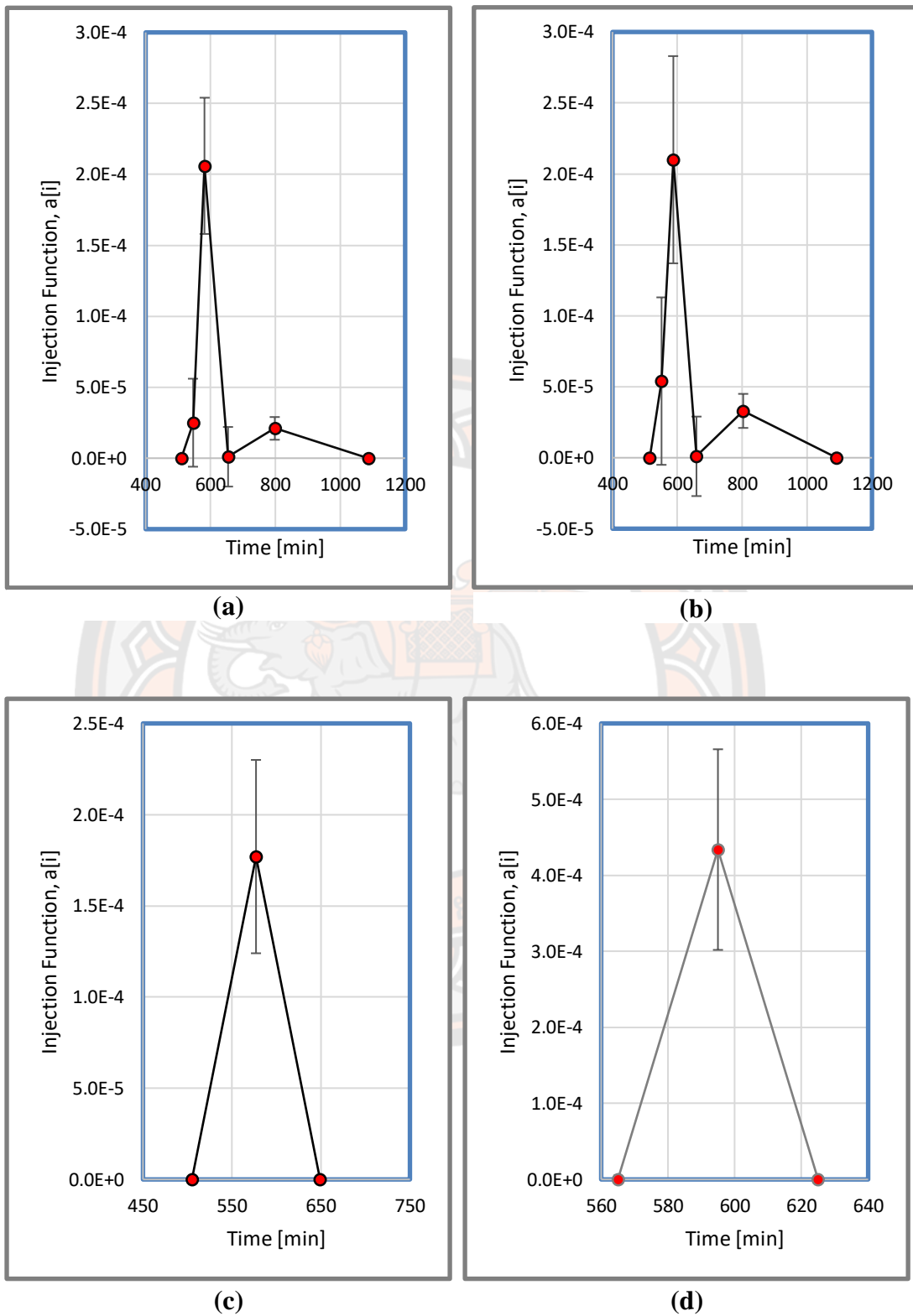


Figure 35: Injection profile for Nitrogen particle at energy level (a) 8.009 MeV/n, (b) 10.660 MeV/n, (c) 13.317 MeV/n, and (d) 16.854 MeV/n.

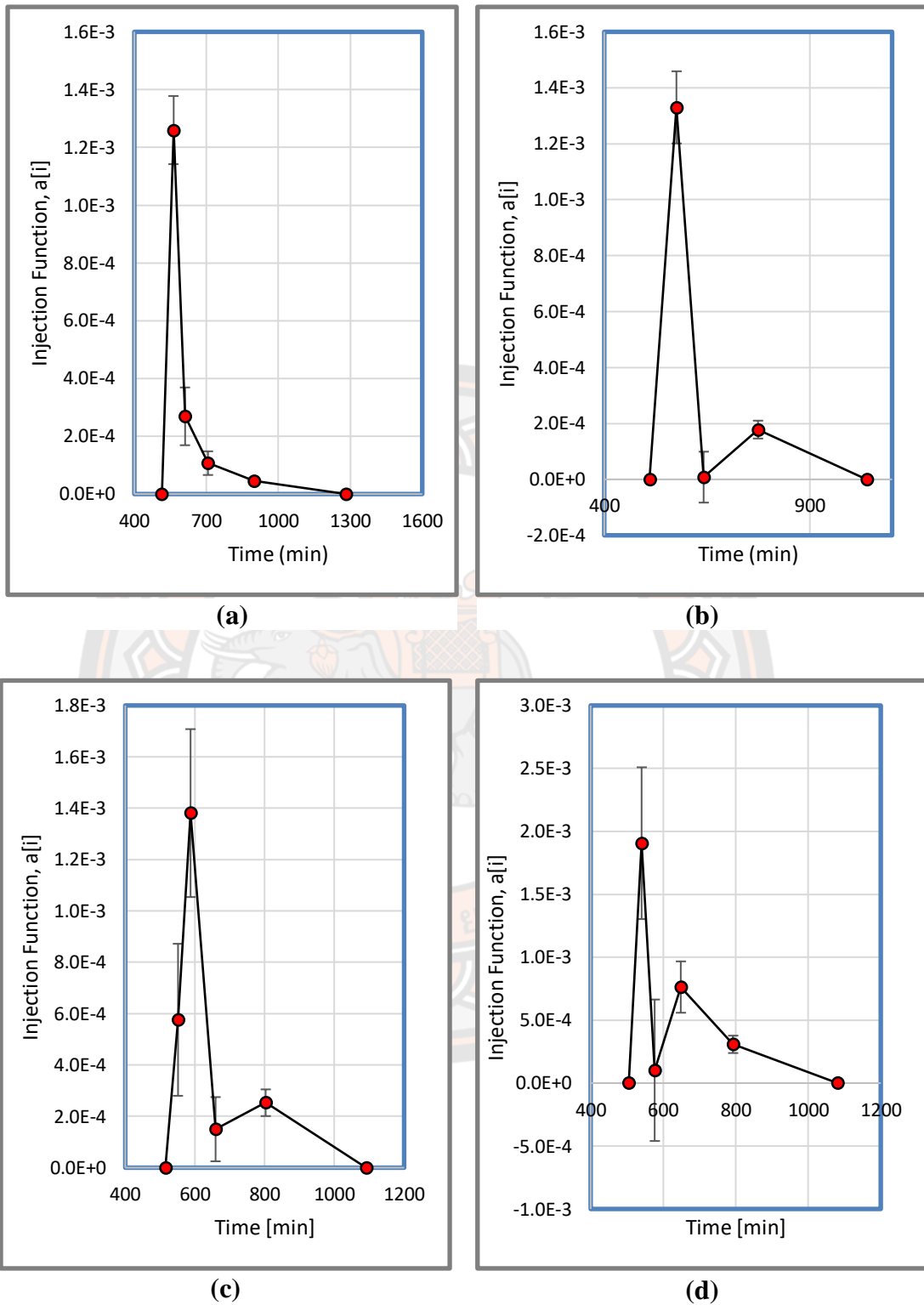


Figure 36: Injection profile for Oxygen particle at energy level (a) 8.538 MeV/n, (b) 11.427 MeV/n, (c) 14.293 MeV/n, and (d) 18.104 MeV/n.

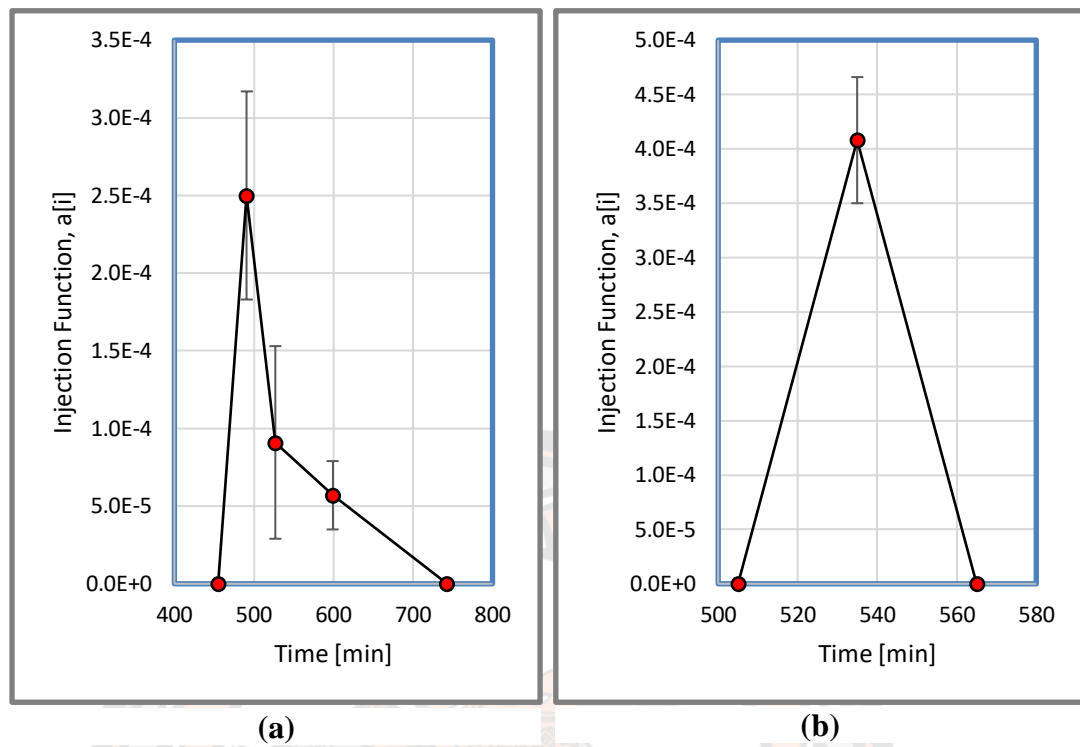


Figure 37: Injection profile for Iron particle at energy level (a) 18.461 MeV/n, and (b) 30.902 MeV/n.

4.4 The simulation result for solar event on August 9, 2011

Table 8, as shown below is simulated by using transport equation of Ruffolo (1995, 1998) in C++ program on ubuntu operating system considering initial value of the collected data. The results are displayed as mean free path λ (AU) and injection time (min) release from Sun to Earth for each element at every energy level.

Table 8: Simulation results for He, C, N, O and Fe

Elements	Energy levels [MeV/n]	Mean free path [AU]	Injection time [min]
Helium	4.032	0.587 ± 0.022	42.689
	5.390	0.667 ± 0.066	45.732
	6.685	0.306 ± 0.036	39.401
	8.418	0.391 ± 0.082	62.351
	11.493	0.497 ± 0.064	30.708
	15.623	0.681 ± 0.132	47.453
Carbon	7.443	0.383 ± 0.030	47.643
	9.839	0.282 ± 0.074	60.074
	12.267	0.310 ± 0.093	79.989
	15.505	0.196 ± 0.084	182.238
Nitrogen	8.009	0.423 ± 0.073	56.662
	10.660	0.466 ± 0.100	60.403
	13.317	0.520 ± 0.318	72.000
	16.854	0.410 ± 0.009	30.000
Oxygen	8.538	0.313 ± 0.054	54.515
	11.427	0.341 ± 0.068	66.200
	14.293	0.546 ± 0.149	71.266
	18.104	0.476 ± 0.140	37.018
	24.838	0.651 ± 0.186	42.100
	33.847	0.613 ± 0.079	30.376
	49.832	0.664 ± 0.171	141.293
Iron	18.461	0.366 ± 0.094	46.302
	30.902	0.16 ± 0.063	30.000

From table 8 we can conclude that, the average injection time and mean free path for Helium element are 44.722 min and 0.530 AU respectively, which is also almost consistent for all energy value considered. Similarly, for Carbon the average injection time is 62.569 min and average mean free path is 0.325 AU for the energy value ranging from 7.443 to 15.505 MeV/n. The release time for Nitrogen from Sun to Earth is found to be 54.766 min for which the mean free path is 0.455 AU which is almost constant for every energy level. The simulated result for release time of oxygen showed 50.246 min with mean free path of 0.515 AU for energy level ranging from 8.538 to 49.832 MeV/n. For high energy particles such as iron, since the error is very high it hard to simulation result, however numerous trial in our thesis showed that average injection time decreases as energy level increased.

4.5 Relationship between solar cycle and galactic cosmic rays

Cosmic rays are the tiny particles (mostly the nuclei of hydrogen or proton) that enters Earth's atmosphere at nearly the speed of light. They are usually formed by supernovae explosion in outer space which reaches Earth and are called primary cosmic rays. It collides with other particles in the Earth's atmosphere creating cascade of particles which showers to the ground. These particles are called secondary cosmic rays and are absorbed by the neutron monitor for measurement.

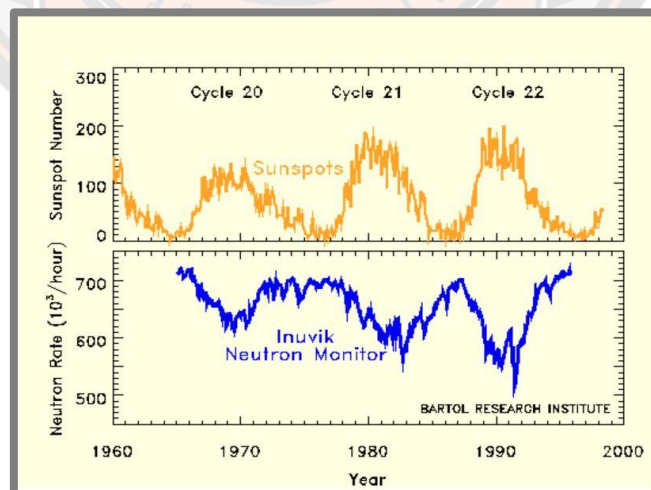


Figure 38: Data collected by Inuvik Neutron monitor illustrating the relationship between sunspot number and neutron rate.

Source: <http://neutronm.bartol.udel.edu/listen/main.html>

During maximum solar cycle the count of sunspots is high and occurrence of solar flare is highly likely. When it arises, the solar energetic particles propagating from the Sun to Earth creates barriers to galactic cosmic rays and sweeps away some of the cosmic rays in its path. Thus, as a result the neutron count rate decreases gradually which is seen in neutron monitor. Figure 38 corresponds to the data collected from Inuvik Neuron monitor illustrating the relationship between sunspot number and neutron count rate. It displays gradual decrease in neutron count rate as number of sunspot increases and vice versa, indicating some circumstances of solar activity (Houseman & Fehr, 1999).

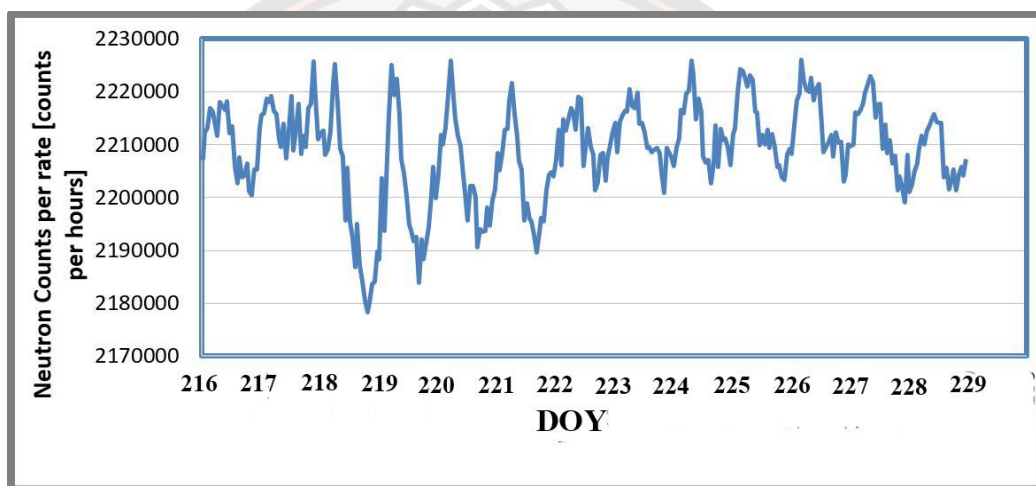


Figure 39: Data collected (Corr Vs Time) for the duration of 216/2011 to 229/2011 from Princess Sirindhorn Neutron monitor, Thailand.

Neutron monitor is ground based detector to measure the number of high energy charged particles (cosmic rays) striking Earth's atmosphere from outer space. We used Princess Sirindhorn Neutron Monitor on Doi Inthanon, Thailand to collected the data at our event of interest on August 9, 2011.

Figure 39 as displayed above, corresponds to the data collected from the Princess Sirindhorn neutron monitor which is the measurement of neutron count rate [counts per hour] corrected for pressure effect versus the DOY (day of year). It was gathered for the duration of DOY 216/2011 to 229/2011 as our solar event of interest was on DOY 221/2011. By closely analyzing the above graph we concluded that there was decrease in number of neutron particles during DOY 218/2011-222/2011 hinting us that there was high probability of the occurrence of solar flare and solar energetic particle reached the Earth.

CHAPTER V

CONCLUSIONS

The research was based on the solar eruption at the maximum phase of solar cycle 24th on August 9, 2011. We studied the solar energetic particles that propagated from Sun to Earth at that particular event. This was done via Ruffolo's (1995, 1998) transport equation using C++ program in ubuntu operating system to simulate the motion of particles. However, the equation was solved using numerical technique of finite difference. The initial values of simulation were prepared from the spacecraft data for basic variable calculating. The simulation results are the particle distribution as a function of time for each energy of the mean free path. We use the technique of the piecewise linear least square method for optimization of the injection duration.

The chapter discusses the major analysis of the results obtained and we draw our interpretation of the behavior of the particles that propagates from Sun to Earth. The reason to select an event was mainly due to fact that it was only the event having X class solar flare of X6.9 at the maximum of 24th solar cycle. The solar wind speed at that particular event was 551.5 kms⁻¹.

5.1 Discussion

As displayed in Table 8, we have simulated for all considered particles, He, C, N, O and Fe. We can see that most particles with higher energy level propagated from Sun to Earth faster than particles with lower energy levels due to their higher speed. The propagation of particles along to the magnetic field with the highest mean free path will be faster than the small mean free path, because of the particle propagation along to the magnetic field with the longest mean free path will be scattered.

As particles with a low mean free path moves to a certain distance, they are reflected or scattered due to the unevenness of the magnetic field lines from the influence of the solar wind. The particle with a high mean free path can move further along the magnetic field line than a particle with a low mean free path. Therefore, it was found that most particles with a high mean free path travel to Earth faster than particles with a lower mean free path.

The transport simulation results show the trend of mean free path to be roughly constant for each event. The mean free path is an important parameter of interplanetary transport, implying interplanetary scattering is approximately energy independent, but the level of scattering varies with time. The injection duration time from the data fitting of the solar event was more than the injection time from spacecraft because of coronal mass ejection, solar wind speed or the irregularity of the magnetic field from the Sun to the Earth affected the particle propagation.

Our solar event of interest started at 7.48 UT and ended at 8.08 UT with injection time of 20 mins and found the CME (coronal mass ejection) at 8.05 UT. There are some fluctuations in injection duration but overall simulated results showed less injection duration for higher energy than for the lower energy particles. If we closely investigate from Table 8, we concluded that the approximate injection time is between 30 – 60 min for each element which is very close to injection time as detected from Sun directly.

Thus, unlike the other solar event with much difference of injection time between simulation result and direct detection result, our solar event of interest didn't had much of effect from the space environment. So, the solar event at maximum of solar cycle had injection time from the Sun to Earth close to injection time at the Sun. The violent explosion of these solar flares didn't affect on the Earth's magnetic field because the Kp-index less than 3, which that means the Earth doesn't get any effect of disturbances in the Earth's magnetic field.

5.2 Conclusion

From the above discussion for our solar event of interest we concluded that most particles with higher energy level propagated from Sun to Earth faster than particles with lower energy levels due to their higher speed. The trend of mean free path is found to be roughly constant for each event.

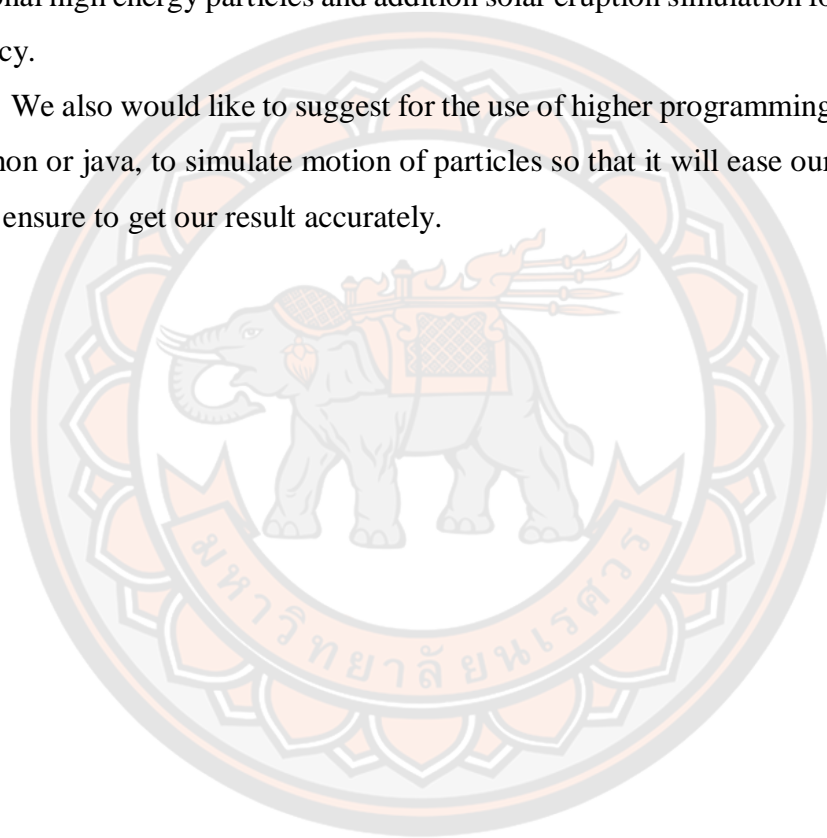
There were some fluctuations in injection duration but overall simulated results showed less injection duration for higher energy than for the lower energy particles. The calculated approximate injection time for our event was between 30 – 60 min for each element which is very close to injection time as detected from Sun directly. Thus, unlike the other solar event with much difference of injection time between simulation

result and direct detection result, our solar event of interest didn't had much of effect from the space environment. So, the solar event at maximum of solar cycle had injection time from the Sun to Earth close to injection time at the Sun.

5.3 Suggestion

The study of solar flare requires very careful and close investigation for proper prediction in future incidents. Therefore, we would like to suggest to consider additional high energy particles and addition solar eruption simulation for precision and accuracy.

We also would like to suggest for the use of higher programming language such as python or java, to simulate motion of particles so that it will ease our work and also would ensure to get our result accurately.



REFERENCES

- Baisri, P., Khumlumlert, T., & Aiemsa-ad, N. (2017). *Solar energetic particle propagation from solar flare*. Paper presented at the Journal of Physics. Conference Series (Online).
- The Classification of X-ray Solar Flares. (n.d.). Retrieved from <https://spaceweather.com/glossary/flareclasses.html>
- Earl, J., Ruffolo, D., Pauls, H. L., & Bieber, J. (1995). Comparison of three numerical treatments of charged particle transport. *The Astrophysical Journal*, 454, 749.
- Fox, K. C. (2011). Solar Cycle Primer. *NASA's Goddard Space Flight Center, Greenbelt, Md.,*. Retrieved from https://www.nasa.gov/mission_pages/sunearth/news/solarcycle-primer.html
- Fox, K. C. (2011, August 9). Sun Unleashes X6.9 Class Flare. *NASA's Goddard Space Flight Center*. Retrieved from https://www.nasa.gov/mission_pages/sunearth/news/News080911-xclass.html
- The glare of the Sun (Solar Flares). (n.d.). Retrieved from http://astro.phys.sc.chula.ac.th/IHY/Solar_storm/Flare.htm
- Gordan D, H. (2006). *The mysterious origins of solar flares*.
- Houseman, J., & Fehr, A. (1999). The Inuvik Neutron Monitor. *Listening for Cosmic Rays*. Retrieved from <http://neutronm.bartol.udel.edu/listen/main.html>
- Paluk, P., Khumlumlert, T., Kanlayaprasit, N., & Aiemsa-ad, N. (2017). *The solar energetic particle propagation of solar flare events on 24th solar cycle*. Paper presented at the Journal of Physics. Conference Series (Online).
- Ruffolo, D. (1994). Effect of adiabatic deceleration on the focused transport of solar cosmic rays. *arXiv preprint astro-ph/9408056*.
- Ruffolo, D., Khumlumlert, T., & Youngdee, W. (1998). Deconvolution of interplanetary transport of solar energetic particles. *Journal of Geophysical Research: Space Physics*, 103(A9), 20591-20602.
- Sharp, T. (2017, November 2). Atmosphere of the Sun : Photosphere, Chromspher & Corona. Retrieved from <https://www.space.com/17160-sun-atmosphere.html>
- Siddiqi, A. A. (July 25, 2019). ACE. *NASA History Program Office, 2018*. Retrieved from <https://solarsystem.nasa.gov/missions/ace/in-depth/>

Solar energetic particles : SEPs. (n.d.). Retrieved from

https://translate.google.com/translate?hl=en&sl=th&u=http://astro.phys.sc.chula.ac.th/IHY/Solar_storm/SEP.htm&prev=search

The Solar Wind. (n.d.). Retrieved from

https://translate.google.com/translate?hl=en&sl=th&u=http://astro.phys.sc.chula.ac.th/IHY/Interplanetary_space/IP_solar_wind.htm&prev=search

Space weather prediction center. (n.d.). Coronal Mass Ejection. Retrieved from

<https://www.swpc.noaa.gov/phenomena/coronal-mass-ejections>

What is a Solar flare? (n.d.). Retrieved from

<https://hesperia.gsfc.nasa.gov/sftheory/flare.htm>

Wikipedia contributors. (2020, March 11). Solar storm. *In Wikipedia, The Free*

Encyclopedia. Retrieved from https://en.wikipedia.org/wiki/Solar_storm

Wikipedia contributors. (2021, February 27). Sun. *In Wikipedia, The Free Encyclopedia*

Retrieved from <https://en.wikipedia.org/wiki/Sun>

Wikipedia contributors. (2021, January 4). Radiation Zone. *In Wikipedia, The Free*

Encyclopedia. Retrieved from

https://en.wikipedia.org/w/index.php?title=Radiation_zone&oldid=937864385

Wikipedia contributors. (2021, January 11). Solar cycle. *In Wikipedia, The Free*

Encyclopedia. Retrieved from https://en.wikipedia.org/wiki/Solar_cycle

APPENDIX A:

A method to determine best mean free path

We will fit distances to simulate the mean free path (λ) compared with the actual data in order to find trend of the best mean free path corresponding to the minimum chi square (χ^2) value from all 3 to 5 neighboring points. The mean free path of particles for solar event on August 9, 2011 is as shown in the Figure 42 – 43 used for simulating the injection profile. We then, obtained the best mean free path by differentiating the equation with respect to x and determining the value of $x = \lambda$.

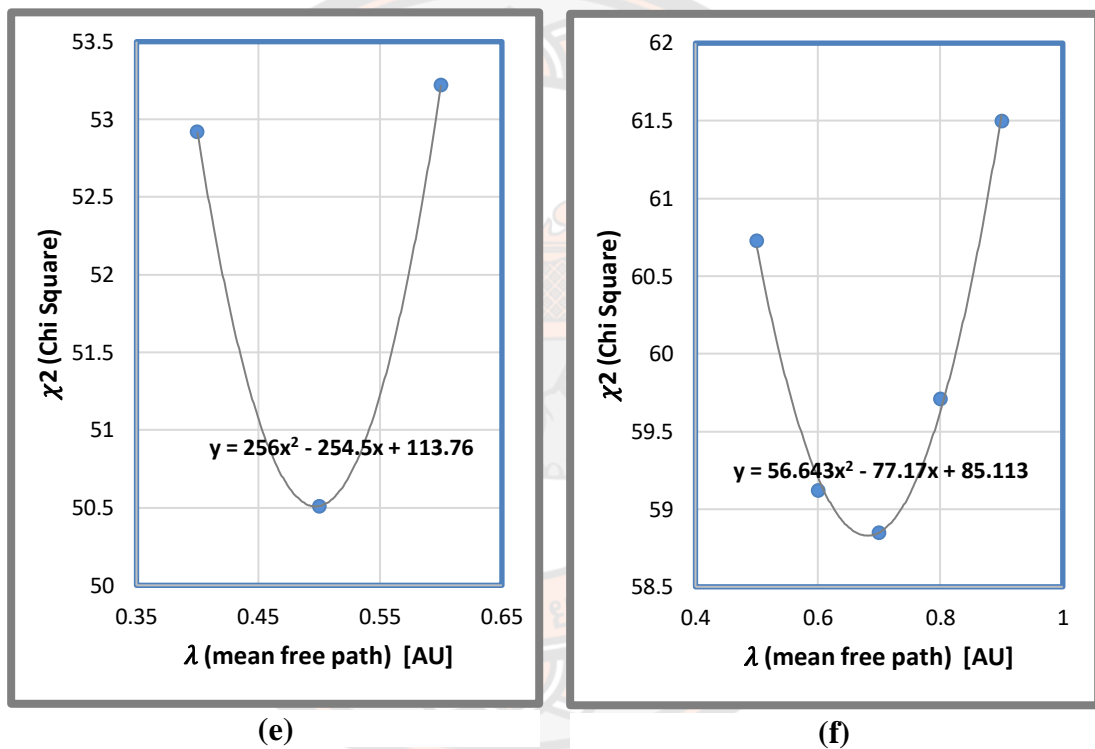


Figure 40: Displaying best mean free path for corresponding minimum Chi square value for Helium particle at energy level (e) 11.493 MeV/n, and (f) 15.623 MeV/n.

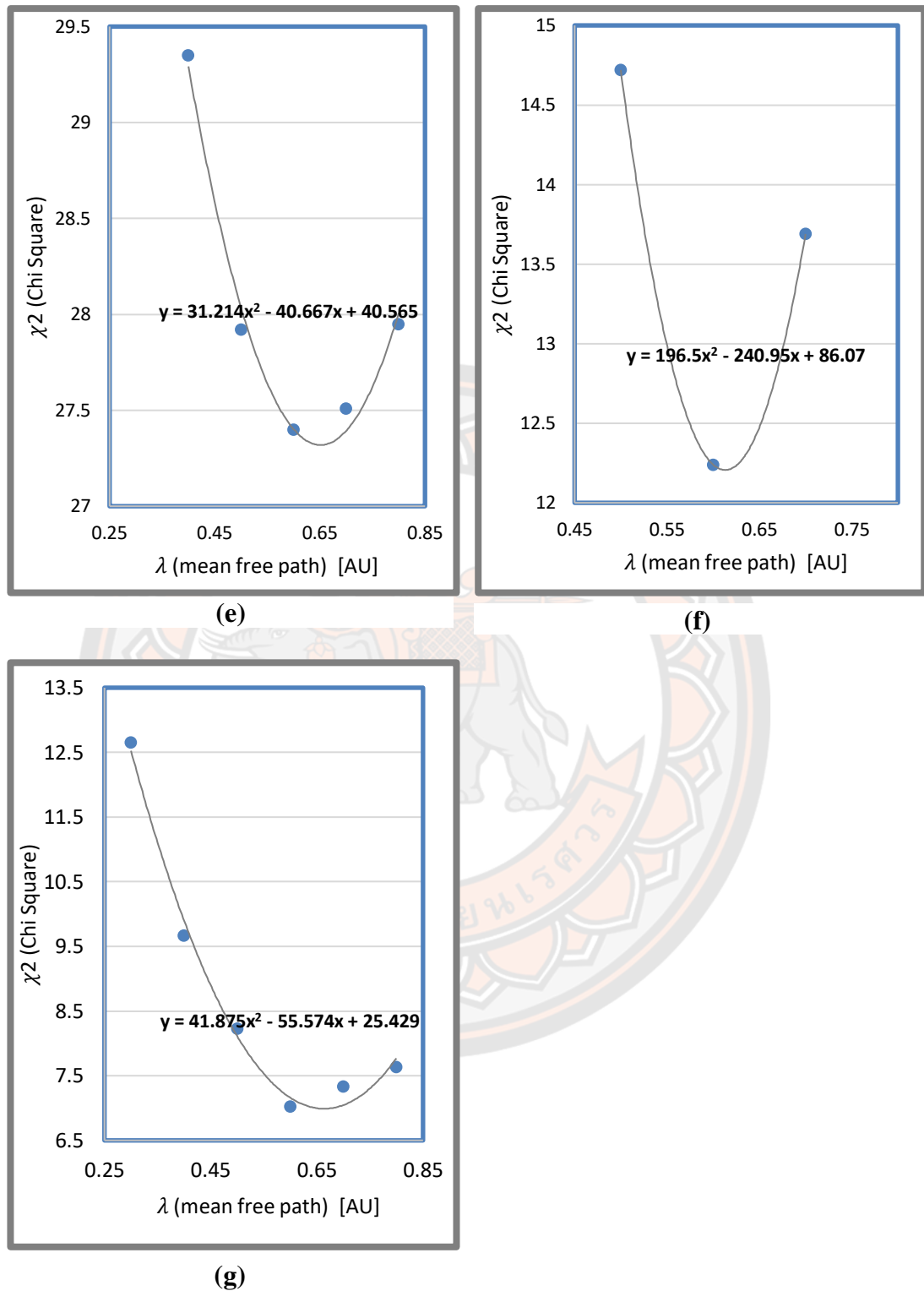


Figure 41: Displaying best mean free path for corresponding minimum Chi square value for Oxygen particle at energy level (e) 24.838 MeV/n, (f) 33.847 MeV/n, and (g) 49.832 MeV/n.

APPENDIX B:

The best fitting result between the spacecraft data and simulation data

The fitting results corresponding to the comparison of actual data from the spacecraft and with those obtained from simulation results for each element at all energy level is as displayed in Figure 44 - 45. We find the best fitting between spacecraft data and simulated data for best mean free path. We use compared fitting method of piecewise linear function between the simulation results and spacecraft data.

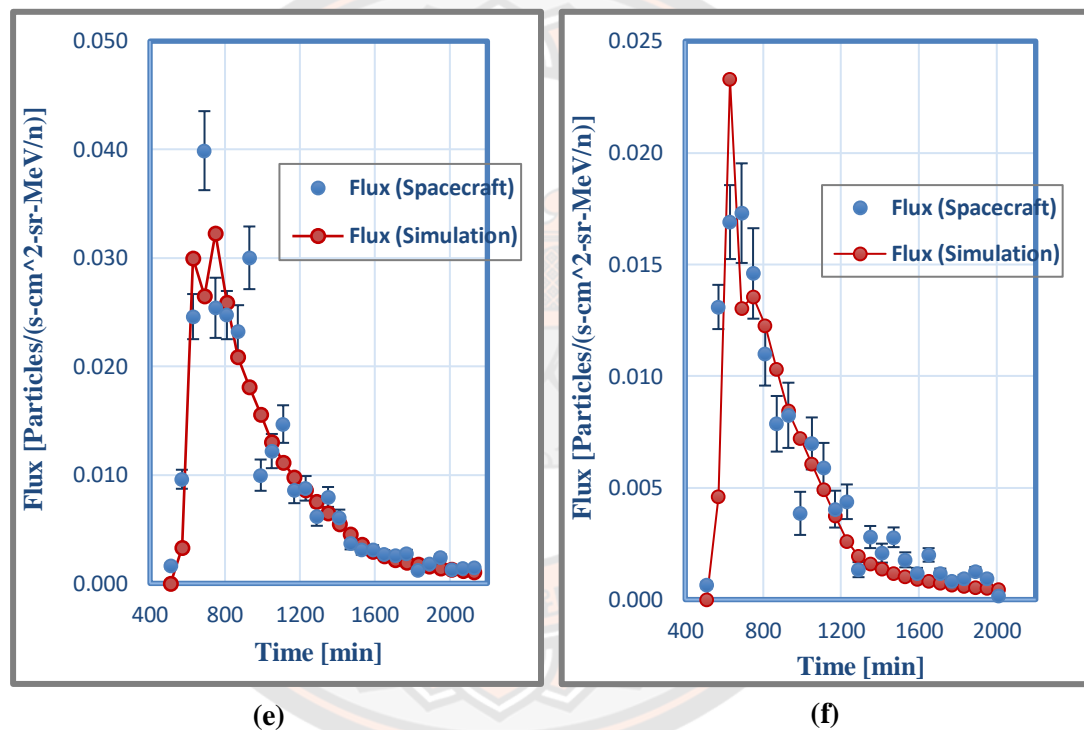
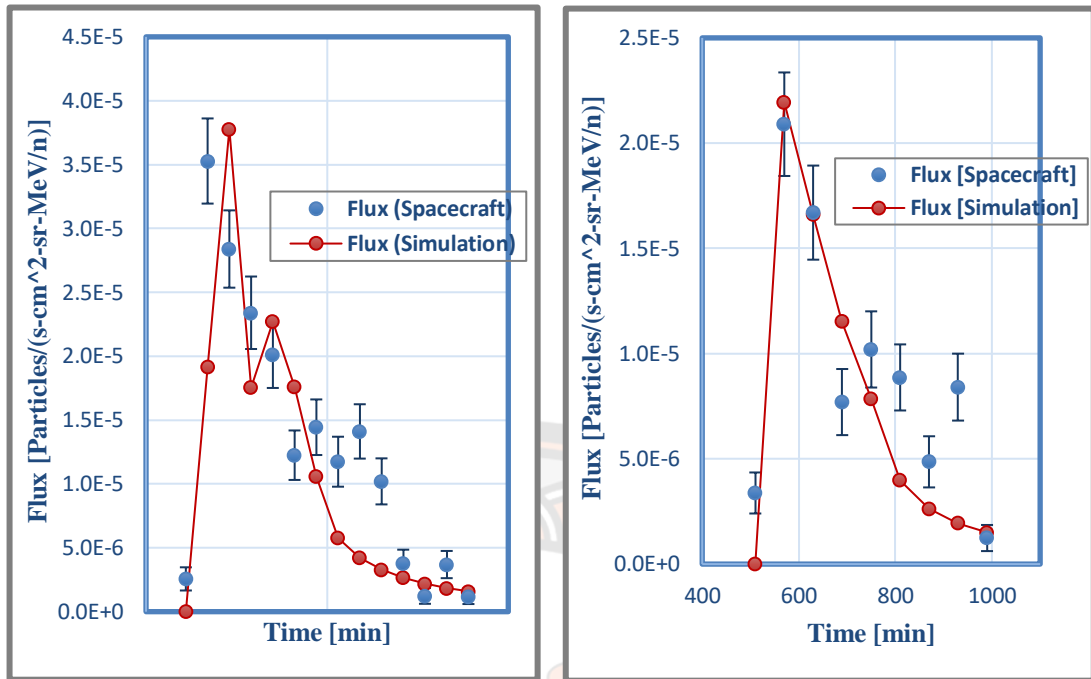
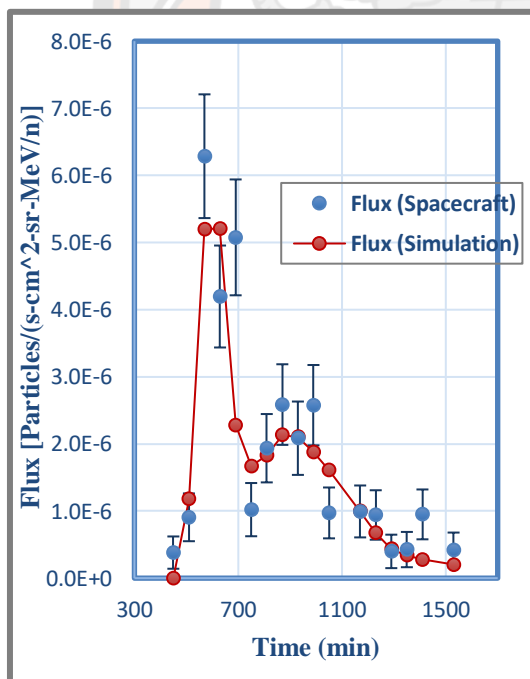


Figure 42: Comparison of simulated data and spacecraft data for Helium particle at energy level (e) 11.483 MeV/n, and (f) 15.623 MeV/n.



(e)

(f)



(g)

Figure 43: Comparison of simulated data and spacecraft data for Oxygen particle at energy level (e) 24.838 MeV/n, (f) 33.847 MeV/n, and (g) 49.832 MeV/n.

APPENDIX C:

The injection profiles

After getting best mean free path and fitting data we then, determine the particle release time by from Sun to Earth by using FWHM (Full Width at Half Maximum) technique in injection profile. We find injection time for every considered element at all energy level. The injection profile as shown in the Figure 46 – 47. The x-axis of the graph is time [min] and y-axis is the injection function, $a[i]$. The calculated injection time is shown in Table 8.

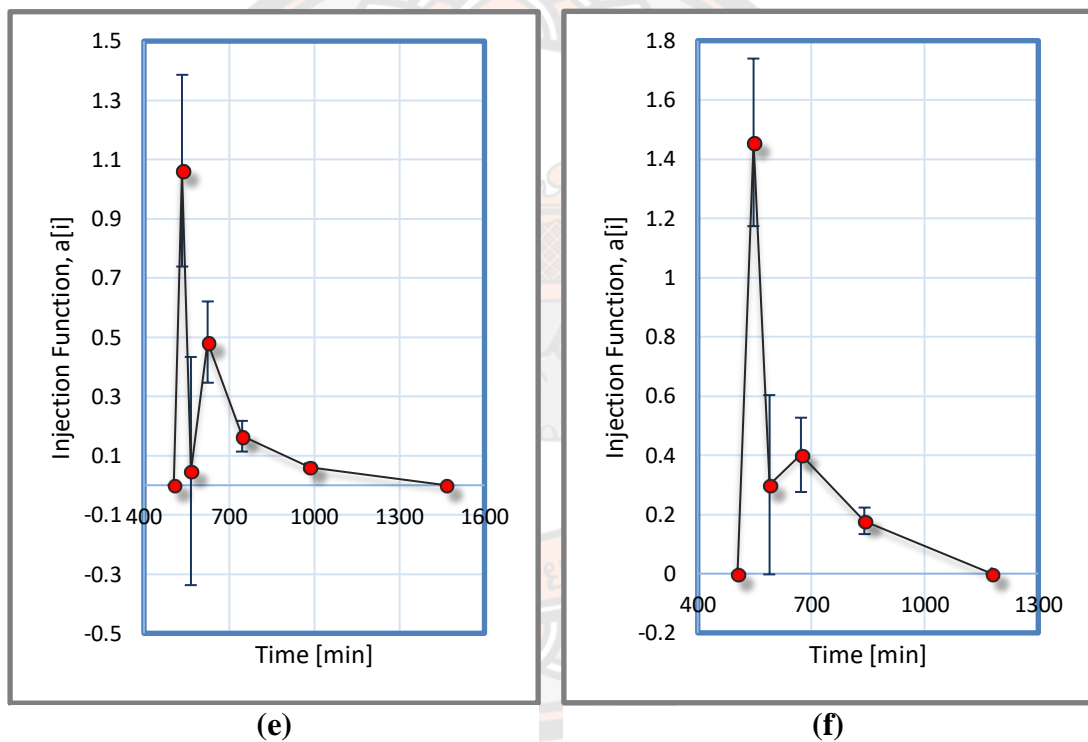


Figure 44: Injection profile for Helium particle at energy level (e) 11.493 MeV/n, and 15.623 MeV/n.

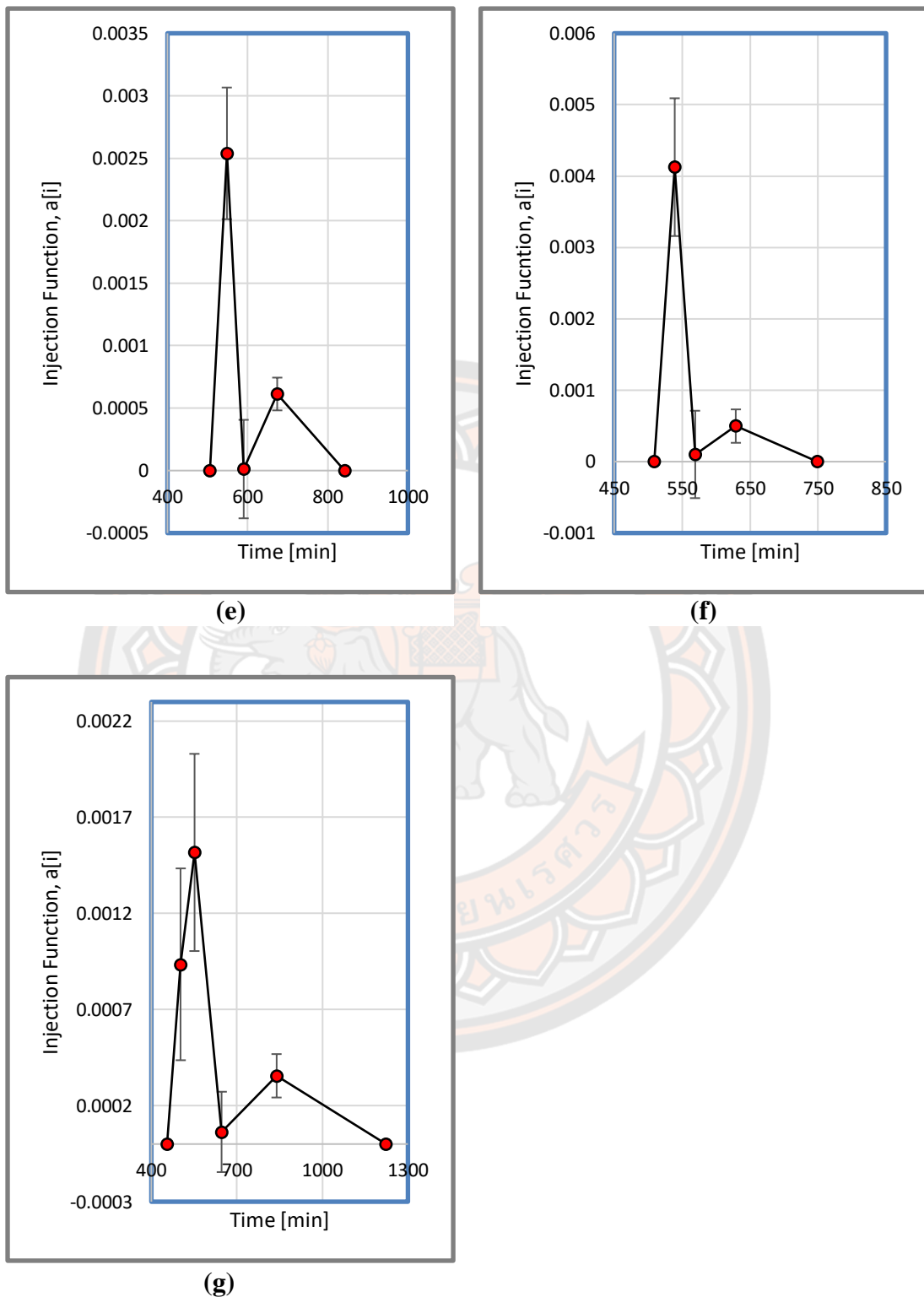


Figure 45: Injection profile for Oxygen particle at energy level (e) 24.838 MeV/n, (f) 33.847 MeV/n, and (g) 49.832 MeV/n.